國 立 交 通 大 學

光電工程研究所

博 士 論 文

無排列缺陷之半 V 型鐵電式液晶元件及其應用

Alignment Defect Free Half-V Switching Mode Ferroelectric Liquid Crystal Devices and Their Applications

研究生：林淇文　　　　　Student：Chi-Wen Lin

指導教授：陳皇銘 博士　　Advisor：Dr. Huang-Ming P. Chen

中 華 民 國 一 百 年 七 月

無排列缺陷之半 V 型鐵電式液晶元件及其應用

Alignment Defect Free Half-V Switching Mode Ferroelectric Liquid Crystal Devices and Their Applications

研究生：林淇文　　　　　**Student：Chi-Wen Lin**

指導教授：陳皇銘 博士　　**Advisor：Dr. Huang-Ming P. Chen**

國 立 交 通 大 學

光 電 工 程 研 究 所

博 士 論 文

A Dissertation
Submitted to Institute of Electro-Optical Engineering
College of Electrical and Computer Engineering
National Chiao Tung University
in partial Fulfillment of the Requirements
for the Degree of
Doctor of Philosophy
in
Electro-Optical Engineering
July 2011
Hsinchu, Taiwan, Republic of China

中 華 民 國 一 百 年 七 月

無排列缺陷之半 V 型鐵電式液晶元件及其應用

博士班研究生：林淇文　　　指導教授：陳皇銘 博士

國立交通大學　　　光電工程研究所

摘要

表面穩定鐵電式液晶(surface-stabilized FLC)元件是目前廣為研究的鐵電式液晶元件技術，除了反應時間快，因為平面的分子運動，其視角也較傳統液晶顯示器大，然而表面穩定鐵電型液晶元件的應用在過去的研究中有兩個主要的問題，缺乏連續的灰階以及難有良好的液晶排列，此缺點嚴重影響到液晶元件的對比度。除了雙穩態之表面穩定鐵電型液晶模式，半 V 型鐵電式液晶(half-V switching mode FLC)模式是以改變光軸方向而達到連續灰階。然而半 V 型鐵電式液晶元件於液晶排列上仍有缺陷存在，在降溫的過程中，半 V 型鐵電式液晶元件由 N^*液晶相轉變成 SmC^*液晶相時，液晶分子雖然順著配向處理的方向排列，卻因層列層(smectic layer)排列方向之不同，使得液晶分子有兩個極性方向之排列，因而產生兩種排列區塊，名為水平山形袖章缺陷(horizontal chevron defect)。半 V 型鐵電式液晶元件於結構上不易排列及衍生出的缺陷是目前我們極欲解決的問題。

此論文以液晶能量的角度探討半 V 型鐵電式液晶元件之水平山形袖章缺陷形成的原因，並研究利用表面處理消除排列缺陷。對於有水平山形袖章缺陷的鐵電式液晶而言，其排列可以分為自發性極化(spontaneous polarization, P_S)指向上的 P_{Sup} 區塊(domain)及指向下的 P_{Sdown} 區塊。當上下基板於相同的配向處理
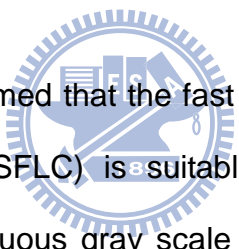
下， P_{Sup} 區塊及 P_{Sdown} 區塊擁有相同的總自由能。換言之，此兩種區塊皆會出現於元件中。如果能設法使兩種區塊的能量產生大小的差異，則液晶分子會傾向排列於能量較低的狀態進而得到單一種排列。依液晶能量公式，控制配向層之極性表面能量可讓兩種區塊產生能量差異。於此，有兩種可能的配向組合: 1. 結合強與弱配向方法：結合研磨配向 (rubbing alignment) 與電漿配向 (plasma alignment)。2. 控制配向層之表面極性，上下基板分別使用極性相反的配向層材料。使用非對稱配向技術，在液晶盒厚度小於 1.8μm 且配向層表面平坦的液晶盒中成功地去除了水平山形袖章缺陷。 鐵電式液晶因快速反應的特性，可於光電元件的應用上，達到光電訊號傳輸上的快速響應。延續使用無排列缺陷的半 V型鐵電式液晶元件製程技術，我們以條狀電極方式製作鐵電型液晶光柵，在有條狀突起電極不平整的基板上研究去除鐵電式液晶之排列缺陷並設計電極寬度提高繞射效率。藉由降低液晶盒厚度，延展鐵電式液晶之螺距及使用非對稱配向可得良好排列的鐵電式液晶元件。然而在面板製程中，其液晶盒間距大於 3 μm 已經比表面穩定鐵電式液晶之間距大了兩倍。我們進一步研究鐵電式液晶於 3.5 μm液晶盒中的排列，延展鐵電式液晶之螺距至 10 μm 以上並使用非對稱配向降低排列缺陷。

Alignment Defect Free Half-V Switching Mode Ferroelectric Liquid Crystal Devices and Their Applications

Doctoral Student: Chi-Wen Lin   Advisor: Dr. Huang-Ming Philip Chen

Institute of Electro-Optical Engineering
National Chiao-Tung University

Abstract

Many studies have confirmed that the fast response of surface-stabilized ferroelectric liquid crystal (SSFLC) is suitable for fast switching devices. However, the lack of a continuous gray scale limits the potential for display application. Half-V switching FLC mode (HV-FLC) with its intrinsic continuous gray scales is more suitable for the driving of active matrix thin-film-transistors (AM TFT). The major drawback in HV-FLC devices is the horizontal chevron alignment defect. This is due to the presence of both spontaneous polarization (P_S) up and down domains when the HV-FLC device cools down from its N^*-SmC^* phase transition. Resolution of the alignment defect remains a challenge to overcome before the potential for display application of HV-FLC can be realized.

In this dissertation, the origin of the horizontal chevron alignment defect is explained by considering the physical aspect of the FLC's free energy. The P_S

up and P_S down domains co-exist because of the same minimum total free energy in the symmetrical cell in which the top and the bottom alignment surfaces have the same polar surface interaction coefficients. As a result, a defect-free alignment texture is only achievable when the orientation of the FLC's P_S direction is the same. According to HV FLC's total free energy, a large difference in the polar surface energy term under asymmetrical alignment conditions may hold the key to lowering the FLC's free-energy level. Two approaches to solve the alignment problem caused by surface pre-treatment were identified. Firstly, by applying rubbing and plasma alignment techniques on both top and bottom substrates, the alignment strength which differentiates values were controlled. Secondly, by using alignment layers with opposite sign of surface polarities, the sign of $\gamma_2^{(b)}$ was changed. The asymmetrical alignment techniques were applied to control the anchoring energy and surface polarity and to validate theoretical predictions. Using the asymmetric alignment technique, based on double-side striped electrodes, the electrically tunable FLC grating, approaching calculated diffraction efficiency is demonstrated. FLC's alignment in the ITO patterned non-uniform surface is studied. The width of thin striped electrodes is designed smaller than half of the grating pitch to compensate for the fringe field effect and thus improve the diffraction efficiency. Good FLC alignment is able to be achieved by small cell gap, certain pitch design, and surface polarity control asymmetric cell. The remaining unsolved issue in display applications is the cell process limitation in manufacture. The cell gap of most TFT-LCDs is controlled larger than 3 μm. The minimum cell gap requirement is, at least, 2 times greater than SSFLC cell. We studied a potential approach which can be applied to minimize the alignment defects in the cell gap 3.5 μm.

Acknowledgement

顯示科技所的創立至今，身為陳皇銘老師第一屆學生，碩博士七年從懵懂無知到獨立成熟真的很感謝老師的指導與嚴格的要求。在老師的保護下學習、犯錯然後成長，老師總是耐心的教誨，指導我正確的研究處世態度。博士班口試結束，老師仍細心指導著要改進的地方，告訴我出社會後要注意的事項。論文口試像是一場成年禮去驗證自己是否有獨當一面的能力，老師就像看著自己的孩子離開家園，開心小孩長大了卻又擔心實力不以面對出社會後更多的挑戰。這些年如果我有所成長、成熟都要感謝老師。

博士班這五年很辛苦，很充實也很開心。一直以來都覺得自己很幸運，一路上都有貴人相助，就像我最喜歡的書"牧羊少年奇幻之旅"裡的一句話"當你真心渴望某樣東西時，整個宇宙都會聯合起來幫助你完成。"感謝實驗室所有成員的陪伴；感謝歷屆液晶團隊的學弟們：昆展、謹瑋、宣穎、智一、家煌，在研究上共同努力；感謝葆如學姐，司芬學姐，玉蓮在研究上的協助；感謝李信榮先生，陳丁振博士對晚輩的照顧，在研究及生活多次幫助；感謝芳正學長及文娟姐在荷蘭時的照顧，讓我在異鄉也有家的感覺；感謝珮宜讓實驗室有良好的制度與研究環境。博士論文能完成真的非常感謝大家的照顧與協助。

我要將這分榮耀與親愛的爸媽、弟妹，還有在天上的阿嬤分享，是家人無盡的愛讓我有勇氣走完這漫長的路。這些年來唯一的煩惱就是無法為家裡分擔家計，感謝爸媽弟妹支持、鼓勵，也是家人以我為驕傲讓我有努力的動力。感謝旻珮、雅娟、俞文、潔如的陪伴，常常幫我打氣，讓我覺得念博士班是很屬害的事！

畢業了，離開學生身份將朝向另一個人生階段邁進。很多人總愛問博士生為什麼要念博士班，為錢？為升遷？為教職？近日才真正了解自己念博士班的原因，很奇怪卻很像我，是為了"不一樣"，想擁有不同的人生。博士班的訓練，荷蘭 Philips 的研習，五年過了，我"不一樣"了吧？感謝自己的毅力與勇氣，讓我有說不完的故事，為人生增添不少色彩。

TABLE OF CONTENTS

FIGURE CAPTIONS

List of Tables

Chapter 1   Introduction

1.1   Introduction

Electro-optical and semi-conductor techniques are highly developed. Liquid crystal devices perform an important function in the application of electro-optical techniques. Liquid crystal (LC) as an electric switchable material with birefringence is widely applied in display and optical devices. Properties of easy fabrication, low cost, and compactness attract consumers to product such as thin-film-transistor liquid-crystal displays (TFT-LCD), e-books, spatial light modulators (SLMs) and liquid crystal gratings. Due to low driving voltage and gray scale characteristics, nematic LC materials are applied in most LC devices. However, application in fast switching devices and novel display techniques is limited by slow response times. Many studies have confirmed that the sub-millisecond fast response of ferroelectric liquid crystal is suitable for fast switching devices. For display applications, the fast switching property allows FLCs to reduce motion blur in large size LCDs and to realize the field sequential color LCD technique. An inevitable challenge with the development of liquid crystal display is improving the response time.

1.2   Liquid Crystal Phases

Liquid crystal is a state between crystalline solid and amorphous liquid. It can be regarded as a liquid material with ordered molecular arrangement. Liquid crystals are generated from organic substances with anisotropic molecules. The molecules are elongated (rod-like) or flat (disc-like). The

ordering of anisotropic molecules produces mechanical, electrical, magnetic and optical properties. Liquid crystal phases are formed by several types of molecules with widely different structures. Usually, the LC molecules applied to electro-optical techniques are rod-like. Disk-like, bend-shape, board-like molecular and other shapes are not discussed in this dissertation.

Nematic

The nematic liquid crystal phase is characterized by molecules that have no positional order but tend to point toward the same direction as shown in Fig. 1-1. In the nematic phase, molecules are optically uniaxial, i.e. oriented with their long axis aligned to the rubbing direction.
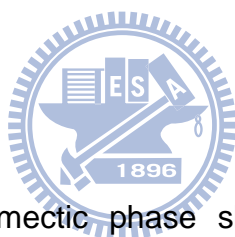
Smectic

Liquid crystals in the smectic phase show an additional degree of positional order with molecules ordered in layers. In the smectic A (*SmA*) phase, layer spacing approximately equals the length of molecule as shown in Fig. 1-1. In the smectic C (*SmC*) phase, molecules are arranged in layers as in the *SmA* phase with the directors tilted at a preferred angle to the layer normal. This indicates that the molecule is confined to a conical surface of which the layer normal is the axis and the cone is the so-called smectic cone. During the phase transition from *SmA* to *SmC* LC molecules tilt at an angle Ɵ, The layer spacing in the *SmC* phase is therefore smaller than that in the *SmA* phase. This property is called layer shrinkage.
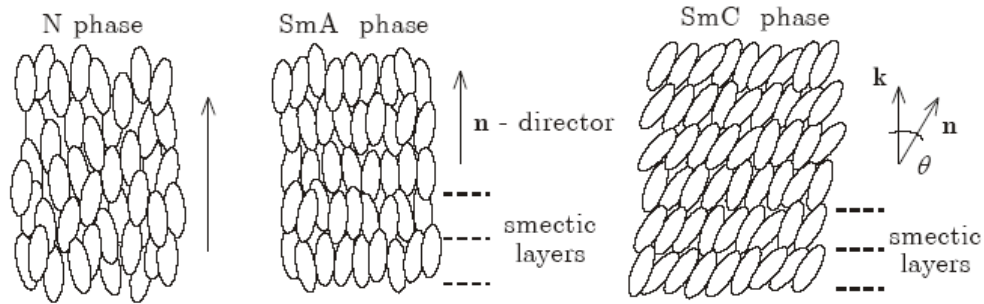
Fig. 1-1. Molecular arrangements of liquid crystal phases [1].

1.2.1 Chirality

Chiral molecules dissolve in achiral LCs inducing twisted LC structures. The chiral molecule itself may or may not have a liquid crystalline phase. A chiral object cannot be superimposed by any translations or rotations onto its mirror image. This is usually due to the presence of an asymmetric carbon atom bonded to four distinct groups. Chiral molecules induce chirality in nematic or smectic phases by intra- and inter-molecular transfer [2]. In intramolecular transfer the center leads to a distortion of the structure of compounds and to the formation of various conformers. Intermolecular transfer may result in a variation of the molecular orientational distribution function. Helical twisting power (HTP) can be utilized for the induction to chiral phases. An approximate linear function of HTP is:

$$HTP = p^{-1}c^{-1} \qquad\qquad (1.1)$$

where p is the helical pitch length, i.e. the distance it takes the director of the LC molecules to rotate a full turn as shown in Fig. 1-2. and c is the concentration of the chiral dopant.

1.2.2 Chiral Nematic

Chiral nematic (or cholesteric) liquid crystal (CLC) phase is composed of nematic mesogenic molecules which contain a chiral center. Usually a CLC is prepared by mixing a chiral dopant with an achiral nematic liquid crystal. The chirality produces an intermolecular force that leads to a twist between each layer. As a result, the director in the chiral nematic (N*) phase is not only oriented uniformly in individual layers but also rotates in space around a helical axis perpendicular to the layer plane, as shown in Fig. 1-2. An important characteristic of a CLC is the helical pitch. A pitch length typically varies between a few hundred nanometers and many micrometers. It relates to the properties of selective reflection.

In a homogenously aligned cell LC molecules are well oriented with their helix axis parallel to the surface normal, the so-called planar state. At the planar state, a cholesteric liquid crystal with a periodic helical structure reflects incident light in line with Bragg's theory. The optical properties of the selective reflection wavelengths follow these equations:

(1) the center reflected wavelength $\lambda_c = n_{ave} \cdot p$, where $n_{ave} = (n_e + n_o)/2$, and p is the pitch length. n_e and n_o are the extraordinary and ordinary refractive indices of the cholesteric liquid crystal respectively.

(2) the reflection bandwidth $\Delta\lambda = (n_e - n_o)p$

(3) the reflected wavelength shows a blue-shift with the incident light at a certain angle, $\lambda = \lambda_{normal} \cos\theta$, where λ_{normal} is the reflected wavelength at normal incident, θ is the incident angle with respect to the layer normal.

When unpolarized light is applied to right-handed cholesteric liquid crystal film, right-handed circular polarized light is reflected at the wavelengths in the reflection band and also passes other lights.
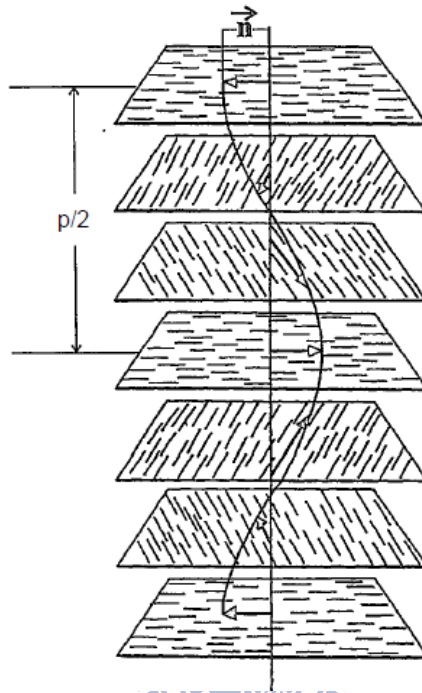
Fig. 1-2. Illustration of a cholesteric liquid crystal structure [3].

1.2.3 Chiral Smectic C

Chiral smectic C (*SmC**) phase is usually formed when chiral dopants are immersed in a *SmC* LC. The chiral dopants induce an intermolecular force leading to a twist between each layer. The *SmC** phase is a continuous rotated layer structure with tilt angle θ, as shown in Fig. 1-3. The distance the director of LC molecules takes to rotate 360°C, is called pitch length.

Ferroelectricity is a characteristic that a material exhibits when the direction of a local polarization field is switched by coupling to an external electric field. R. B. Meyer et al. first demonstrated ferroelectricity in the chiral

smectic liquid crystal in the tilted phase [4]. Ferroelectricity is produced as a result of the unusual combination of symmetrical and asymmetrical properties. Thus, chiral smectic C liquid crystal is a ferroelectric liquid crystal. Because of the asymmetric chemical structure in the *SmC** phase each LC molecule has a polarization field, called spontaneous polarization (P_S) the direction of which is perpendicular to the long axis of the molecule.
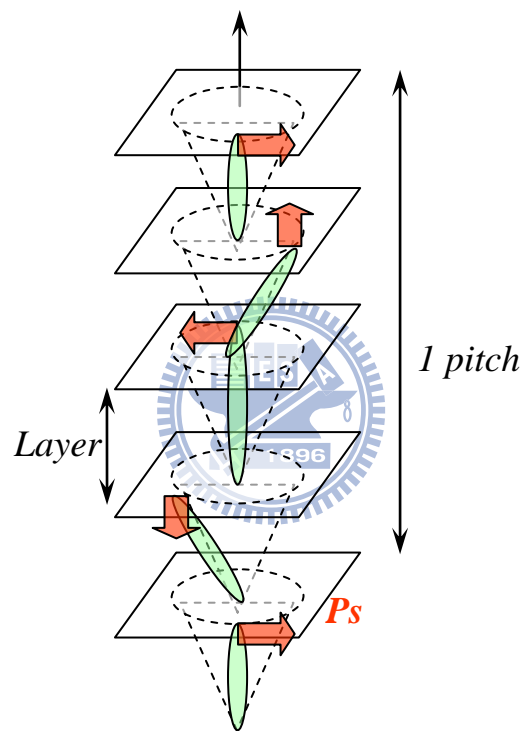
Fig. 1-3. Helix layer structure of a *SmC** liquid crystal.

1.3 Fast Switching LC Modes

Multi-domain vertically aligned (MVA) [5] and in-plane switching (IPS) [6] are currently the mainstream LC modes applied in the LCD industry. The wide viewing angle property of these modes meets the requirement for large size LCD-TV application. However, the slow LC responses (10~20 ms) limit

potential for high-frame-rate display application. Several fast switching LC modes such as optically compensated bend (OCB) [7], blue phase LC [8-9], and half-V shaped switching ferroelectric LC (HV-FLC) [10-11] with response time below 3 ms are proposed.

The OCB cell delivers fast switching response times under 3 ms due to no backflow effects during molecular relaxation in the bend state [12-13]. The OCB cell is normally operated at the bend state. Because the ground state is the splay state, a nucleation transition is completed before operation to circumvent the topological difference between the two states. The processing time to complete the splay-to-bend transition process as shown in Fig. 1.4, which may take a few seconds to minutes, is controlled by the applied voltage.
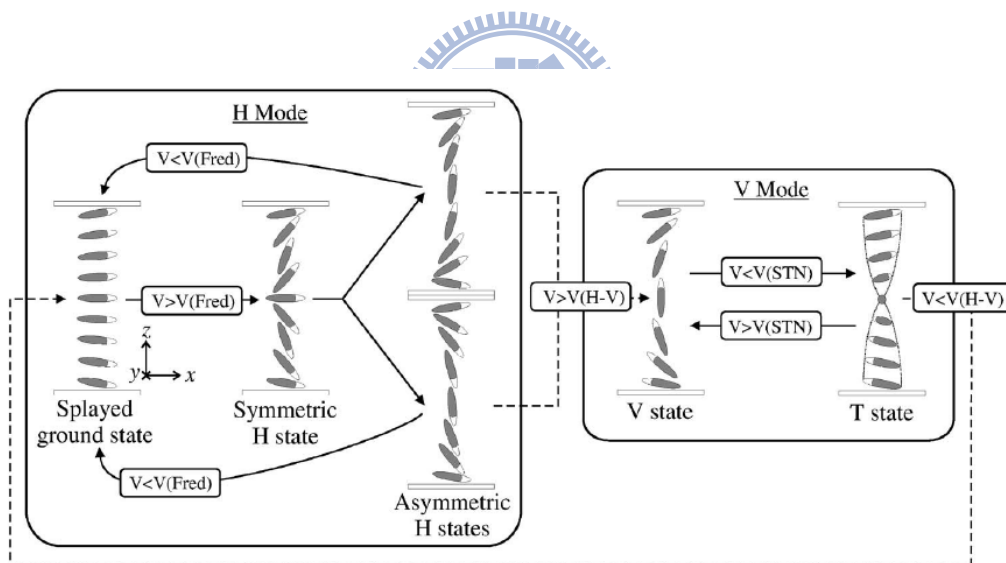
Fig. 1-4. The transition states of an OCB cell [14].

Blue phases with excellent fast switching below 1 ms was recently widely studied. The blue phase appears during the transition from the chiral nematic to the isotropic phase in a very narrow temperature range. The blue phase forms when the structure delicately balances between a local energetic minimum, double twist alignment of the molecules and minimal defects as

shown in Fig. 1-5. The defects known as disclination lines tend to break the stability of the structure. This explains existence only in a narrow temperature range. Blue phases are distinguished into three structure types, BP I (blue phase I), BP II and BP III. BP I and BP II are respectively body-centered and simple cubic structures, while BP III is still an unknown structure.
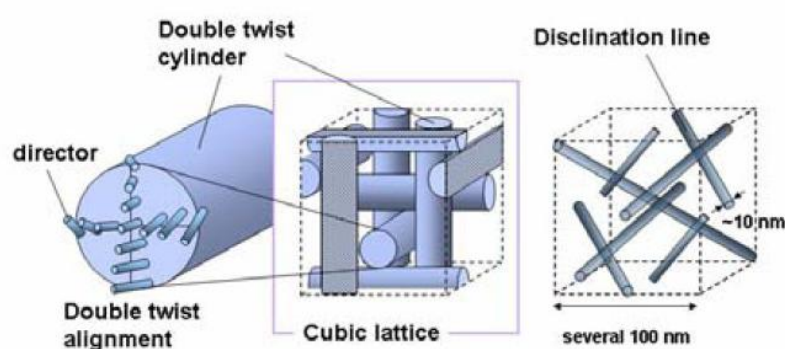
Fig. 1-5. Illustration of the structure of blue phase I [9].

At field off state, blue phases are initially optically isotropic because of the symmetric structure (LC orientation). Alignment surface pre-treatment is therefore not necessary. When an external electric field is applied, molecules tend to reorient following the electric field leading to an optically anisotropic state. Despite potential advantages of fast switching and free surface pre-treatment the intrinsic issues of blue phases limit their application. Blue phases are only available in a narrow temperature range. To increase the operation temperature range polymer-stabilized blue phases were proposed [15-16]. Another restrictive factor is high driving voltage. In comparison to the TN LC device which operates below 5 V blue phases require extremely high driving voltages above 20 V to break the double twist alignment structure.

Another fast switching LC mode with sub-millisecond fast response is the

half-V switching mode ferroelectric liquid crystal (HV-FLC) device. The low driving voltage below 10 V has the potential to fulfill current IC design. HV-FLC is a mono-stable ferroelectric liquid crystal mode with gray-scale capability and low temperature dependence. HV-FLC uses a FLC material with *N*-SmC** in comparison to the surface-stabilized FLC (SSFLC) mode which uses FLC material with *N*-SmA-SmC** phase sequences [17]. The conditions for preparing an HV-FLC device are similar to that of an SSFLC device. These include a thin cell gap under 2 μm with a parallel or antiparallel rubbed alignment pre-treatment and a pitch length of HV-FLV material larger than the cell gap.

HV-FLC with N*-SmC* phase sequence displays intrinsic continuous gray scale characteristics which are more suitable for the driving of active matrix thin-film-transistors (AM TFT). The major unsolved drawback in HV-FLC devices is the horizontal chevron alignment defect. This is due to the presence of both spontaneous polarization (P_S) up and down domains when the HV-FLC device cools down from its *N*-SmC** phase transition as shown in Fig. 1-6. The alignment defects limit HV-FLC's potential for display application. In this study the horizontal chevron defect problem is addressed based on FLC's total free energy. A defect free result can be realized by degenerating the energy levels between spontaneous polarization (P_S) up and down domains. Suppression of the alignment defect is proposed by employing the asymmetric alignment technique with a difference in polar surface coefficient (γ_2). The contrast ratio of the asymmetric aligned HV-FLC device improves.
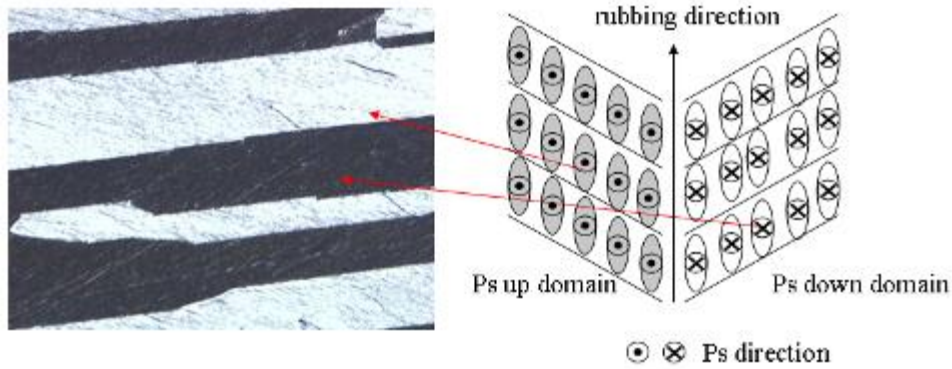
Fig. 1-6. Microscopic texture and illustration of the horizontal chevron defects.

1.4 Motivation and Objective of This Dissertation

Many studies have confirmed that the fast response of ferroelectric liquid crystal is suitable for fast switching devices. For display application the fast switching property allows FLCs to reduce motion blur in large size LCDs enabling the field sequential color LCD technique.

One of the FLC modes, half-V mode FLC, displays intrinsic continuous gray scale characteristics which has the potential for the driving of active matrix thin-film-transistors (AM TFT). The major drawback in HV-FLC devices is the horizontal chevron alignment defect. The alignment defect reduces the contrast ratio of HV-FLC devices and limits potential for display application.

In this theoretical study, resolution of the intrinsic defect problem is based on examining HV-FLC's total free energy. FLC's alignment is improved by diluting the pitch length. In addition, the asymmetric alignment technique is proposed to suppress the alignment defects and present the defect free H-V FLC grating.

1.5 Organization of This Dissertation

The operational principle, the electro-optical properties and LC alignment of a surface stabilized ferroelectric liquid crystal (SSFLC) are presented in Chapter 2. The bistability, chevron layer structures and the zigzag defect are also described. In addition, the half-V switching mode FLC (HV-FLC) with continuous gray scales is introduced. The electro-optical properties and horizontal chevron defect are also discussed. In Chapter 3, the horizontal chevron defect is studied based on HV-FLC's total free energy. Formation of the horizontal chevron defect and how the defect can be suppressed is explained. Furthermore, according to HV-FLC's total free energy, asymmetric alignment techniques are proposed. In Chapter 4, the experimental results of defect free HV-FLC devices are presented and discussed. Alignment of HV-FLC is studied in the uniform surface pre-treated cell with the cell gap below 1.8 μm. First the alignment of the HV-FLC device is improved by increasing FLC's pitch length. Then a horizontal chevron defect free HV-FLC device is prepared without applying external voltage. Besides the pitch length in the HV-FLC cell good alignment quality importantly depends on polar surface interaction. The alignment textures, electro-optical properties of the asymmetric cells controlling polarities and anchoring energies of the alignment layers are presented. In Chapter 5, FLC's alignment is studied in a patterned ITO surface, the ferroelectric liquid crystal grating based on striped electrodes. Thin ITO coated substrate is applied to improve FLC's alignment. The surface-polarity-controlled asymmetric cell is applied to suppress the horizontal chevron defect. The defect-free FLC grating presents high diffraction efficiency. The calculated results and findings of the experimental

diffraction yield are discussed. In Chapter 6, we studied a potential to minimize the alignment defects in the cell gap 3.5 ± 0.3 µm. Good FLC alignment is able to be achieved by small cell gap, certain pitch design, and surface polarity control as discussed in previous chapters. The remaining unsolved issue in display applications is the cell process limitation in manufacture. The cell gap of most TFT-LCDs is controlled larger than 3 µm. Large cell gap posts a great challenge for obtaining a good cell performance in HV-FLC and SSFLC cells due to the effective surface boundary condition. Less alignment defect FLC devices are approached by lengthening FLC's pitch length and controlling the surface polarities. Finally, the summary of the dissertation and future works are presented in Chapter 6.
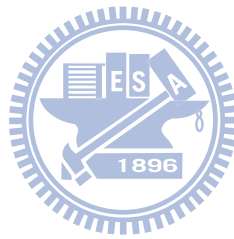
Chapter 2   Surface-Stabilized Ferroelectric Liquid Crystal Devices

2.1   Introduction

Many studies presented the fast switching (below 1 ms) and good memory properties of surface stabilized ferroelectric liquid crystal (SSFLC) devices. The LC reorientation switched by an electric field is similar to the in-plane switching mode (IPS mode) and also enables a natural wide viewing angle. However, the mechanism to achieve an alignment-defect-free SSFLC is complicated. In this chapter, the structure of the SSFLC device and its electro-optical properties is first presented. The alignment of the SSFLC device is then discussed.

2.2   Structure of the Surface-Stabilzed FLC

Many studies of ferroelectric liquid crystals (FLCs) have been presented since N. A. Clark [17] first proposed surface-stabilized ferroelectric liquid crystal (SSFLC) in 1980. An FLC is filled when the planar, aligned, parallel, rubbed cell constrains the position of the LC director to the surface plane. The SSFLC's pitch length must be larger than the cell gap, which, in turn must be less than 2 μm. Under these two conditions, the helical structure of FLC material is unwound by strong surface forces as shown in Fig. 2-1. In the ideal case, the smectic layers are perpendicular to the surface (rubbing direction), the so-called bookshelf geometry [18]. In the bookshelf layer structure, two homogeneously aligned domains with opposite P_S directions, coexist in the cell.

The P_S vectors of the two domains are parallel to the surface normal while the two states align in opposite directions to each other.
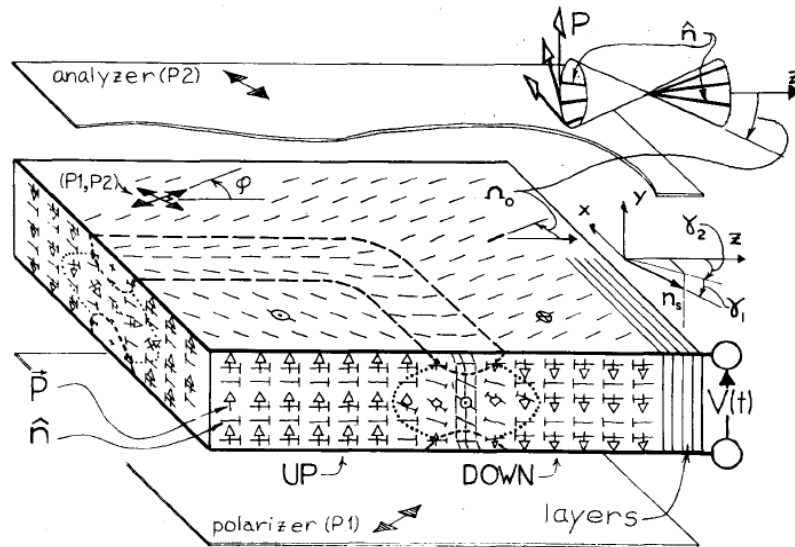
Fig. 2-1. Illustration of the structure of a SSFLC [17].

2.3 Electro-Optical Properties of a SSFLC

The simplest SSFLC device structure, shown in Fig. 2-2, with the long axes of molecules parallel to one of the crossed polarizers is the dark state. When an external electric field is applied across the device, FLC molecules are reoriented with their spontaneous polarization directions following the electric field. The device sandwiched between two crossed polarizers behaves as a wave plate with the incident polarized light retarded by FLC molecules. This is the bright state. The molecular axis of FLC's switching between two states is always parallel to the surface plane as in the in-plane switching (IPS) mode, resulting in a natural, wide, viewing angle. The transmittance of light passed through the analyzer is a function of the cone angle, Δn of FLC, cell thickness and the input wavelength as presented in Eq. 2.1 [19].

$$I = I_0 \sin^2(4\theta) \sin^2(\frac{\Delta n \cdot d \cdot \pi}{\lambda}) \qquad (2.1)$$

where Δn is the birefringe, d is the cell gap, 2θ is the cone angle and λ is the wavelength of light.
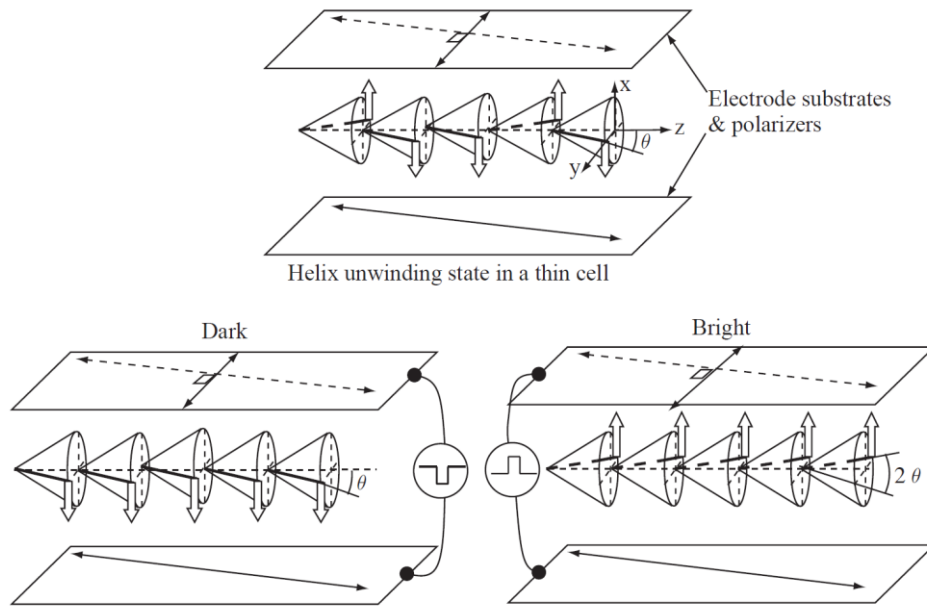
Fig. 2-2. Illustration of the operation principle of a SSFLC [18].

Positive and negative polarization of an external electric field applied across an SSFLC cell, switches the molecules between the two states. FLC molecules are reoriented according to the ferroelectric torque equation:

$$\Gamma_f = P_S \times E \tag{2.2}$$

where, P_S is the spontaneous polarization of an FLC and E is the applied electric field.

The dynamic molecular switching in an SSFLC cell can be expressed as:

$$\eta \frac{d\phi}{dt} = P_S E \sin \varphi \tag{2.3}$$

where η is the coefficient of viscosity, ϕ the, rotational angle of an FLC molecule and φ the angle between P_S and E.

The general solution of eq. 2.3 is:

$$\varphi(t) = 2\tan^{-1}(\tan\frac{\varphi_0}{2}e^{-t/\tau}) \tag{2.4}$$

where φ_0 is the angle at t=0. Thus the response of an SSFLC to which an electric field is applied, is expressed as $\tau = \eta / P_s E$ [17].

Fig. 2-2 illustrates the operational principle of an SSFLC to which an external electric field is applied. The two switched states are equally stable because that the layer normal in a SSFLC cell is parallel to the rubbing direction and bisects the two FLC switching states. Thus the last switched state is maintained after the applied electric field is turned off. The SSFLC presents bi-stable switching which results in the hysteresis loop in the voltage-dependent transmittance curve as shown in Fig. 2-3.
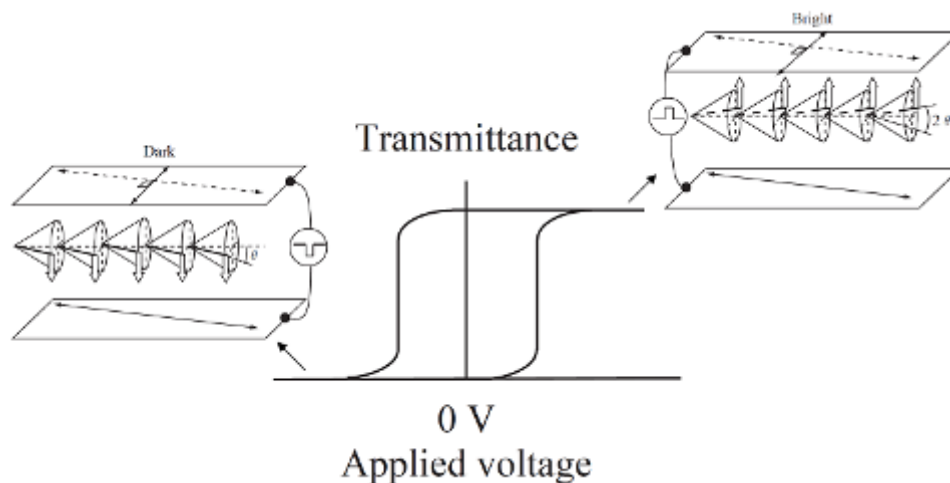
Fig. 2-3. Relationship between applied voltage and transmittance in the SSFLC [18].

2.4　Alignment of SSFLC

2.4.1　Smectic Layer Structures

The alignment of an FLC material is strongly related to the surface pre-treatment of an LC cell. Under varying alignment conditions, FLC devices present different smectic layer structures as shown in Fig. 2-4. In a homeotropic cell, FLC molecules are vertically aligned and the smectic layer normal is formed parallel to the surface normal, as shown in Fig. 2-4(a). In a homogenous cell with antiparallel alignment, a tilted smectic layer structure is presented as shown in Fig. 2-4(b) [20].In a homogenous cell with parallel alignment, in most SSFLCs, a chevron shaped layer structure is formed, as shown in Fig. 2-4(c). This special layer structure is confirmed by X-ray measurement [21]. The formation of the chevron layer structure is explained by the difference in layer spacing between the SmC* and SmA phases. When a homogeneous cell cools down from the SmA to the SmC* phase, FLC molecules tend to tilt at an angle (layer tilted angle) as shown in Fig. 2-5. The layer spacing in the SmA phase is designated as d_A. When the SSFLC cell cools down in the transition from the SmA to the SmC^* phase, the layer spacing shrinks from d_A to d_C. Thus the smectic layers tilt from both top and bottom substrates and form the vertical chevron structure. The relation between d_A and d_C is expressed as $d_C = d_A \cos \delta_C$, where δ_C is the layer tilted angle in the SmC* phase.
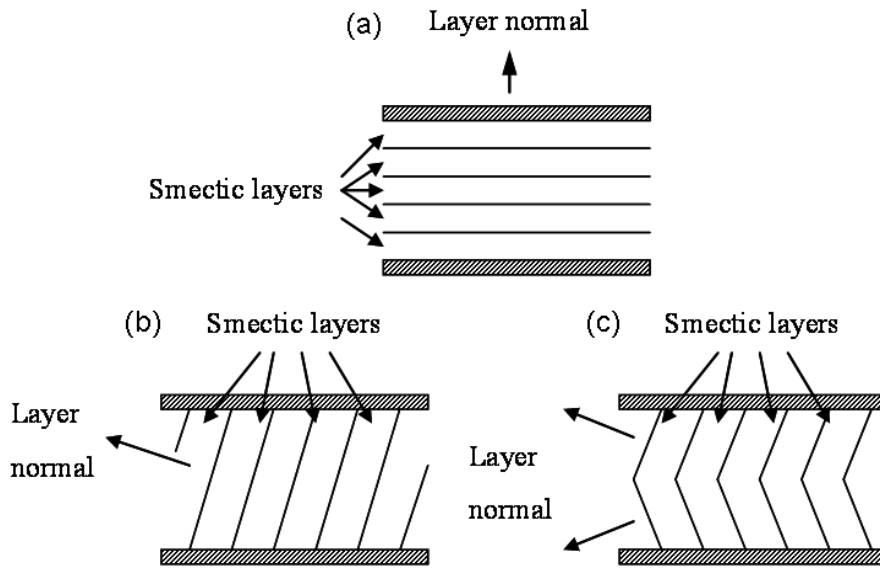
Fig. 2-4. Smectic layer structures in various alignment layers. (a) Homeotropic;
(b) Tilted; (c) Chevron [18].
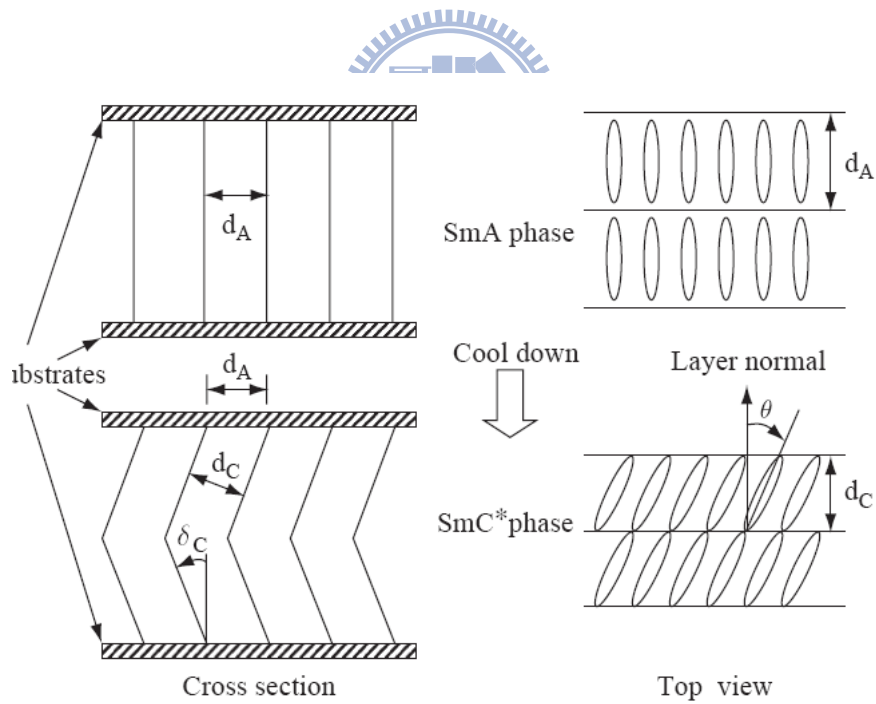
Fig. 2-5. Origin of the chevron layer structure [18].

2.4.2 Chevron Layer Structure

Two classifications shown in Fig. 2-6 define FLC molecular orientation in the chevron structure. The first relates to the tilting direction of the chevron structure and the surface pre-tilt. When the chevron structure tilts towards the rubbing direction, the molecular orientation is named the C2 state. Conversely, when the chevron structure tilts opposite to the rubbing direction it is the C1 state.
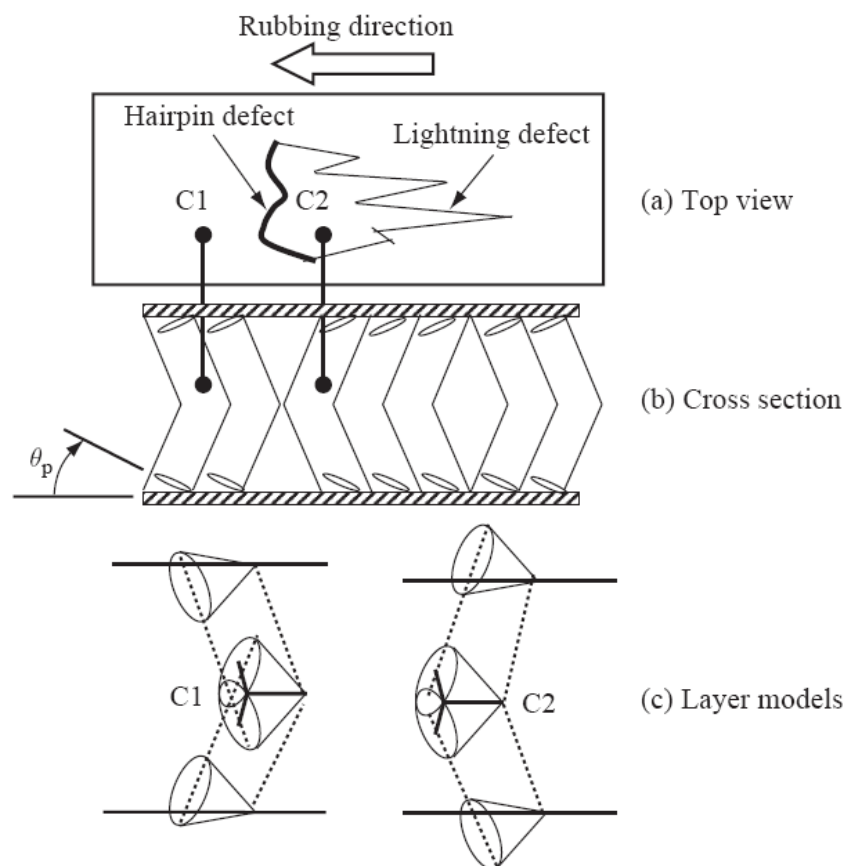
Fig. 2-6. Illustration of C1 and C2 states, distinguished by directions between the chevron layer structure and the surface pre-tilt [22].

The second classification is based on the optical properties of an SSFLC device viewed through a polarizing optical microscope (POM). This classification defines two different alignment states viz. the uniform state (U)

and the twisted state (T) [23-24]. When an SSFLC cell is rotated, the uniform state shows extinction positions, while the twisted state shows only positions of colouration without any extinction.
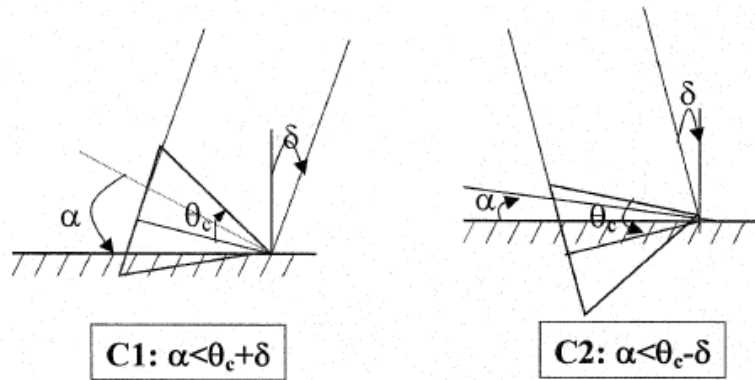
Fig. 2-7. Schematic illustration of the geometrical conditions for C1, C2 states. α, $2\theta_c$, and δ are pretilt angles, cone angles, and layer tilt angles respectively [22].

The conditions required for existence of the C1 and C2 states are shown in Fig.2-7 [22]. In a cell with low pretilt angle surface pre-treatment, both C1 and C2 states exist. In a cell with high pretilt angle surface pre-treatment, only the C1 state exists. In the C2 state the FLC director cannot lie on the switching cone. Based on these criteria, when an SSFLC device cools down in the transition from the *SmA* to *SmC** phase, only the C1 state presents because the cone angle and layer tilt angle near the *SmA* phase are still very small. At lower temperatures as $\theta_c - \delta$ increases gradually, the C2 state starts to present. Finally, the C1 and C2 states coexist and form the zigzag defect as shown in Fig. 2-8.

Zigzag defects form when the chevron structures of C1 and C2 states point to opposite directions as shown in Figs. 2-6(a-b). Zigzag defects limit

display applications for SSFLC devices while the alignment defects reduce the contrast ratio.
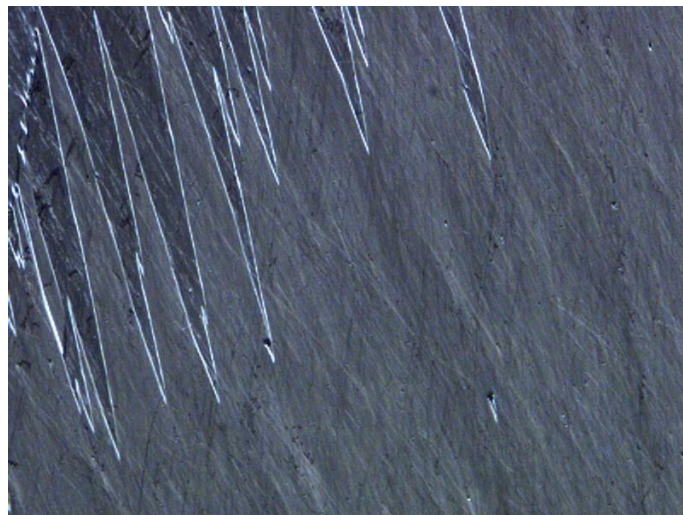
Fig. 2-8.   Zigzag defects of a surface stabilized ferroelectric liquid crystal in the chevron geometry.

2.4.3   Zigzag Defect Free SSFLC Devices

Zigzag Free C1 Structure

As previously mentioned in section 2.4.3, the chevron structure of the C1 state tends to exist in a cell with a high pre-tilt alignment surface. This is a precondition for the existence of a zigzag-free C1. Several groups attempted to achieve zigzag-free C1 structures [22, 25-26].Canon achieved a zigzag-free C1 structure by using polyimide film with a high pre-tilt angle of 18° [27]. However, the polar interaction between FLC's Ps and alignment layers caused a twisted C1 state in the parallel aligned cell with no extinction position [25]. A cross-rubbing alignment (±10° with respect to the rubbing direction) can improve the twisted C1 state and achieve a high contrast bi-stable C1 SSFLC.

A high pre-tilt SiOx alignment in which the pre-tilt angle was close to the chevron angle in the SmC* phase [26] also achieved a zigzag-defect free C1 state. Good bistability and a large memory angle, resulted in high brightness.

Zigzag Free C2 Structure

Zigzag-free C2 structures were developed in the cells by applying very low pre-tilt angle alignment pre-treatments [28-33]. Specifically, a very smooth polyimide RN-1199 (from Nissan Chemical) was applied at a pretilt angle of about 1° [34]. In C2 configuration, the splay-twist elastic deformation energy is lower than that of C1. The FLC director in the C2 configuration lies at the top or bottom of the switching cone, nearly parallel to the rubbing direction. A prerequisite for the FLC molecule to be bound to the alignment surface is a strong anchoring energy.
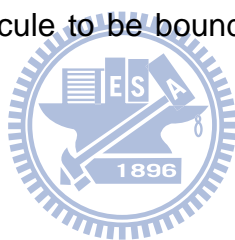
2.5 Issues of SSFLC

The lack of continuous gray-scale limits application of SSFLC. The presence of analogue gray-scale levels is limited by the bistability and hysteresis loop of an SSFLC device. FLC molecules tend to reorient to both bistable states, negating availability of intermediate states. Based on bistable switching, SSFLC displays with gray scales were first developed by applying spatial and temporal dither techniques [35]. An LC display, employing the spatial dither technique, reduces resolution while increasing the number of sub-pixels. In addition, control of the divided sub-pixels requires doubling of, the number of data lines and electrodes which, in turn, slows down signal writing speed. In contrast, the downside of the temporal dither technique is the

increase in power consumption when the LC device is rapidly switched.

Despite the fast switching and bistability properties of SSFLCs, their application as main stream materials is retarded by high driving voltage, lack of gray scale, poor well LC alignment and other factors. Numerous FLC modes were previously proposed to generate gray scale capability [36-41]. In particular, the half-V switching ferroelectric liquid crystal mode [a] (HV-FLC, also known as Continuous Director Rotation-FLC) was developed in the 90's to achieve continuous gray scale, resulting in the feasibility of the FLC active matrix display application [40-41].

2.6   Half-V shaped switching FLC mode (HV-FLC)
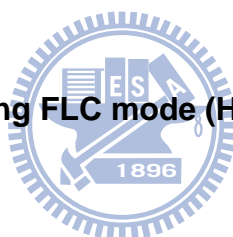
2.6.1   Introduction

Numerous studies exploring surface-stabilized ferroelectric liquid crystal as a fast switching device have been conducted. However, lack of a continuous gray scale limits the potential for display application. These limits are caused by strong temperature dependencies, hysteresis, and bistability. A mono-stable ferroelectric liquid crystal mode is proposed with gray-scale capability and low temperature dependence. The new FLC mode is named half V-shaped switching FLC (HV-FLC). HV-FLC utilizes an FLC material with

---

[a] A V-shaped FLC device has the electro-optical properties of hysteresis free and threshold voltage less. The device is switched by both positive and negative electric fields. The FLC device with N*-SmC* phase transition only switched by a positive electric field (for FLC material with positive spontaneous polarization) is named half V-shaped switching FLC. However, the device has hysteresis and threshold voltage.

N*-SmC* phase sequences, unlike SSLFC which uses FLC material with *N*-SmA-SmC** phase sequences. The conditions for preparing a HV-FLC device are similar to that of an SSFLC device. These include a thin cell gap under 2 μm with a parallel or antiparallel rubbed alignment pre-treatment and a pitch length of HV-FLV material larger than the cell gap. In this chapter, the electro-optical properties and LC alignment of HV-FLC devices are discussed.

2.6.2   Electro-Optical Properties of HV-FLC

Unlike SSFLC, HV-FLC devices are only switched by one of the polarities of the electric field as shown in Fig. 2-9. The E-O properties are characterized by 1 Hz triangular waves. The voltage-transmittance curve displays asymmetric switching behavior which strongly responds to positive polarization of the applied electric field. When a negative polarization of electric field is applied, FLC molecules are oriented following the rubbing direction (also the initial alignment state). Ideally, for an H-V FLC device free of horizontal chevron defects, there must be no light leakage when a negative polarization of electric field is applied.

The E-O properties of an H-V FLC device presents hysteresis loop as shown in Fig. 2-9. In general, a liquid crystal device with hysteresis cannot be applied to analogue gray-scale display. In principle for an AC-driven HV-FLC mode, the hysteresis loop does not need to be considered. In a well aligned HV-FLC device, LC molecules do respond to negative polarization of the applied electric field; however, it induces no retardation. LC molecules remain in their initial alignment state when either a negative or no electric field is applied. Thus, under crossed polarizers, the previous state of each gray-scale

level is determined by the black state. Since an AC driving scheme includes a negative polarization of the applied electric field, the hysteresis loop existing in a HV-FLC device can be ignored.
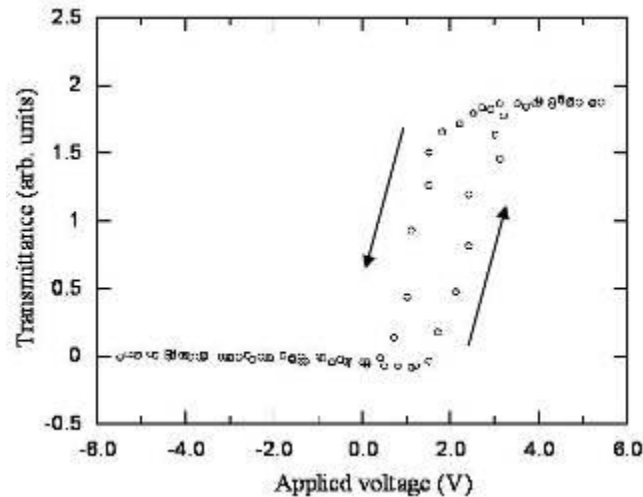
Fig. 2-9. E-O properties when applying a triangular wave with a 3 Hz driving frequency.

The transmittance of a HV-FLC device varies with different applied voltages as shown in Fig. 2-10. The E-O properties are determined by applying a bipolar pulse through increasing driving voltage. The transmittance increases with increasing applied voltage. The voltage dependent transmittances indicate the potential for analogue gray scales using active matrix driving. The voltage-transmittance curve as shown in Fig. 2-11 indicates that the temperature dependences of HV-FLC devices are minimal.
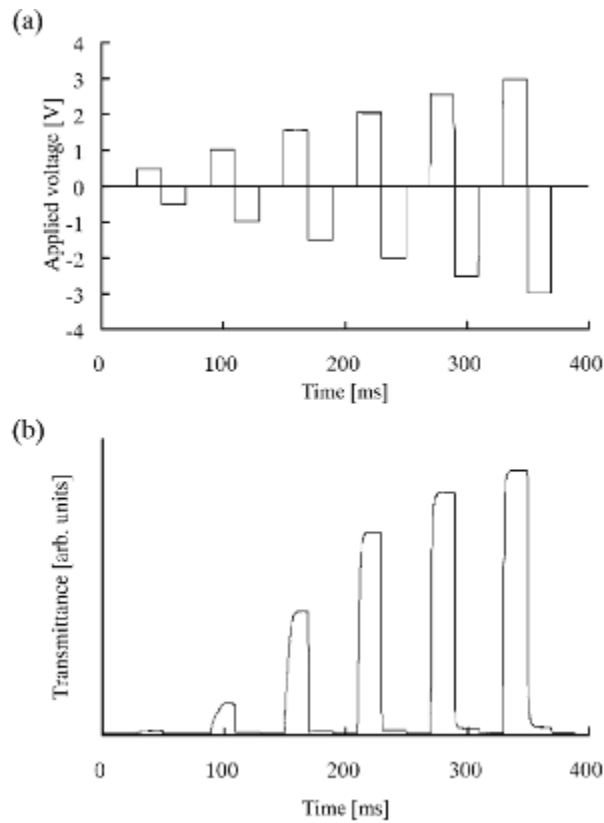
Fig. 2-10. Electro-optical characteristics under the applied bipolar pulse (a) the driving scheme and (b) transmittance [40].
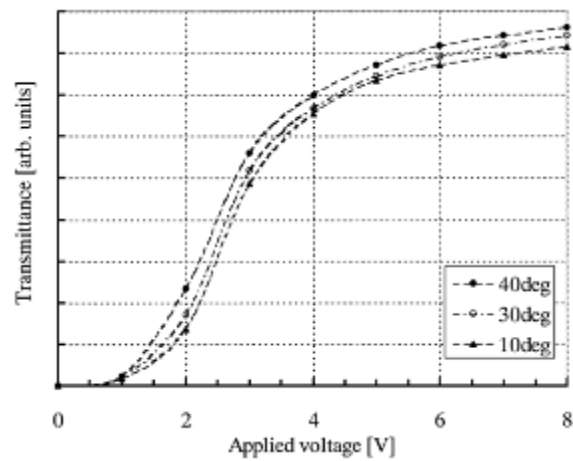
Fig. 2-11. Electro-optical properties of the H-V FLC device characterized at various temperatures [40].
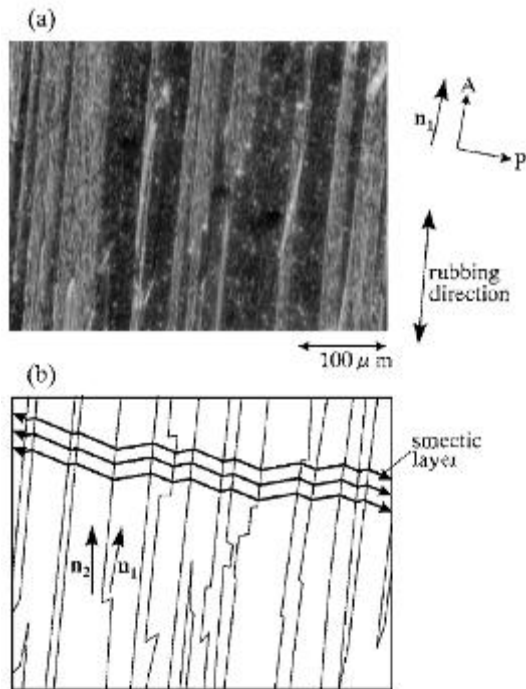
Fig. 2-12. (a) polarizing micrograph and (b) schematic illustration of the H-V FLC device [40].

2.6.3 Alignment defects of H-V FLC

HV-FLC devices present intrinsic continuous gray scales, which are more suitable for driving active matrix thin-film-transistors (AM TFT). The major, unsolved drawback is the horizontal chevron alignment defect. This is due to the presence of both spontaneous polarization (P_S) up and down domains when the HV-FLC device cools down from its N^*-SmC^* phase transition as shown in Figs. 2-12 and 2-13. Resolution of the alignment defect remains a challenge to overcome before the potential for display application of HV-FLC can be realized.

In an HV-FLC cell, LC molecules in the N^* phase are oriented with their optical axis parallel to the rubbing direction. When the HV-FLC cools down from N^* to SmC^* phase transition, LC molecules deviate a finite angle with

respect to the rubbing direction because of the surface electronic effect [42]. As shown in Figs. 2-13(c-e), the HV-FLC shows extinction angle of 2 degree with respect to the rubbing direction.
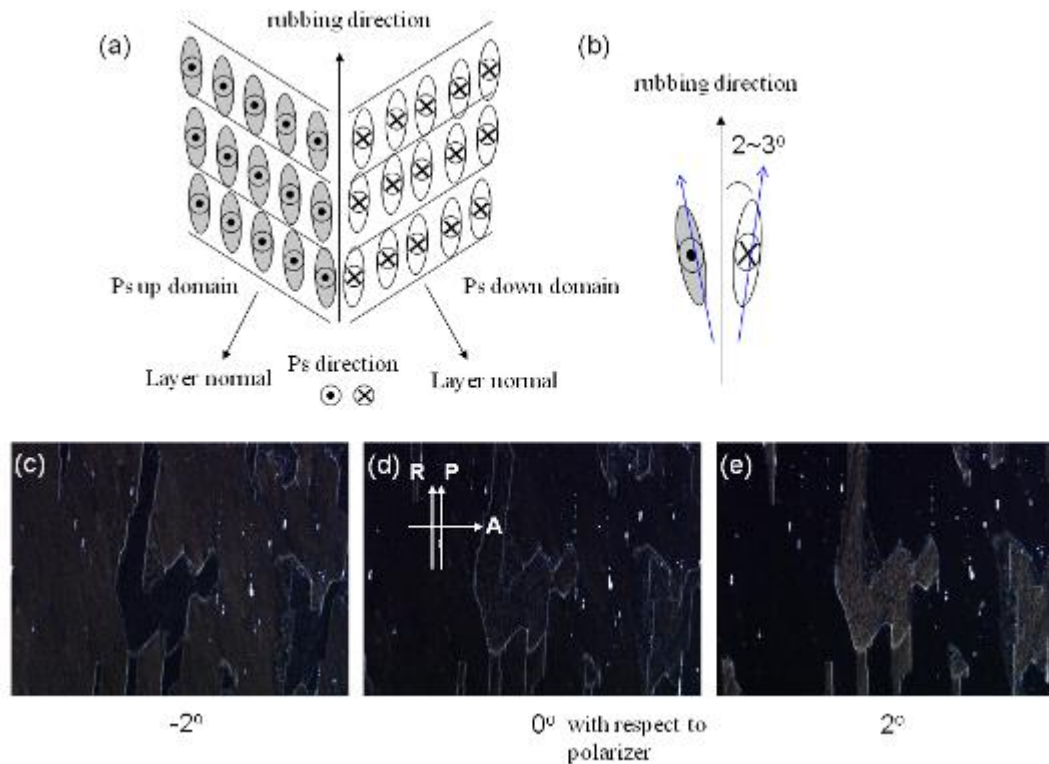
Fig. 2-13. (a-b) illustrations of the HV-FLC with horizontal chevron defect and (c-e) the microscopic textures of P_S up and down domains with an extinction angle of 2 degree with respect to the rubbing direction.

2.6.3.1 Methods to suppress the horizontal chevron defect

The horizontal chevron defect forms during the phase transition from N^* to SmC^*. The formation and tilting of smectic layers irregularly occurs. The smectic layers tilt at an angle θ with respect to the rubbing direction. The smectic layers, which tilt clockwise or counter-clockwise, form P_S up and P_S down domains as shown in Fig. 2-13. The following discussion highlights

several methods proposed to solve the problem.

(a) Electric field annealing process

Horizontal chevron defects are found in the alignment texture of the HV-FLC device as shown in Figs. 2-14(a) and 2-15(a). When a DC electric field is applied, FLC molecules tend to reorient with their P_S direction following the electric field as illustrated in Fig. 2-14 (b). The defects are suppressed by applying a DC electric field during the annealing process of HV-FLC's N^*-SmC^* phase transition [10]. The microscopic textures of a HV-FLC device with and without the DC annealing process are presented in Fig. 2-15.
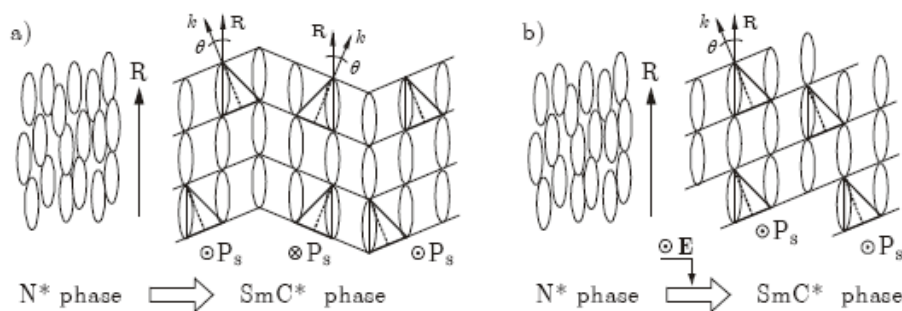
Fig. 2-14. Illustration of the smectic layers after the phase transition from the N^* to SmC^* phase in a HV-FLC device. (a) horizontal chevron defects with P_S up and P_S down domains and (b) A mono-domain structure obtained by applying a DC field during the phase transition from N^* to SmC^*.
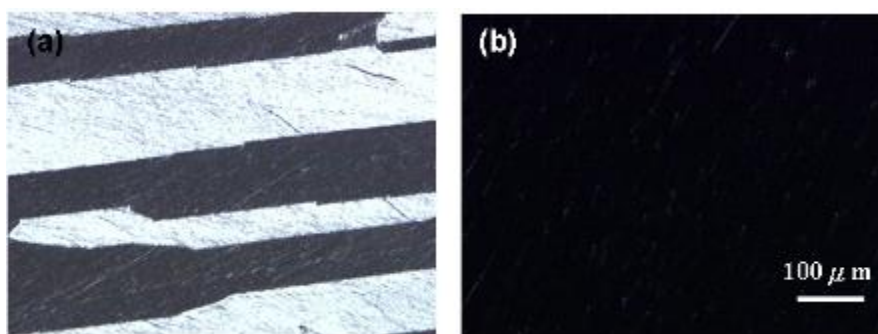
Fig. 2-15. Polarizing microscopic texture of a HV-FLC device (a) without the DC annealing process and (b) with an applied DC field during the phase

transition from *N* to SmC**.

In addition to DC electric field application, AC field annealing processes were also proposed to suppress horizontal chevron defects. AC electric fields use triangular, [43], square wave [44], and asymmetric rectangular waveform [45] were proposed. From a display manufacturing perspective, the electric field annealing process is complex. Alignment pre-treatment methods offer more promise.

(b) Hybrid alignment combining rubbing and photo-alignment

The alignment textures of HV-FLC devices in which the DC annealing process applications and different surface pre-treatments were discussed by S. Kobayashi, et. al. [46] as shown in Fig. 2-16. The horizontal chevron defects present in the rubbed cell as shown in Fig. 2-16(a-1). The defects suppressed after the DC annealing process are shown in Fig. 2-16(a-2). After the device is heated up to the isotropic temperature, the HV-FLC material cools down to room temperature and alignment defects present again as shown in Fig. 2-16(a-3). The DC annealing process does not reverse the defect-free alignment texture. Poly-domains present in HV-FLC's alignment texture under the surface pre-treatment of photo alignment are shown in Fig. 2-16(b-1). Photo alignment induces weaker anchoring energy of about 10^{-5}-10^{-4} J/cm^2 in comparison to that of rubbing (approximately 10^{-3} J/cm^2). The surface boundary condition is not strong enough to control FLC's alignment. Thus, alignment defects still present after the DC annealing process as shown in Fig. 2-16(b-2). The hybrid alignment cell, which combines rubbing and photo

alignment initially, presents a mono-domain alignment texture without application of the DC annealing process as shown in Fig. 2-16(c-1). The defect-free alignment texture presents again after thermal annealing as shown in Fig. 2-16(c-3). The experimental results show that the asymmetric alignment surfaces with different anchoring energies suppress horizontal defects. However, the results do not precisely prove that anchoring energy dominates HV-FLC's alignment since this hybrid alignment cell utilizes different alignment materials. The properties of alignment material may also affect HV-FLC's alignment.
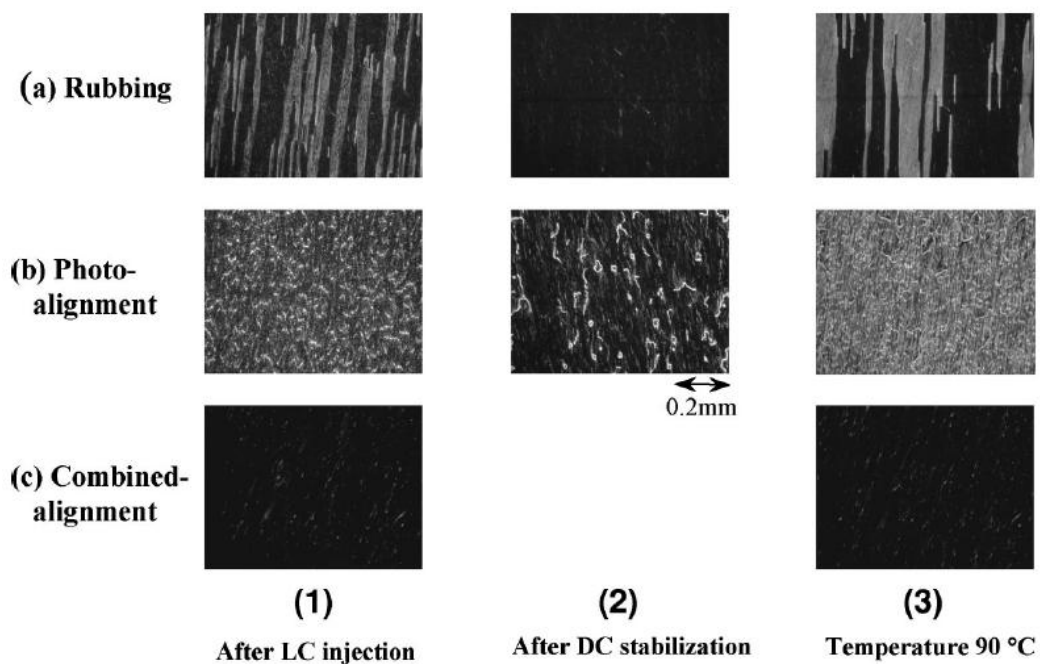
Fig. 2-16. Microscopic textures of the HV-FLC cells aligned by (a) rubbing, (b) photo alignment, and (c) hybrid alignment. The textures are captured under the following conditions: (1) after the LC injection, (2) after the DC annealing process, and (3) after the temperature cycling test (heating up and cooling down between room temperature and 90°C) [46].

(c) Hybrid Alignment Using Linearly-Photo-Polymerized Materials and Liquid Crystal Polymers

Alignment of FLC is very sensitive to the surface roughness of the alignment layer. A rubbed alignment layer, contaminated with dust particles may induce alignment defects. M. Okabe proposed the horizontal chevron defect free HV-FLC device using the photo alignment method [47]. Linearly-photo-polymerized (LPP) and liquid crystal polymer (LCP) materials were applied as asymmetric alignment surface pre-treatments as illustrated in Fig. 2-17. In a series of LPP and LCP materials, the alignment surfaces treated by LPP/LCP: ROP-103/ROF-5101 and LPP: ROP-102 respectively, present less horizontal chevron defects as shown in Table. 2-1. The experimental results show that among the LPP and LCP materials, the combination of LPP/LCP: ROP-103/ROF-5101 and LPP: ROP-102 give best alignment with less defects. In this literature, the mechanism of improving HV-FLC's alignment was not discussed.
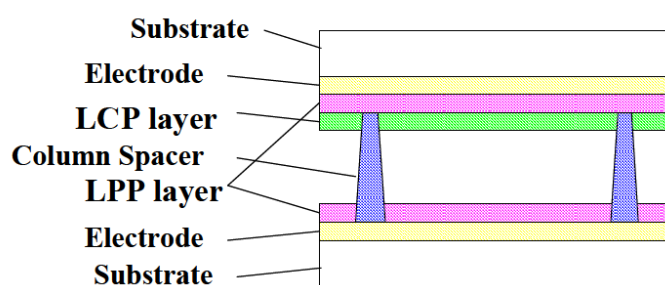
Fig. 2-17. Structure of the asymmetric cell using LCP and LPP [47].

Table 2-1. Ratio of positive P_S domains
under different alignment conditions [47].

Sample No.	Substarete 1 (Front side)	Substarete 2 (Backlight side)	Ratio of Positive Ps
	LPPs/LCPs	LPPs	(%)
1	ROP-103 ----	ROP-102	79.3
2	ROP-102/ROF-5101	ROP-103	80.9
3	ROP-102/ROF-5102	ROP-103	88.1
4	ROP-103/ROF-5102	ROP-102	92.8
5	ROP-103/ROF-5101	ROP-102	99.7

Based on S. Kobayashi's and M. Okabe's studies, asymmetric alignment conditions may hold the key to suppression of the horizontal chevron defect. However, the mechanism to minimize the alignment defect is not clear.

In the next chapter, the formation of the horizontal chevron defect is first discussed in terms of FLC's total free energy. We not only prove how the DC annealing process suppresses the alignment defect, but also propose two kinds of asymmetric alignment cells with defect-free alignment textures.

Chapter 3   The Proposed Asymmetric Alignment Techniques

3.1   Theoretic study of the horizontal chevron defects

The alignment mechanism of HV-FLC devices can be studied by examining LC free energy. The coordinate system of a HV-FLC cell is illustrated in Fig. 3-1.
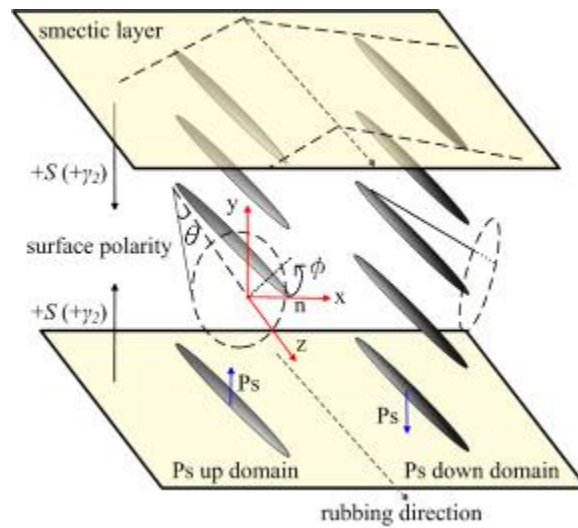
Fig. 3-1 The coordinate system of a HV-FLC cell.

The molecular director can be expressed as:

$$\hat{n} = (\sin\theta\cos\phi, \sin\theta\sin\phi, \cos\theta) \tag{3.1}$$

where θ and ϕ represent the tilt angle and azimuthal angle, respectively. When the molecular director of uniformly aligned FLC is parallel to the z-axis, the one-dimensional total free energy per unit area of the FLC cell can be

expressed as [48]:

$$F = \int_{-d/2}^{d/2} W_d \, dy + F_s \qquad (3.2)$$

where W_d is the elastic free energy density, F_s is the surface energy per unit area, d is the cell gap. W_d of a SmC^* material can be written in Oseen-Frank form as:

$$W_d = (K_1/2)(div\,\hat{n})^2 + (K_2/2)(\hat{n} \cdot rot\,\hat{n} - q_t)^2 \\ + (K_3/2)(\hat{n} \times rot\,\hat{n} - \hat{q}_b)^2 \qquad (3.3)$$

where K_1, K_2, K_3 are the elastic constants, q_t, the wave vectors of spontaneous twist and $\hat{q}_b$, the spontaneous bend given by

$$q_t = -q \sin^2 \theta \qquad (3.4)$$

$$\hat{q}_b = q \cos \theta (\hat{n} \times \hat{z}) \qquad (3.5)$$
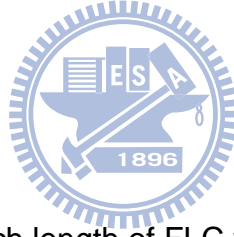
where $|q| = 2\pi/p$, p is the pitch length of FLC with the sign of q specifying the handedness of the FLC helicoids. If the variation of ϕ is restricted in the y axis with constant cone angle in a simple HV-FLC cell, the elastic free energy density can be expressed as:

$$W_d = \frac{1}{2}\phi_y^2 \sin^2 \theta \, [\, K_1 \cos^2 \phi + (K_2 \cos^2 \theta + K_3 \sin^2 \theta) \sin^2 \phi \,] \\ + \phi_y q (K_2 - K_3) \sin^3 \theta \cos \theta \sin \phi \\ + \frac{1}{2} q^2 \sin^2 \theta (K_2 \sin^2 \theta + K_3 \cos^2 \theta) \qquad (3.6)$$

where ϕ_y is the partial derivative of ϕ with respect to the y axis. It is assumed that the well alignments of FLC molecules are without variation at the y axis, i.e. $\phi_y = 0$ or $\phi = $constant. The elastic free energy density of this uniform

state can be simplified as:

$$W_d = \frac{2\pi^2}{p^2} \sin^2\theta \, (K_2 \sin^2\theta + K_3 \cos^2\theta) \qquad (3.7)$$

where K_2 and K_3 are the elastic constants and p is the pitch length of FLC.

The surface energy per unit area is the energy summation of the top *(t)* and bottom *(b)* substrates, which can be expressed as:

$$\begin{aligned}
F_s &= \sum_i [\gamma_1^{(i)} (\hat{n} \cdot \hat{s})^2 + \gamma_2^{(i)} (\hat{p} \cdot \hat{s})] \\
&= \sin^2\theta \, (\gamma_1^{(t)} \sin^2\phi_t + \gamma_1^{(b)} \sin^2\phi_b) \mp (\gamma_2^{(t)} \cos\phi_t - \gamma_2^{(b)} \cos\phi_b)
\end{aligned} \qquad (3.8)$$

where γ_1 and γ_2 are the non-polar and the polar surface interaction coefficients, respectively. $\hat{p}$ and $\hat{s}$ are the unit vectors of polarization to the surface normal. The negative and positive values correspond to P_S up and P_S down domains in the horizontal chevron defects. When FLC molecules are well oriented by the rubbing direction in the HV-FLC cell ($\phi_t = \phi_b = \phi$), the surface free energies can be rewritten as:

$$F_s = \sin^2\theta \, (\gamma_1^{(t)} \sin^2\phi + \gamma_1^{(b)} \sin^2\phi) \mp (\gamma_2^{(t)} - \gamma_2^{(b)}) \cos\phi \qquad (3.9)$$

Thus, the total free energy per unit area of P_S up and P_S down domains can be expressed as:

$$\begin{aligned}
F &= \frac{2\pi^2 d}{p^2} \sin^2\theta \, (K_2 \sin^2\theta + K_3 \cos^2\theta) \\
&+ \sin^2\theta \, (\gamma_1^{(t)} \sin^2\phi + \gamma_1^{(b)} \sin^2\phi) \mp (\gamma_2^{(t)} - \gamma_2^{(b)}) \cos\phi
\end{aligned} \qquad (3.10)$$

Regardless of P_S up or P_S down domains, the LC molecules have the same minimum total free energy. The top and the bottom alignment surfaces

have the same polar surface interaction coefficients, i.e. $\gamma_2^{(t)} = \gamma_2^{(b)}$. As a result, a defect free alignment texture can be produced if the direction of the FLC's spontaneous polarization is oriented in one direction. One significant approach to suppress alignment defects is application of an external DC electric field during the annealing process during FLC's *N*-SmC** phase transition. The electrostatic energy, W_E, can be expressed as:

$$\int_{-d/2}^{d/2} W_E \, dy = -\int_{-d/2}^{d/2} P \bullet E \, dy = -P_S \cdot E d \cos\phi \tag{3.11}$$

where $P_S = |P|$. The energy levels between P_S up and P_S down domains degenerate into:

$$F = \frac{2\pi^2 d}{p^2} \sin^2\theta (K_2 \sin^2\theta + K_3 \cos^2\theta) \\ + \sin^2\theta (\gamma_1^{(t)} \sin^2\phi + \gamma_1^{(b)} \sin^2\phi) \mp P_S \cdot E d \cos\phi \tag{3.12}$$

The minus (-) and plus (+) signs before the electrostatic energy term indicate the energy of P_S up and P_S down domains, respectively. Unfortunately the DC electric field annealing process, generates residual charge in the FLC device [49].

To solve the alignment issue by surface pre-treatment, according to Eq. (3.10), a large value of $(\gamma_2^{(t)} - \gamma_2^{(b)})$ for asymmetric alignment surfaces (i.e. $\gamma_2^{(t)} \neq \gamma_2^{(b)}$) is necessary to degenerate FLC's free energy into two energy levels, when the polar surface energy [50-51] term is not zero. Thus, the uniform molecular alignment yielded from the uniform P_S direction can be obtained at the lowest free energy level in the asymmetrical alignment surface.

There are two approaches to asymmetric alignment conditions. Firstly, degeneration of the value between $\gamma_2^{(t)}$ and $\gamma_2^{(b)}$ can be realized by controlling the alignment strength. Secondly, the sign of $\gamma_2^{(b)}$ can be changed by using the alignment layer with the opposite surface polarity. In this study, theoretical predictions were validated by applying asymmetric alignment techniques to control anchoring energy [52] and surface polarity [53].

The theoretical studies are firstly approached by applying rubbing and plasma alignment techniques on top and bottom substrates, respectively. The alignment strength which differentiates values were controlled. Secondly, by using alignment layers with opposite sign of surface polarities, the sign of $\gamma_2^{(b)}$ was changed. The asymmetrical alignment techniques were applied to control the anchoring energy and surface polarity and to validate theoretical predictions.

3.2   Surface Pre-treatments

3.2.1   Plasma Alignment Technique

Plasma irradiation is generated by an anode layer thruster (ALT), which consists of an inner and outer cathode and an anode, as shown in Fig. 3-2. A permanent magnet generates a magnet pole at the outer cathode. The plasma flux is generated by a cross electric field and a magnetic field. Fig. 3-3 is a diagrammatic and photographic depiction of the ALT plasma system. In the system, several operating parameters, such as incident angle, energy, and

manufacturing gas volume, can be adjusted. The volume of gas applied in the plasma alignment controls the properties of the alignment layer.

The plasma alignment technique was developed for large scale non-contact alignment. The flux of the plasma beam obliquely treats the alignment surface creating anisotropic properties.
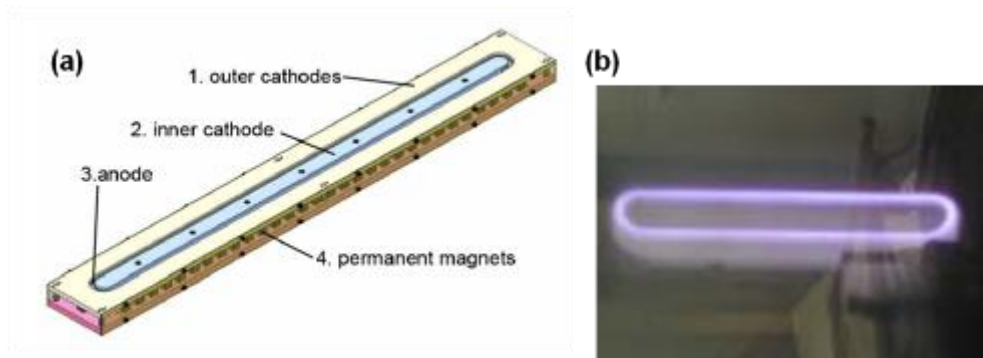
Fig. 3-2. Schematic diagram and photo of anode layer thruster (ALT).
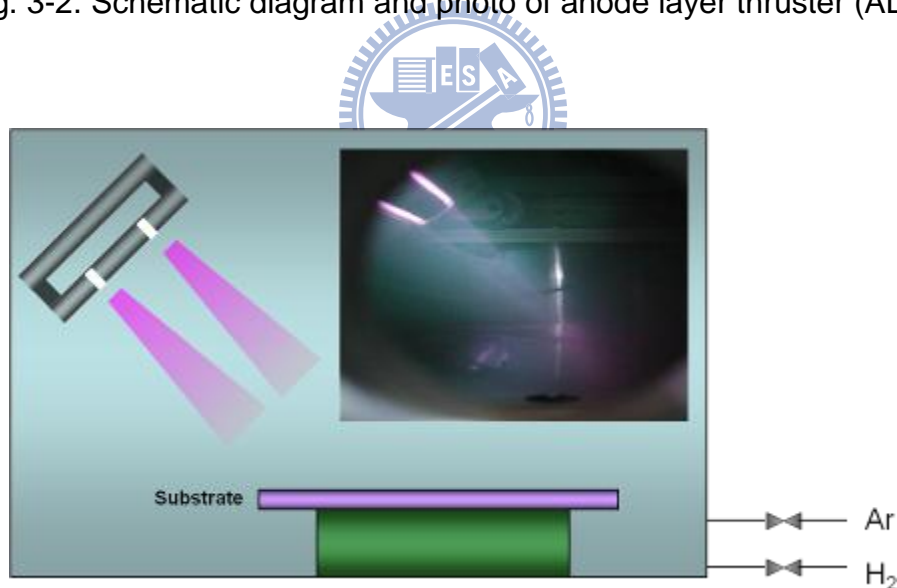
Fig. 3-3. Schematic diagram and photo of ALT plasma system.

3.2.2 Surface Polarity

Surface polarity (S) interacts with the spontaneous polarization affecting FLC's alignment [50]. In the proposed asymmetric cells the polar surface interaction coefficient γ_2 holds the key to control FLC's alignment. The

intensity of the polar surface property is determined by characterizing the polar part of the surface tension of alignment layers. The surface tension (dynes/cm) is characterized by using the physicochemical technique [50], measuring the contact angles of two liquids on the same alignment surface.

In the second proposed asymmetric cell, alignment layers with opposite surface polarity are applied to change the sign of $\gamma_2^{(b)}$. The sign of surface polarity is determined by the cross rubbed cell [54]. In the twisted FLC mode (cross rubbing), the direction of the smectic layer is determined by the sign of the spontaneous polarization and the direction of the polarity of the alignment layer surfaces. With the same FLC material, the opposite layer direction of the alignment textures indicates opposite signs of surface polarity from poly vinyl alcohol (PVA) and polyimide (PI) as shown in Fig. 3-4. In this study the sign of surface polarity is taken positive for an outward polar surface. Positive surface polarity materials applied in this study were PVA, hexamethyldisilizane (HMDS), and Nylon 6; PI is a negative surface polarity material. The intensities and signs of alignment layers are listed in Table 3-1.

Table 3-1. Surface tension of the tested layers (dynes/cm) [50]

Alignment layers	γ_1	γ_2	Surface sign
HMDS	26	17	+
PVA	28.5	19.5	+
PA6	32	16.6	+
PI	36.5	9	-
SiO$_2$	31	44	-
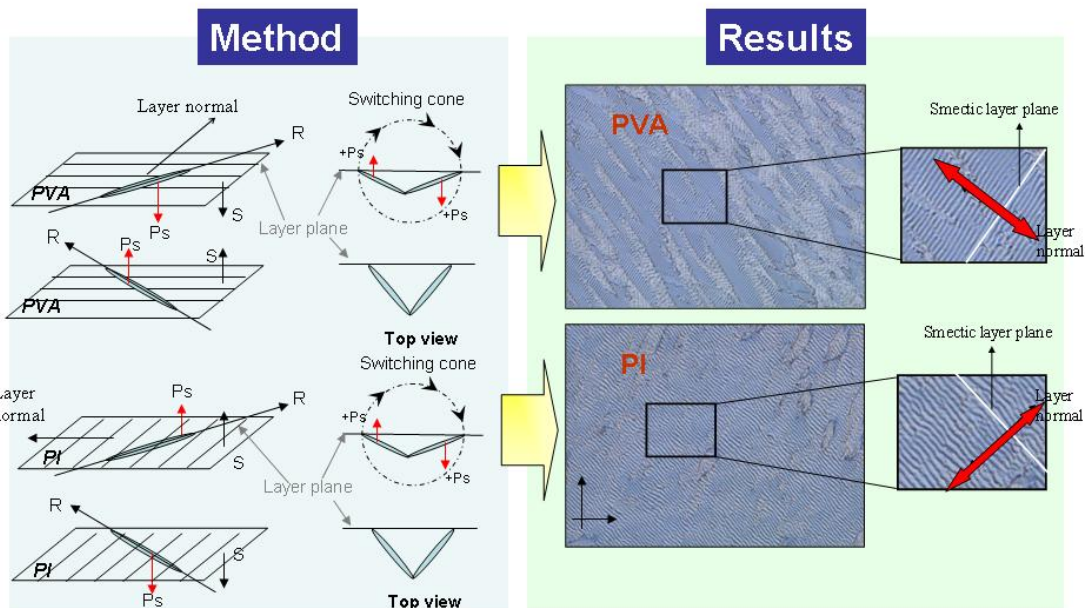
Fig. 3-4. The diagram of the twisted FLC mode and the microscopic textures.
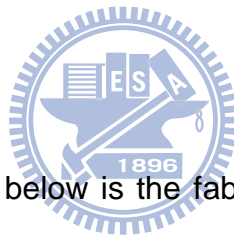
3.3 Cell Preparation

The flow chart as shown below is the fabrication process of a H-V FLC device:
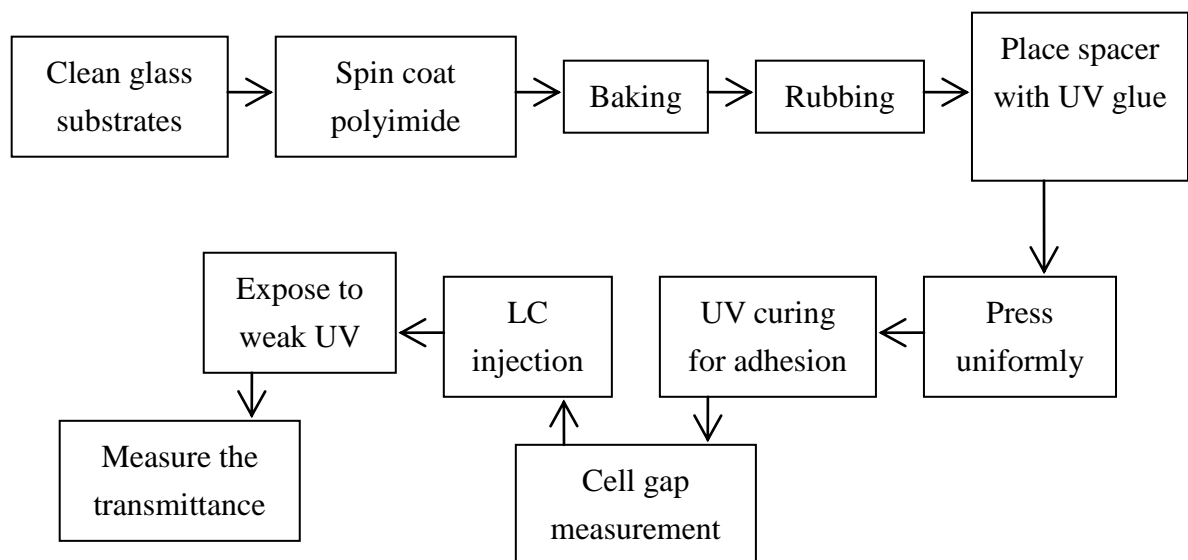
A. Each piece of glass is rinsed with detergent and carefully cleaned by

hand. Then, wash the glass with DI water until the water flows along the surface smoothly. After that, put the glass into DI water and clean by ultra sonication for 30 minutes.

B. Blow the surface of glass by compressed air to remove water, and then bake on the hot plate for 60 min. at 110 ^{o}C. Next, using UV-ozone to treat the glass surface for 20 min. before coating polyimide.

C. Polyimide (PIA-X201-G01, Chisso) and PVA (Mw 13,000-23,000, 98% hydroldyzed, Sigma-Aldrich) are spin coated under the conditions of:

D.

2.5 wt.% PVA (dilute in water)			50% Polyimide (dilute in solvent)		
	Speed	Time		Speed	Time
1st spin	500rpm	10s	1st spin	500rpm	10s
2nd spin	1500rpm	60s	2nd spin	5000rpm	60s

After spin-coating, the polyimide film is pre-baked at 100 ^{o}C for 10s, and then baked at 200°C for 1 hr; the PVA film is baked at 100 ^{o}C for 1 hr. The film thickness of 2.5 wt.% PVA is 1000Å, and the thickness of 50 wt.% polyimide is about 350Å.

E. After the substrate cools down, polyimide coated glass substrate is rubbed by rubbing machine at the rotating speed of 500 rpm and advancing speed of 10 mm/s.

F. Drop a small amount of UV glue (NOA-65, from Norland) mixed with 1.6 μm spacer at four corners of the bottom substrate. Cover with the top substrate following the parallel rubbing direction. Next, place the cell under UV irradiation to cure the glue, so that an empty cell is prepared.

G. Measure the cell gap of an empty cell by a spectrometer using the interferometric method [54]; the cell gap should be controlled from 1.5 to 1.8 μm.

H. The H-V FLC mixture is filled into a cell by capillary force at 100°C (over the isotropic temperature of LC material). Then, the H-V FLC device is slowly cooled down at the cooling rate of 1 ^{o}C/min.

3.4 Surface Morphology

The surface morphology and film thickness were characterized by using atomic force microscope (AFM) as shown in Fig. 3-5. The film thickness of 50 wt.% PI and 2.5 wt.% PVA are 25 nm and 95 nm, respectively. The surface roughness (root-mean-square) of the rubbed PI and PVA films are 0.62 nm and 0.48 nm, respectively. The plasma alignment treated PI film shows more uniform surface morphology with the roughness of 0.274 nm.
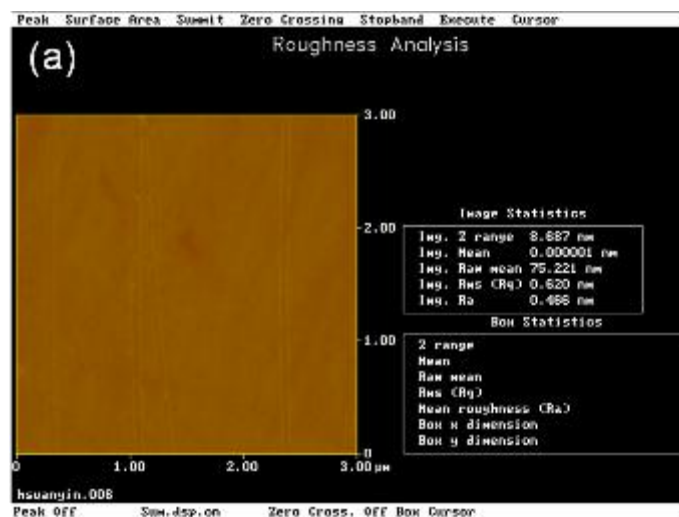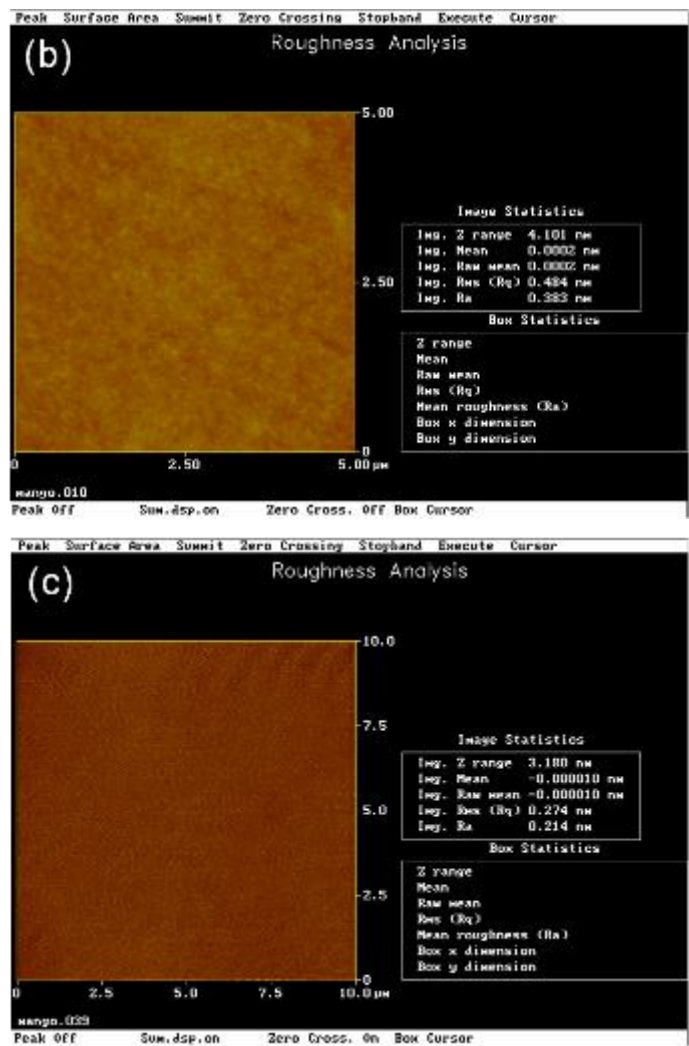
Fig. 3-5. Surface morphology of the (a) 50% PI diluted in solvent after rubbing, (b) 2.5% PVA diluted in water after rubbing, and (c) 50% PI diluted with solvent after plasma alignment treatment.

Chapter 4   Defect Free HV-FLC Devices

4.1 Introduction

In this chapter, the experimental results of defect free HV-FLC devices are presented and discussed. First the alignment of the HV-FLC device is improved by increasing FLC's pitch length. Then a horizontal chevron defect free HV-FLC device is prepared without applying external voltage. Besides the pitch length in the HV-FLC cell good alignment quality importantly depends on polar surface interaction. The alignment textures, electro-optical properties of the asymmetric cells controlling polarities and anchoring energies of the alignment layers are presented.
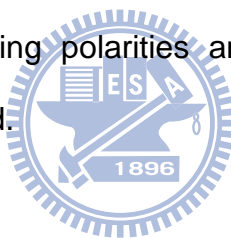
4.2   H-V FLC Material Preparation

The HV-FLC material R3206 (*Iso* 109.9 *N** 79.5 *SmC** -17.9 *C*, P_S=20.1 nC/cm^2, $V_{sat.}$ at 3.5V, pitch=0.8±0.2 μm, from AZ Electronic Materials) was employed as the model compound. Pure R3206 presents poly-domains in a polyimide (PI) treated cell (1.8±0.1 μm) as shown in Fig. 4-1(a). FLC molecules align as helical, splayed and uniform states dependent on pitch length and cell gap as shown in Fig. 4-1(b) [56]. With the cell gap at 1.6 μm and the pitch length at 0.8 μm, pure R3206 aligns at the helical state, presenting poly-domains. Lengthening the pitch length changes R3206's alignment to the uniform state.
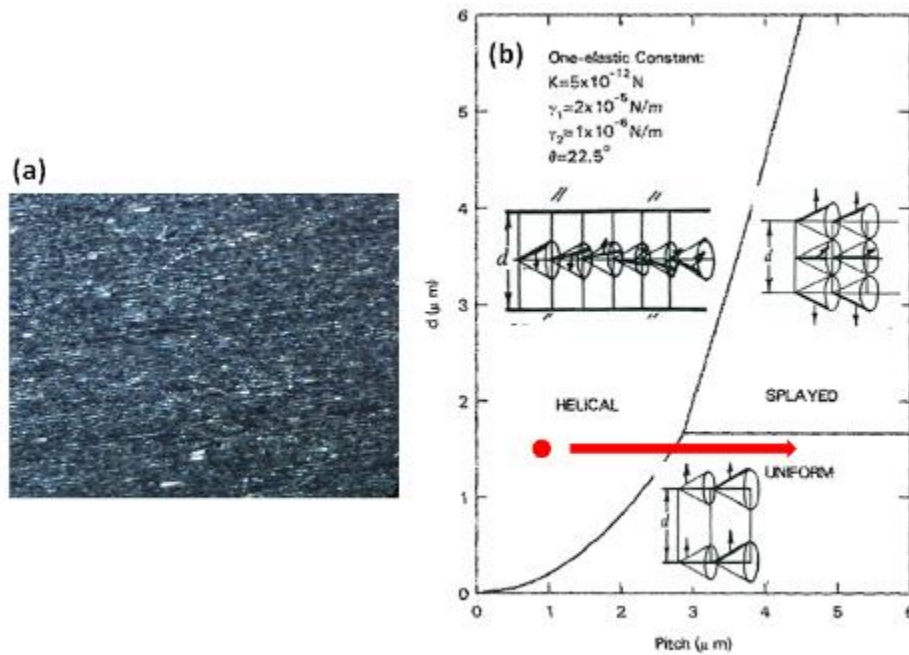
Fig. 4-1. (a) Microscopic texture of R3026 and (b) Phase diagram as a function of th cell thickness and pitch.

The *SmC* host R3206H (*Iso* 110.7 *N* 73.8 *SmC* -29.7 *C*), a racemic mixture of R3206, is prepared to adjust the pitch length of R3206. A series of weight differentiated R3206H was mixed into R3206. The alignment textures of R3206 with various mixtures prepared from polyimide (PI) cells (1.8±0.1 μm) were captured by a polarizing optical microscope (POM). The diluted R3206 mixtures appear to align better than the pure R3206 as shown in Fig. 4-2. Horizontal chevron domain defects are larger when the weight percentage of R3206 is lower than 70%, as shown in Figs. 4-2(c-d).

Thermal properties of ferroelectric liquid crystal (R3206), smectic C host (R3206H) and their mixtures were measured by using DSC at cooling rate of 10 ^{o}C /min. The mesophase temperature of R3206, R3206H and their mixtures are listed in Table 4-1. R3206 and their mixtures shown the phase transition of

Isotropic-N*-SmC*-Crystalline. R3206 and R3206H have wide *SmC*/SmC* temperature from 79.45 °C to -17.90 °C and 73.77 °C to -29.73 °C, respectively.

Table 4-1. Phase sequence temperature of pure R3206 and their mixtures characterized at cooling rate of 10 °C /min.

Materials	Phase sequence temperature (°C)
R3206H	*Iso* 110.66 — *N 73.77* — *SmC* -29.73 *Cry*
R3206	*Iso 109.88* — *N* 79.45* — *SmC** -17.90 *Cry*
R3206_70	*Iso 109.39* — *N* 76.81* — *SmC** -21.85 *Cry*
R3206_50	*Iso 110.63* — *N* 77.19* — *SmC** -23.39 *Cry*

Iso : Isotropic, N : Nematic, Sm : smectic, Cry : Crystalline, * : chiral
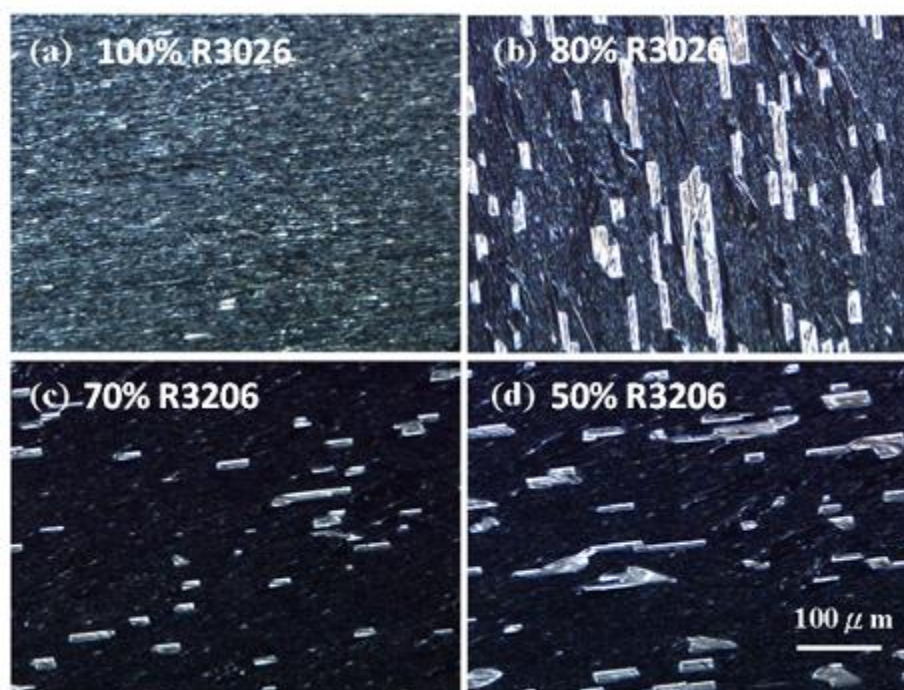
Fig. 4-2. Polarizing optical micrographs of (a) R3206, (b)80% R3206, denoted as R3206-80 (c) R3206-70, and (d) R3206-50 in the 1.8±0.1μm PI cells.

The pitch length shown in Fig. 4-3 was generated by applying a parallel rubbed cell with a cell gap of 60 μm [57]. The distance between two stripes indicates the FLC's pitch length. The pitch length of R3206 mixtures is linearly reduced as the amount of R3206 is increased. See Fig. 4-3(b).
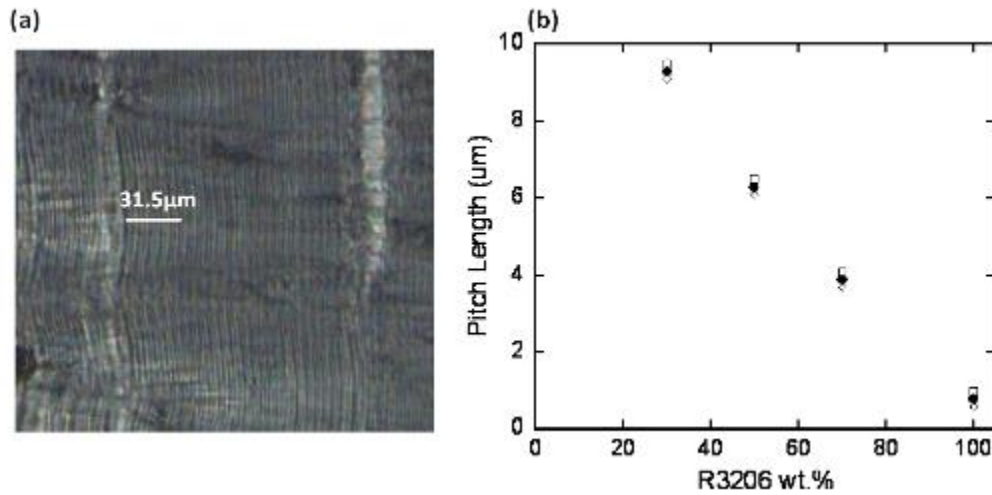
Fig. 4-3. (a) Microscopic texture of R3206-50 in a parallel rubbed cell with the cell thickness of 60 μm and (b) pitch lengths of R3206 mixtures; R3206-30: 9.3±0.2μm, R3206-50: 6.3±0.2μm, and R3206-70: 3.9±0.2μm.

In the series of R3206 mixtures, P_S values are almost linearly dependent on R3206 weight percentage as shown in Fig. 4-4. When the saturation voltage ($V_{sat.}$) increases, P_S decreases. The low frequency triangular driving waveform confirms that both pure R3206 and its mixtures are half-V switching mode FLC materials as shown in Fig. 4-5.
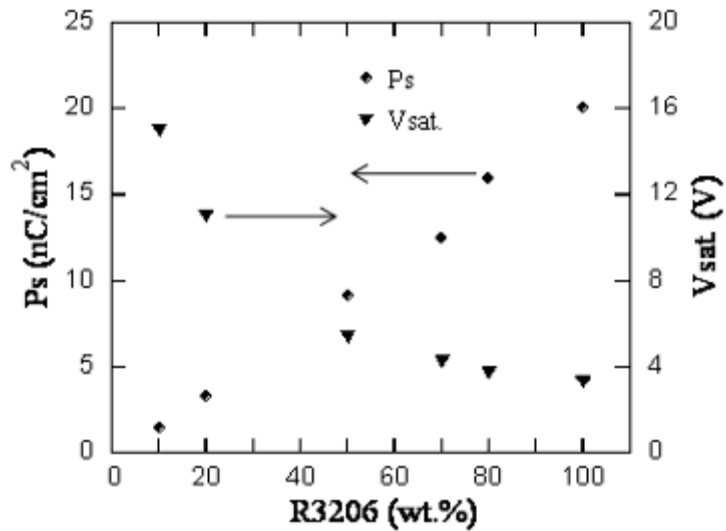
Fig. 4-4. Spontaneous polarizations and saturation voltages of R3206 and its mixtures. Spontaneous polarization was enabled by the liquid crystal analysis system (LCAS-1) with 5 μm pre-made cells (from LC Vision). Saturation voltage was characterized by a 100Hz square wave under 1.8 μm cells.
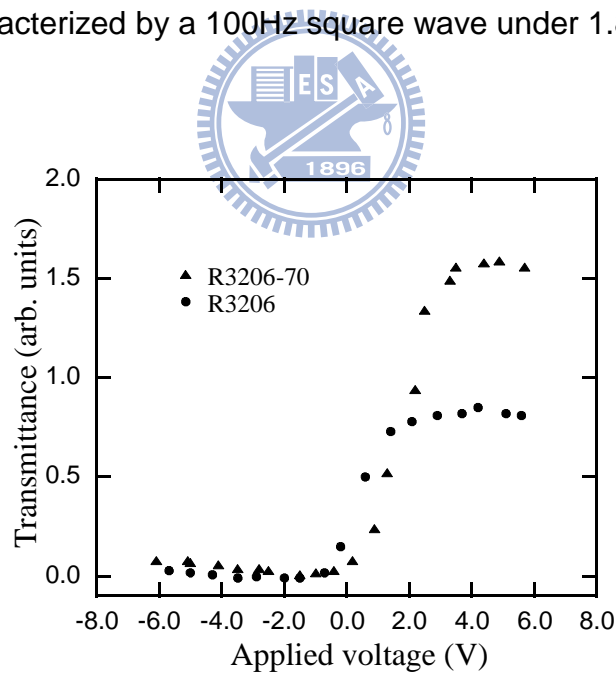
Fig. 4-5. Electro-optical properties of R3206 and R3206-70 driven by a 30 Hz triangular wave.

4.3 Asymmetric Hybrid Alignment Techniques

The P_S up and P_S down domains co-exist because of the same minimum total free energy in the symmetrical cell, where the top and the bottom alignment surfaces have the same polar surface interaction coefficients, i.e. $\gamma_2^{(t)} = \gamma_2^{(b)}$. As a result, a defect-free alignment texture is only achievable when the direction of the FLC's spontaneous polarization is directed in the same orientation. One of the significant approaches to suppress the alignment defects is to apply an external dc electric field during the annealing process under the FLC's *N*-SmC** phase transition. Uniform alignment can be obtained when the degenerate energy levels of the HV–FLC's total free energy is under a dc electric field. The dc-electric-field annealing process, unfortunately, is not applicable for display applications because it caused residual charges in the LC devices. According to Eq. (3.10), a large value for $(\gamma_2^{(t)} - \gamma_2^{(b)})$ under asymmetrical alignment surfaces (i.e. $\gamma_2^{(t)} \neq \gamma_2^{(b)}$) may hold the key to lowering the FLC's free-energy level. Thus, the alignment issue caused by surface pre-treatment can be solved by the following two approaches of the asymmetrical alignment conditions: first, controlling the alignment strength differentiates the values between $\gamma_2^{(t)}$ and $\gamma_2^{(b)}$; second, the use of opposite-surface-polarity alignment layers changes the sign of $\gamma_2^{(b)}$. The asymmetrical alignment techniques were applied to control the anchoring energy and surface polarity to validate our theoretical predictions.

HV-FLC materials, R2301 (*Iso* 86.8 *N** 64.7 *SmC**, Ps=4 nC/cm^2, AZ Electronic Materials) and R3206-50 [9] (*Iso* 108.7 *N** 75.7 *SmC** -24.8 *C*, Ps=9 nC/cm^2, AZ Electronic Materials) were utilized in this research. The cell gap

was controlled by 1.5 μm spacer. The polar anchoring energy of rubbed polyimide (PIA-X201-G01, Chisso) was measured to be within the order of 10^{-4}-10^{-3} J/m^2, and the plasma-treated PI surfaces were measured to be within the order of 10^{-5} J/m^2 [58]. The surface polarities of alignment layers were determined by the cross-rubbed cell [59]. Polyimide as the negative-surface-polarity material was applied. The positive-surface-polarity materials, such as polyvinyl alcohol (PVA), hexamethyldisilizane (HMDS), and Nylon 6, were applied.

4.3.1　Anchoring-Energy-Controlled Asymmetric Cell

In order to differentiate the subtle changes of $\gamma_2^{(t)}$ and $\gamma_2^{(b)}$ in the same alignment material, we fabricated FLC cells with two different surface treatments for the top and bottom alignment surfaces. The plasma alignment technique and rubbing alignment were treated on top and bottom surfaces, respectively. With one order of lowering anchoring strength than the rubbing process, the subtle changes in polar surface interaction coefficients can be easily observed. In the anchoring-energy-controlled asymmetrical cell, FLC molecules were mainly controlled by the rubbing alignment surface. Thus, the asymmetric anchoring energies lowering the energy levels of two domains as shown in Fig. 4-6. The alignment defect under a symmetrical cell and mono-domain texture under an asymmetrical cell are presented in Figs. 4-7(a) and 4-7(b), respectively. The difference in polar anchoring energy was observed to possess good alignment as predicted.
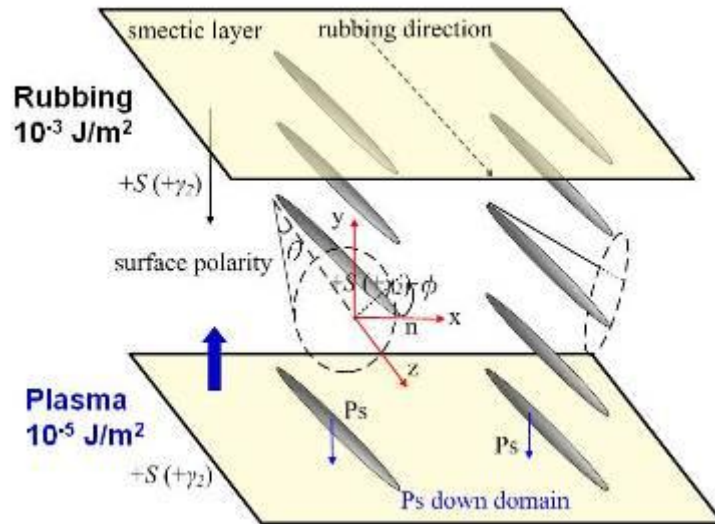
Fig. 4-6. Illustration of the anchoring-energy-controlled asymmetric cell.
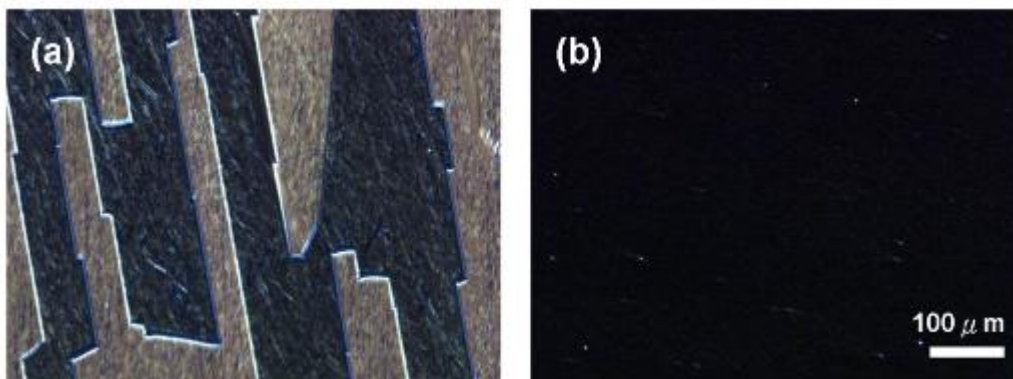
Fig. 4-7. Polarizing optical micrographs of R3206-50 under (a) plasma-alignment-treated symmetric cell and (b) anchoring-energy-controlled asymmetric cell.

4.3.2 Surface Polarity Controlled Asymmetric Cell

Surface polarity which affects the FLC's alignment has been demonstrated in the literature [60]. P_S up and P_S down domains coexist in the symmetrical-alignment condition, as shown in Fig. 3-1. By changing the surface polarity direction of the bottom surface, an asymmetrical cell with a

uni-surface polarity direction was proven achievable as shown in Fig. 4-8.
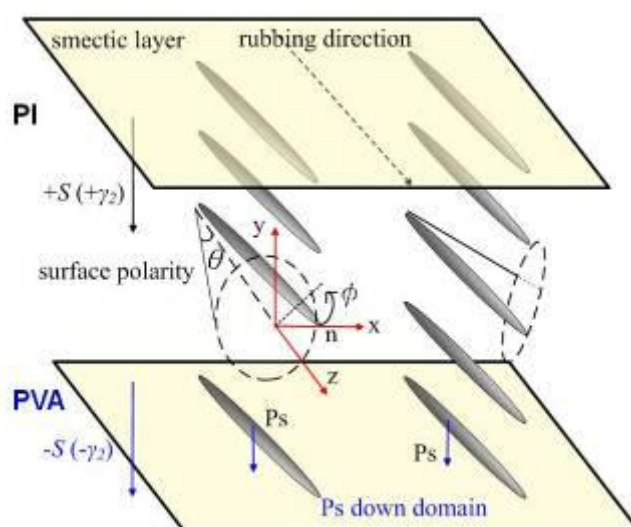
Fig. 4-8. Illustration of the surface-polarity-controlled asymmetric cell.

In this study, we verified the importance of controlling the direction of spontaneous polarization in the asymmetrical-alignment technique and extended the method to various low-driving-voltage FLC materials under different pairs of alignment materials. Pure smectic C, R3206H ($P_S = 0$ nC/cm^2), was applied to verify the usefulness of controlling the spontaneous polarization's direction in the asymmetrical-alignment technique. Two alignment domains were present due to a lack of spontaneous polarization in *SmC*, as shown in Fig. 4-9(a). In contrast, the alignment defects were eliminated in the *SmC**, even doped as low as 1% R3206 in R3206H ($P_S < 0.3$ nC/cm^2), as shown in Fig. 4-9(b). This experiment indicated the importance of the polar surface interaction with the FLC's spontaneous polarization.
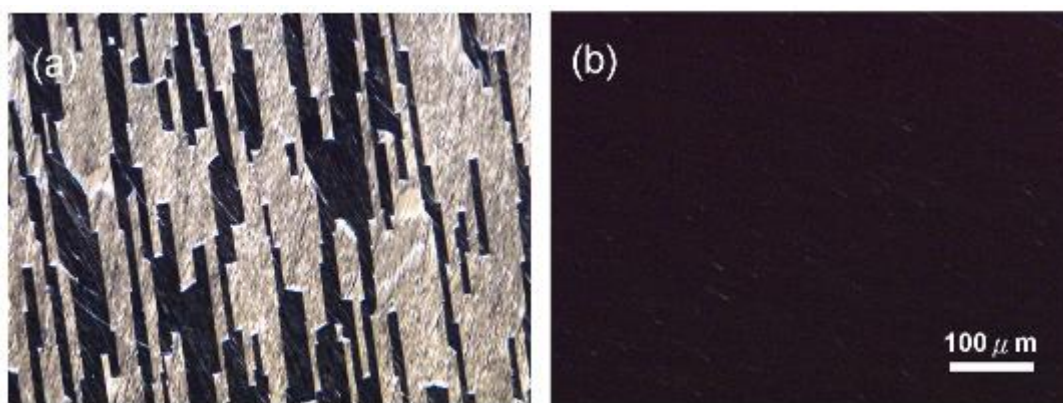
Fig. 4-9. Polarizing optical micrographs of (a) R3206H and (b) 1% R3206 doped in R3206H in the PVA$_{rub}$-PI$_{rub}$ asymmetric cells.

LC alignment textures of H-V FLC materials, R3206-50 and R2301, in the PI coated symmetric cells were captured under POM as shown in Figs. 4-10(a-b), respectively. Both have horizontal chevron defects. Opposite surface polarity alignment layers, PVA and PI, were utilized in asymmetrical cells to control the direction of the FLC spontaneous polarization. The horizontal chevron defects of R3206-50 and R2301 were eliminated in the asymmetric cells as shown in Figs. 4-10(c-d), respectively. The alignment of R3206-50 and R2301 was greatly improved by the asymmetrical cell approach compared to a conventional symmetric cell. Furthermore, different alignment layers were utilized to verify a surface-polarity-controlled asymmetrical cell. The positive-polarity alignment layers, such as HMDS and Nylon 6, were utilized to assemble asymmetrical cells with PI. Both HMDS and Nylon 6 hybrid cells successfully suppressed the horizontal chevron defects of R2301 as shown in Figs. 4-10(e-f), respectively.

The defect free alignment texture with a uniform LC orientation and layer structures are shown in Fig. 4-9(a); however, for FLC's orientation

following smectic layers, the alignment is sensitivity to shocks and vibrations, as shown in Fig. 4-11(b).
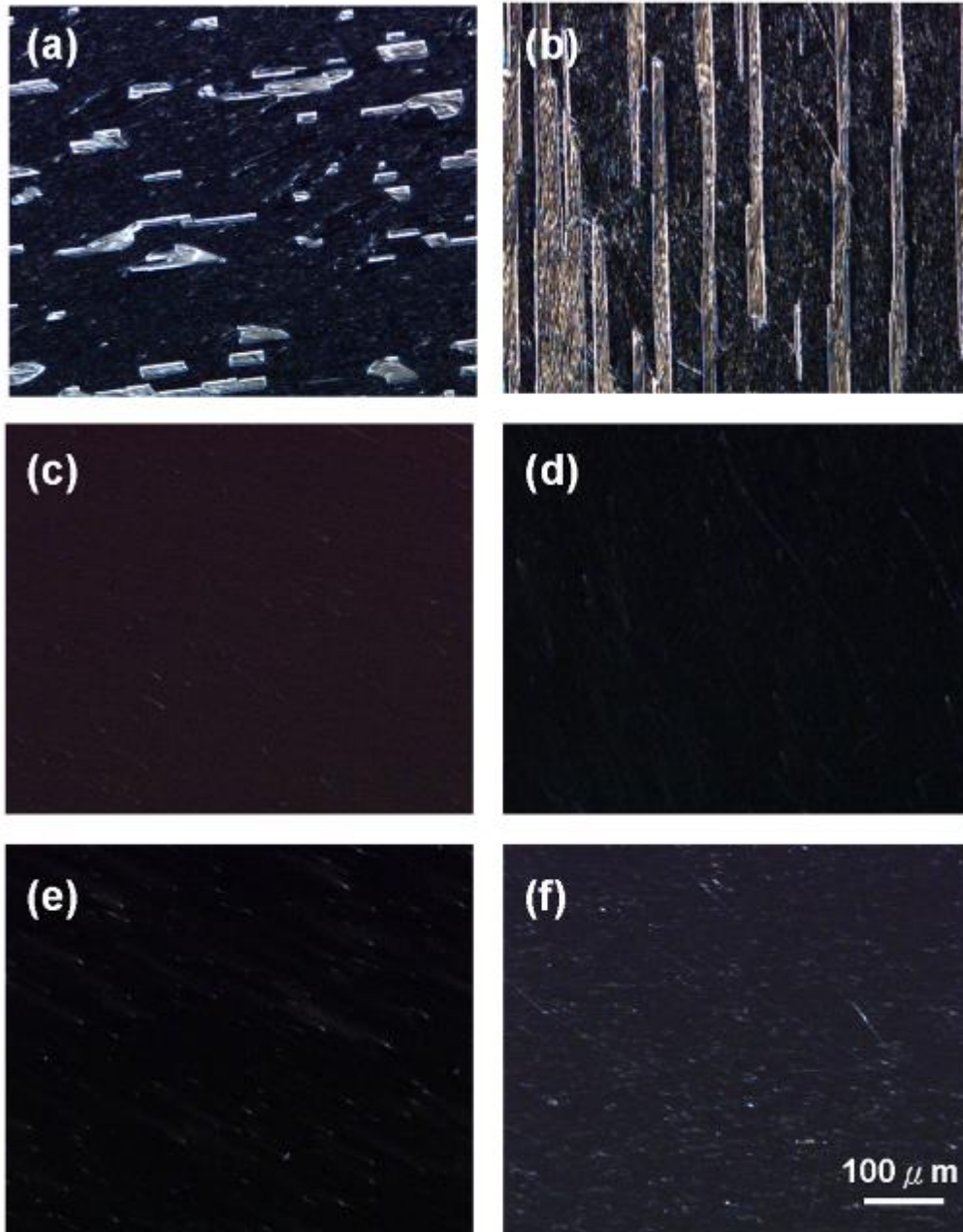
Fig. 4-10. Alignment textures of (a) R3206-50 in the PI rubbed symmetric cell, (b) R2301 in the PI rubbed symmetric cell, (c) R3206-50 in the asymmetric cell, (d)R2301 in the asymmetric cell, (e) R2301 in HMDS-PI asymmetric cell, (f) R2301 in the Nylon 6-PI asymmetric cell.
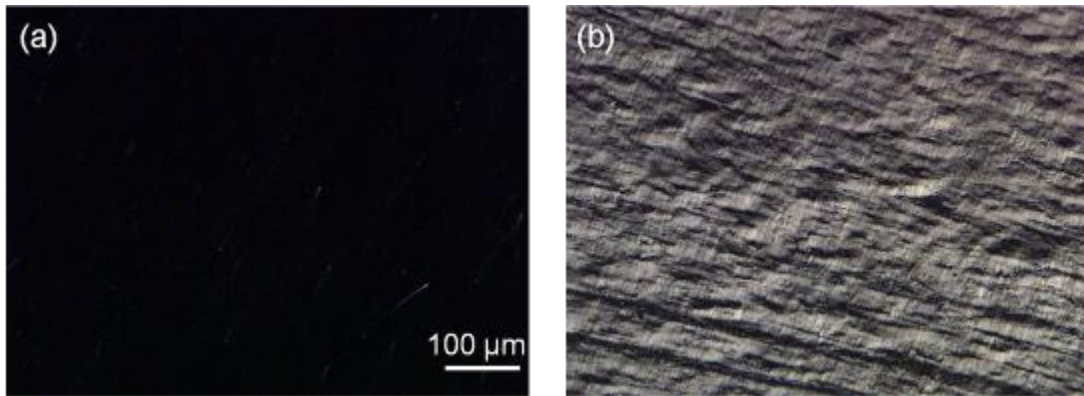
Fig. 4-11. Microscopic textures of a PVA-PI asymmetric cell (a) after thermal annealing and (b) after stress test.

4.3.3   Alignment Ability of All Asymmetric Cells

The difference between $\gamma_2^{(t)}$ and $\gamma_2^{(b)}$ was achieved by controlling the sign of γ2 and its value. The conditions were fulfilled by utilizing alignment materials with opposite surface polarities and alignment techniques with different alignment strengths. By controlling the surface polarity and polar-anchoring energy, the $(\gamma_2^{(t)} - \gamma_2^{(b)})$ value was increased progressively under the asymmetrical-alignment conditions of $(\gamma_{2strong}^{(t)}, \gamma_{2weak}^{(b)})$, $(-\gamma_{2strong}^{(t)}, \gamma_{2weak}^{(b)})$, and $(-\gamma_{2strong}^{(t)}, \gamma_{2strong}^{(b)})$, in which the minus "−" sign denotes the surface-polarity direction with strong or weak alignment strengths. The photos of the R3206-50's alignment textures under different asymmetrical-alignment conditions and various cooling rates were captured under a polarizing optical microscope. The cooling rate was controlled by a hot stage (FP82HT, METTLER TOLEDO). The alignment abilities of asymmetrical cells, PI$_{rub}$ − PI$_{plasma}$ (i.e., rubbed PI and plasma-treated PI surfaces), PVA$_{rub}$ − PI$_{plasma}$, and

PVA$_{rub}$ – PI$_{rub}$, were progressively increased $(\gamma_2^{(t)} - \gamma_2^{(b)})$ values. These were also evaluated by the alignment defects generated at various cooling rates. Based on Eq. (3.10), H–V FLC molecules tend to align as a mono-domain texture when increasing the $(\gamma_2^{(t)} - \gamma_2^{(b)})$ value. Under the smallest cooling rate of 0.1°C/min., the horizontal chevron defect was suppressed in all-asymmetrical cells, as shown in Fig. 4-12(a). When the cooling rate increased to 1.0°C/min, the horizontal chevron defect was presented in the PI$_{rub}$–PI$_{plasma}$ cell, as shown in Fig. 4-12(b). Under a cooling rate of 2.0°C/ min, slight light leakage was present in the PVA$_{rub}$–PI$_{plasma}$ cell, as shown in Fig. 4-12(e). The PVA$_{rub}$–PI$_{rub}$ cell, with a larger difference in the γ_2 value, appeared to have better molecular alignment than the other asymmetrical cells at a higher cooling rate, as shown in Figs. 4-12(g–i). The defect-free cooling-rate tolerance for PI$_{rub}$–PI$_{plasma}$, PVA$_{rub}$–PI$_{plasma}$, and PVA$_{rub}$–PI$_{rub}$ asymmetrical cells were 0.1, 1.0, and 3.0°C/min., respectively. Among these asymmetrical cells, the PVA$_{rub}$–PI$_{rub}$ cell has better alignment even at a fast cooling rate.
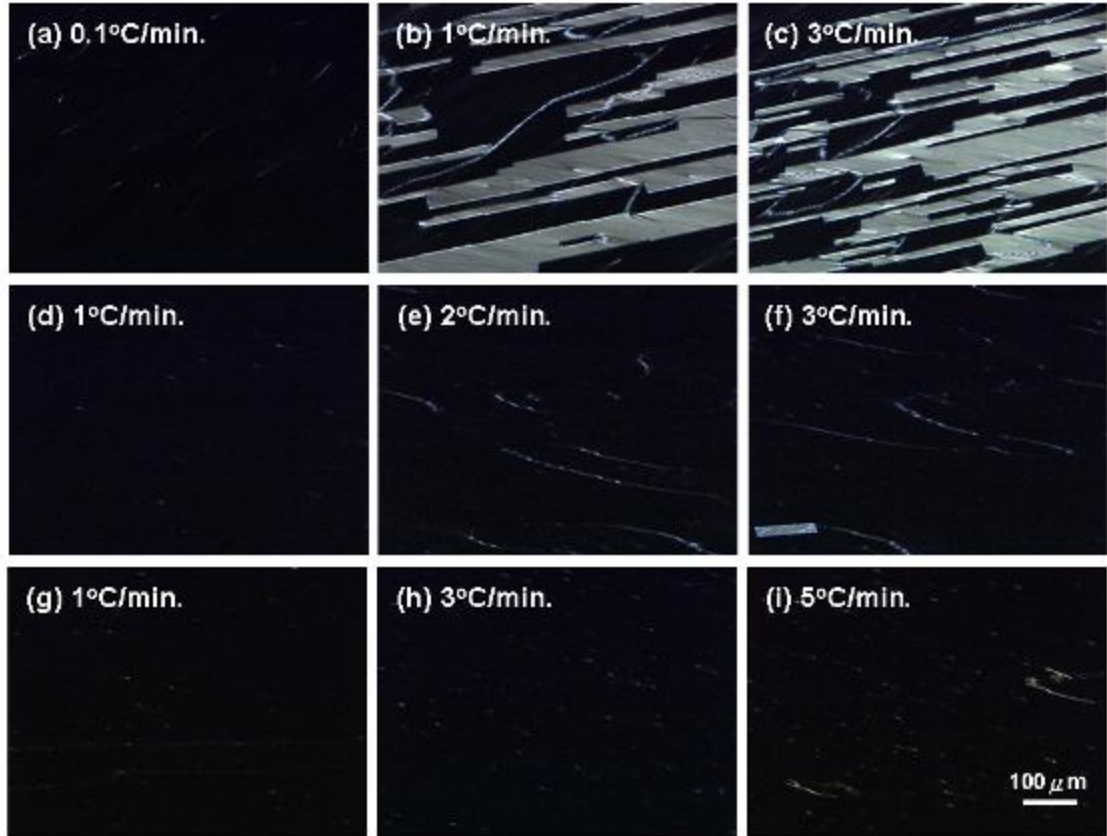
Fig. 4-12. Polarizing optical micrographs of R3206-50 under different cooling rates in the (a-c) PI_{rub}-PI_{plasma}, (d-f) PVA_{rub}-PI_{plasma}, and (g-i) PVA_{rub}-PI_{rub} asymmetric cells.

4.3.4 Electro-optic Properties

The electro-optical properties were characterized by a 100Hz square wave. R3206-50 possesses threshold voltage under 1.2 V and the saturation voltages is 4.5 V as shown in Fig. 4-13. Temperature-insensitive and continuous electro-optical responses were presented. When continuous bipolar squares are applied from 1 V to 5 V, analogue gray scales are presented as shown in Fig. 4-14. The HV-FLC is only switched by a positive electric field. Compare to a symmetric cell, the contrast ratio of R3206-50 in the PVA_{rub}–PI_{rub} treated asymmetric cell was greatly improved from 76:1 to

780:1. R3206-50 demonstrated fast response of below 1 ms as shown in Table 4-2. The rise time and fall time were characterized by squares waves as shown in Fig. 4-14(a). The field off time was characterized by applying a positive pulse as shown in Fig. 4-14(b). In the results of fall time, in addition the interaction between electric field and P_S, strong surface force increase the LC response; thus, R3206-50 shows faster fall time than rise time. Without applying voltage, the field off time is longer than fall time.
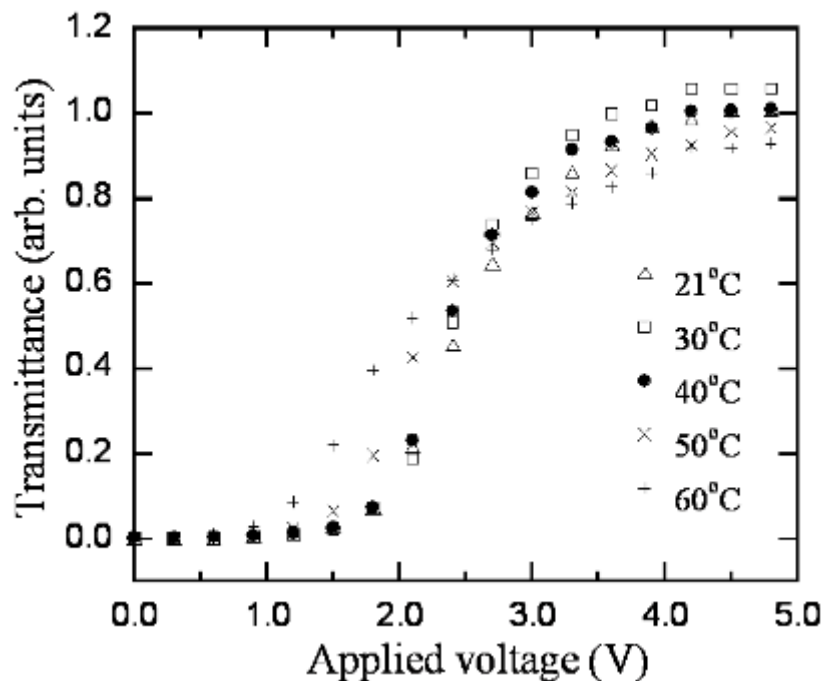
Fig. 4-13. Voltage-transmittance curves of R3206-50 in the PVA$_{rub}$–PI$_{rub}$ asymmetric cell varying with temperature.

Table 4-2. Response time of R3206-50.

R3206-50, cell gap: 1.5µm			
Voltage	Rise Time (+V)	Fall Time (-V)	Field Off Time (0V)
2 V	6 ms	0.24 ms	0.96 ms
3 V	1.12 ms	0.24 ms	0.96 ms
4 V	0.64 ms	0.24 ms	0.88 ms
5 V	0.48 ms	0.24 ms	0.88 ms
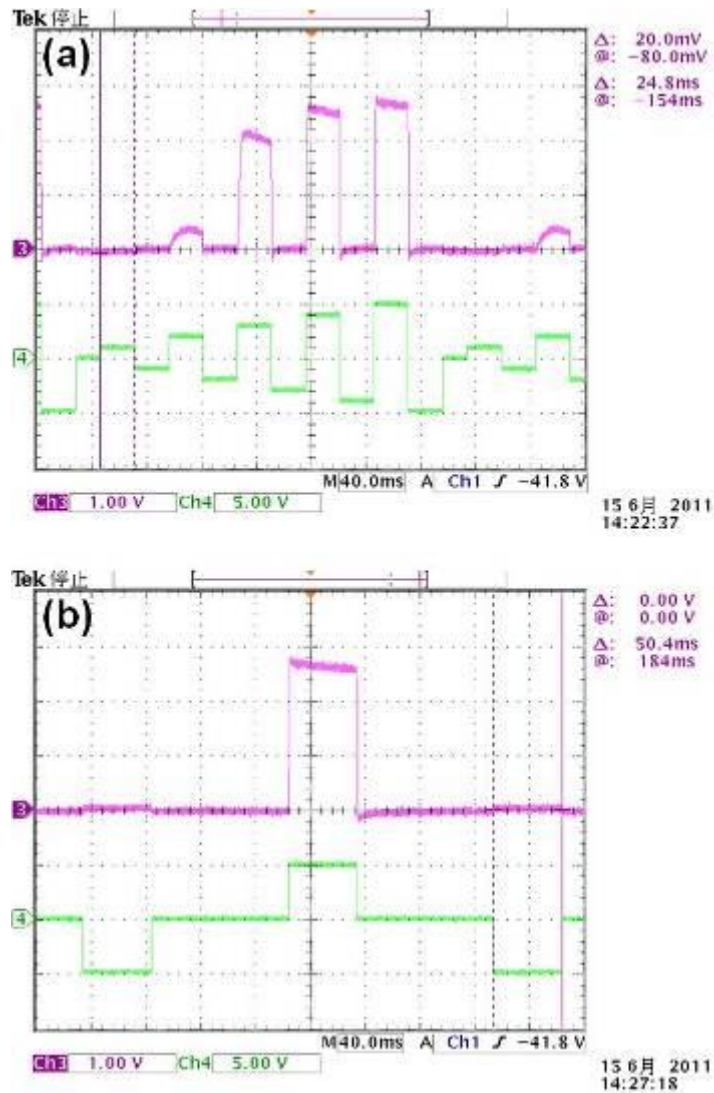
Fig. 4-14. Electro-optical properties of R3206-50 characterized by (a) continuous bipolar square waves at various voltages, and (b) a pulse of 3V, 20 ms.

4.3.5　Prototype FLC Display

The PVA$_{rub}$-PI$_{rub}$ asymmetrical surfaces were applied to prepare a 2.4" prototype FLCD. The defect free alignment texture and display images are shown in Fig. 4-15. The driving scheme applied in this FLCD is a 60 Hz bipolar square wave with a driving voltage of 5 V. The homemade FLCD was

fabricated without utilizing photo-spacers on top of the TFT. The cell gap was controlled by applying 1.5 μm spacer mixed UV glue around the edge of the panel. The cell gap of the 2.4" prototype FLCD is not uniform. Due to manufacturing complications, defects are still present.
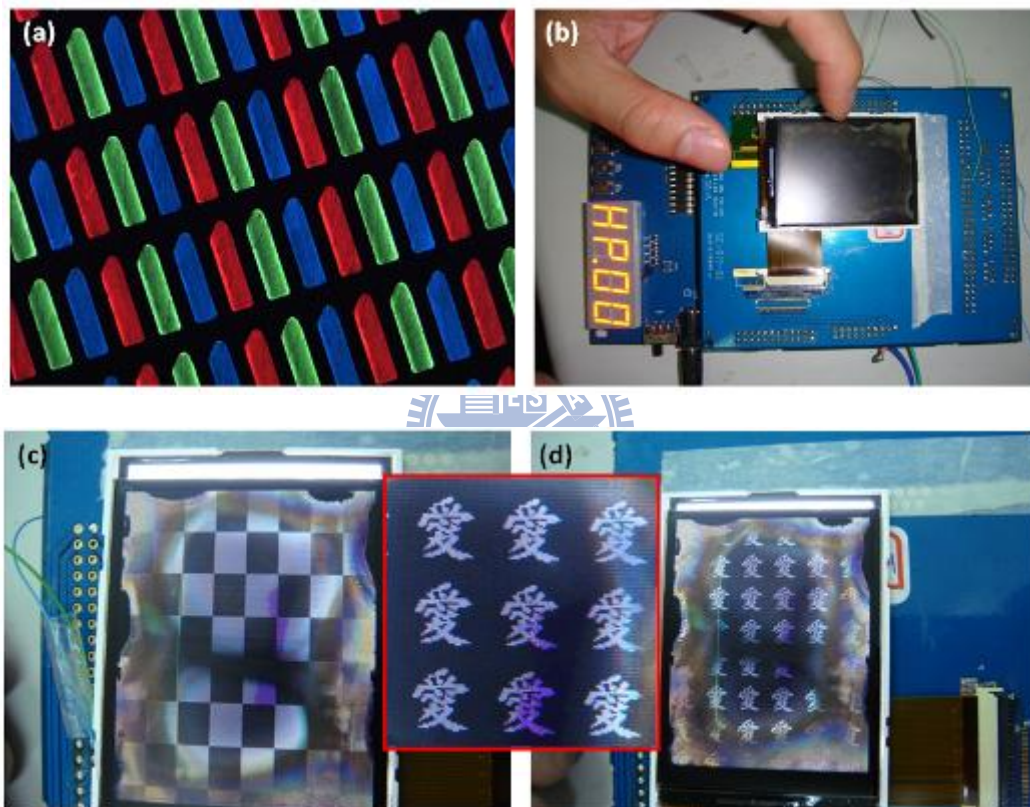
Fig. 4-15. (a) The alignment texture of 2.4" the FLC display, (b) the FLC display and its control panel, (c-d) the display images. The resolution is 240 × 3(RGB) × 320 with the sub-pixel size of 30 μm × 124 μm.

Chapter 5　　Ferroelectric Liquid Crystal Grating Based on Striped Electrodes

The horizontal chevron defect of HV-FLC devices is suppressed by applying the asymmetric alignment techniques discussed in Chapter 4. In this chapter, the surface-polarity-controlled asymmetric cell is applied to fabricate a defect-free HV-FLC grating. The defect-free FLC grating has a high diffraction efficiency. The calculated results and findings of the experimental diffraction yield are discussed and matches well to each other.

5.1　Introduction

Liquid crystal (LC) gratings, with electric switchability, have much potential in optical communication, three-dimensional, projection displays and other applications [61-62]. Numerous studies have explored the good alignment, low driving voltage, low cost and compact features of nematic LC gratings. However, slow response times limit potential application.

Ferroelectric liquid crystals (FLCs) with sub-millisecond response times, were extensively studied since surface-stabilized ferroelectric liquid crystals (SSFLC) were first proposed. Alignment defects are the main problem with FLC devices. In applications employing LC gratings, the diffraction efficiency is extremely sensitive to the alignment of the LC molecules. FLC gratings, containing LC polymers, suppress alignment defects [63-64]. However, the photo crosslink process is complex and the unswitchable photo-crosslinked

monomers with birefringence reduce diffraction efficiencies. Several LC gratings such as patterned electrodes, patterned photo-polymerization, hybrid photo-alignment and holographic alignment techniques [65-70] are proposed. Among these, the striped-electrodes method is the simplest process for manufacturing LC gratings. The simulation shows that an LC grating utilizing double-side striped electrodes has less fringe field effects than comparable single-side striped electrodes [71].

5.2 Proposed FLC Grating

In this study, an alignment defect free FLC grating using double-sided striped electrodes is proposed. The special alignment surface pre-treatment suppresses HV-FLC's alignment defects without utilizing photo-curable LC. A LC grating, with equal stripe width between alternative domains, has an optimal diffraction yield. However, the fringe field effect increases the switched domain width. To compensate, the width of striped electrodes is designed smaller than that of the electrode-etched stripes. Thus, the switched and unswitched domain widths are balanced when voltage is applied.
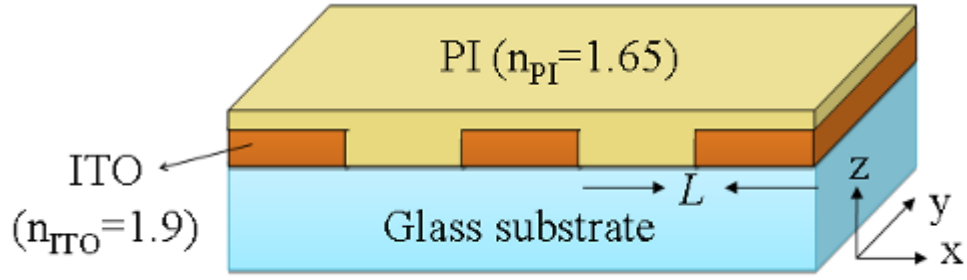
Fig. 5-1. Scheme of the alternating ITO stripes covered by polyimide (PI).

Striped indium-tin-oxide (ITO) glass substrate covered by polyimide (PI) is illustrated in Fig. 5-1. The optical axis of FLC rotates 2 degrees with respect to the rubbing direction (y axis) with the grating vector along the x axis. The input light is polarized along FLC's optical axis. When applying an electric field, the effective refractive index (n_{eff}) of the switched domain is given by [72]:

$$n_{eff} = n_o n_e / [n_e^2 \sin^2 \theta + n_o^2 \cos^2 \theta]^{1/2} \qquad (5.1)$$

Where n_o and n_e represent the ordinary and extraordinary refractive indices of an FLC molecule, respectively. θ is the angle between the polarization of the incident beam and FLC's optical axis (2θ also represents FLC's cone angle when FLC is fully switched) and d is the cell gap. The n-order diffraction efficiency of a LC grating is given by [73]:

$$\eta_n = \frac{\left|1 - \exp^{j\phi}\right|^2}{n^2 \pi^2} \sin^2(\frac{n\pi a}{L}), \quad n \neq 0 \qquad (5.2)$$

where $\phi = 2\pi d (n_e - n_{eff}) / \lambda$ is the relative phase difference between two alternating striped domains. λ is the input wavelength of a light source. a is the switched domain width. L is the ITO stripe period. The ideal first order diffraction efficiency (40.5%) is reached when $\phi = \pi$ and $a = L/2$ (i.e. the same width between switched and un-switched domains).

5.3   Effects of ITO Thickness

Half-V mode FLC (HV-FLC) is applied in the FLC grating. The horizontal chevron alignment defects exist in an HV-FLC device, due to the alignment of the spontaneous polarization (P_S) up and down domains when the FLC is cooled down from the N^*-SmC^* phase as shown in Fig. 5-2(a). A DC electric field applied during the N^*-SmC^* phase transition suppresses the defects. The DC electric field annealing method doesn't function at the region without electrodes in a cell with striped electrodes. This is not practical in the striped structure. In this research, the alignment issues are studied by examining alignment surfaces. Surface roughness strongly affects alignment [46]. For normal ITO thickness of about 94 nm, the spin coated PI film incompletely fills the etched concaves.   Thus, the interface between P_S up and P_S down alignment domains are mostly observed along the edges of ITO stripes as shown in Figs. 5-2(a-b). In addition, different refractive indices for ITO, PI and FLC cause initial phase differences between the alternative striped domains. Reducing the thickness of striped electrodes is prerequisite to obtain uniform surface alignment and   lower initial phase difference. The proposed FLC grating is fabricated using thin (16 nm) striped electrodes. The PI completely fills the etched concave. The uniform alignment surface above the interface of the ITO stripes is shown in Fig. 5.2(c). To further solve the defect problem, FLC's P_S direction is controlled by proposing the asymmetric surface polarity controlled hybrid cell which suppresses alignment defects as discussed in Chapter 4.
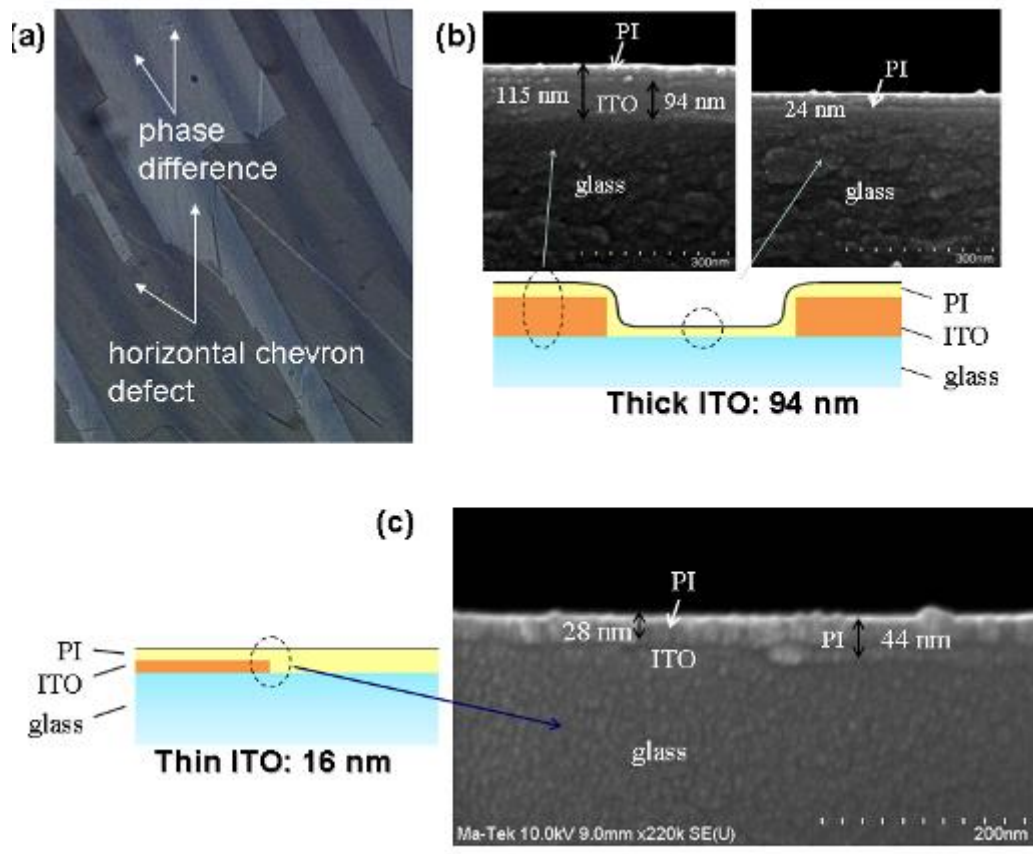
Fig. 5-2. (a) Polarizing optical micrograph of the HV-FLC grating based on striped ITO; the cross-section of polyimide coated surface using (b) thick (94 nm) and (c) thin (16 nm) ITO stripes.

5.4 Alignment of the HV-FLC Grating

Low driving voltage HV-FLC material, R3206-50 ($V_{sat.}$ at 4.7 V, Iso 108.7 N* 75.7 SmC* -24.8 C, cone angle=46°, Δn=0.18, P_S=9 nC/cm^2, from AZ Electronic Materials) is used in the FLC grating. The asymmetric hybrid alignment surfaces use both a positive surface polarity material, poly vinyl alcohol (PVA) and a negative surface polarity material, polyimide (PIA-X201-G01, Chisso). Fig. 5-3 shows the alignment textures of FLC grating. The first FLC grating was fabricated with the striped ITO with at 20 μm and the

grating pitch is 40 μm, as shown in Figs. 5-3(a-c). The surface pretreated FLC grating shows defect-free alignment texture as shown in Fig. 5-3(a). As the applied voltage increases, fringe field effect increases the switched domain width as shown in Figs. 5-3(b-c). At 5V (the saturation voltage of R3206-50), the switched domain width is 23 μm, while the striped ITO width is 20 μm. To reduce the fringe field effect, it can be approached by increasing the cell gap or pitch of grating. Increasing the cell gap, however, may affect FLC alignment. Pitch of the FLC grating is increased from 40μm to 80μm with the striped ITO width of 40μm as shown in Fig. 5-3(d). At the applied voltage of 5V, the FLC grating shows lower fringe field effect; the switched domain width is 41.6 μm.
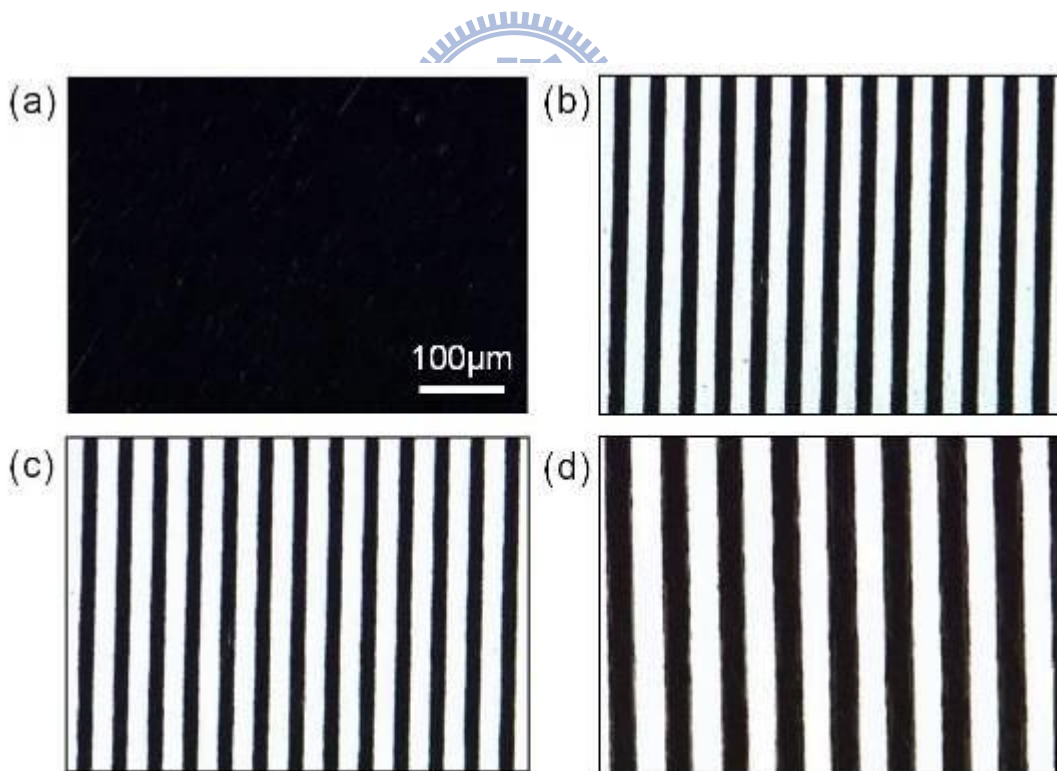
Fig. 5-3. Polarizing optical micrographs of 20/40μm (ITO striped width/pitch of grating) H-V FLC grating driven at (a) 0 V, (b) 3 V, (c) 5 V, and (d) 40/80 μm grating driving at 5 V. The FLC gratings were driven by 100 Hz bipolar square waves.
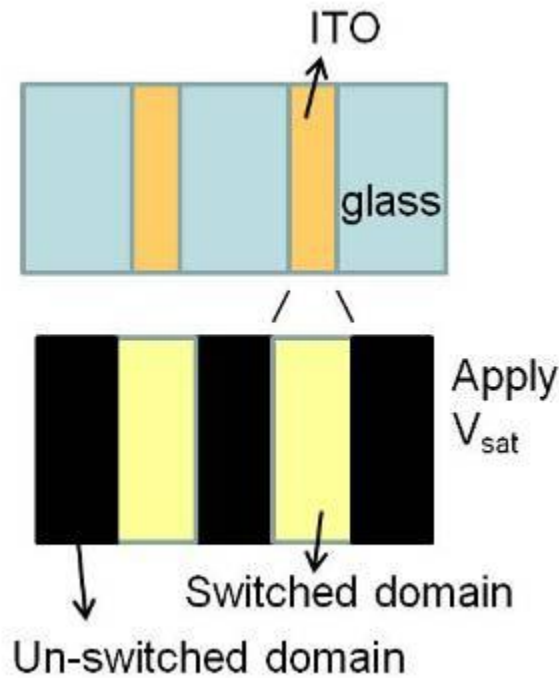
Fig. 5-4. Illustration of the asymmetric electrodes.

Since fringe field effect can not be completely eliminated, we design the striped electrodes with the width smaller than half of the pitch to compensate the fringe field effect as shown in Fig. 5-4. When the external electric field is applied, the switched domain width increases and balances the widths of alternative domains. As shown in Fig. 5-5, when the applied voltage is above 3V, increasing the switched domain width for about 0.53 μm/V results in the fringe field effect. At the saturation voltage of R3206-50, the switched domain width increases for about 2.4 μm. The unequal widths between two alternative striped domains decrease the diffraction efficiency based on Eq. (5.2). To compensate for the fringe field effect, the 38 μm-ITO-stripes are applied in this research with the grating pitch at 80 μm.

The surface pre-treated HV-FLC grating displays alignment defect free textures as shown in Fig. 5-5. The switched domain width is originally smaller

than that of the un-switched domain as shown in Figs. 5-5(b-c). When increasing the applied voltage, the fringe field effect increases the switched domain width. The alternative domain widths are balanced at about 5V as shown in Fig. 5-5(d). When the applied voltage is above 5 V, the switched domain width is larger than the un-switched domain as shown in Fig. 5-5(e-f). The applied voltage dependent, switched domain widths are presented in Fig. 5-6. The unbalanced domain widths reduce the diffraction efficiency by the factor of $\sin^2(\frac{n\pi a}{L})$ according to Eq. (5.2). At various driving voltages, the fringe field compensated FLC grating displays a domain width factor of 0.999 from 3 V to 5 V as shown in Fig. 5-6.
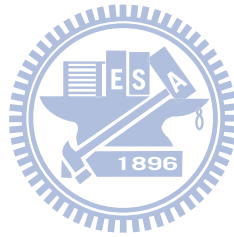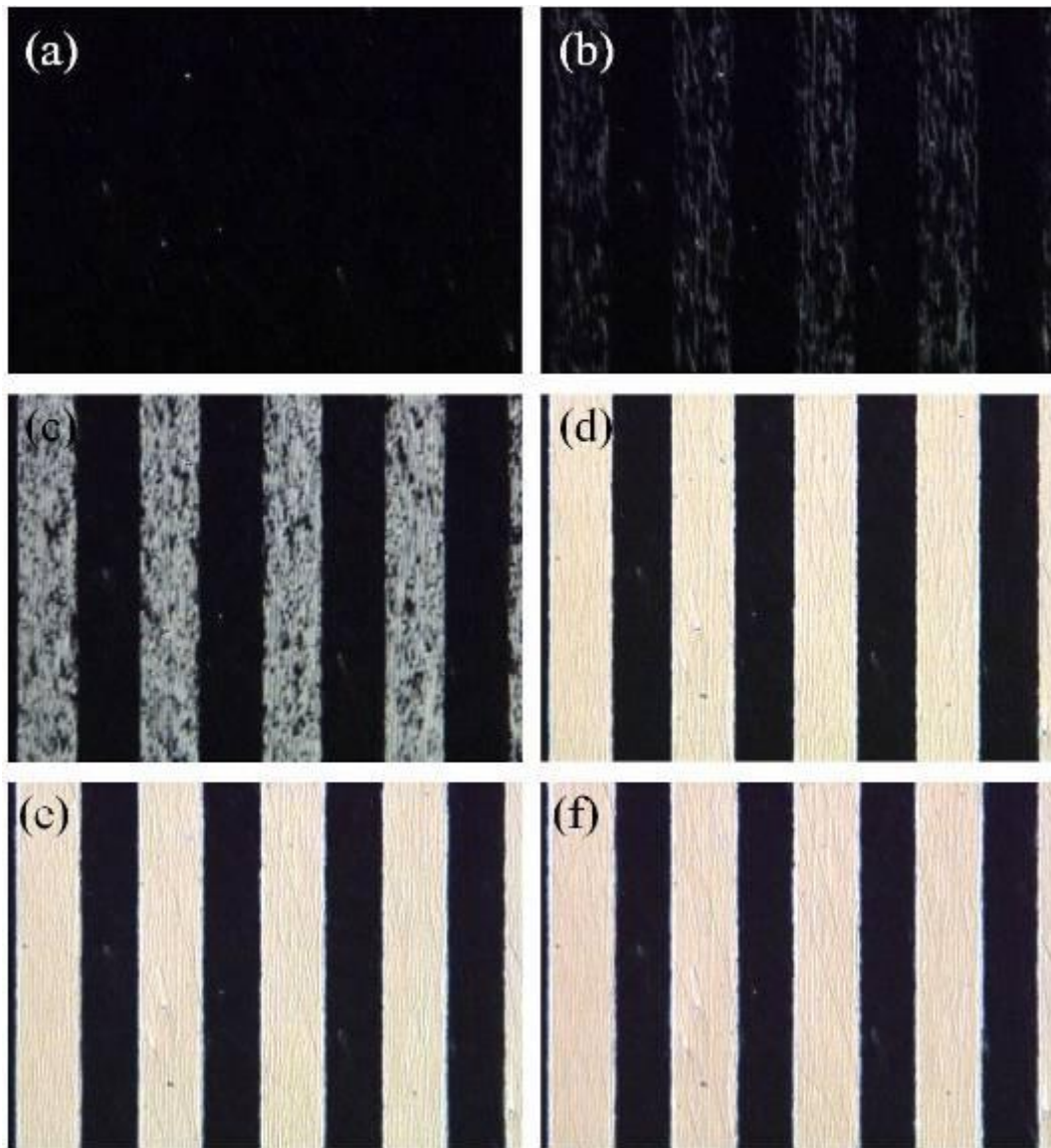
Fig. 5-5. Polarizing optical micrographs of H-V FLC grating driven by 100 Hz bipolar square waves at (a) 0V, (b) 1.5V, (c) 2V, (d) 5V, (e) 7V, (f) 10V in the 1.9 µm cell.
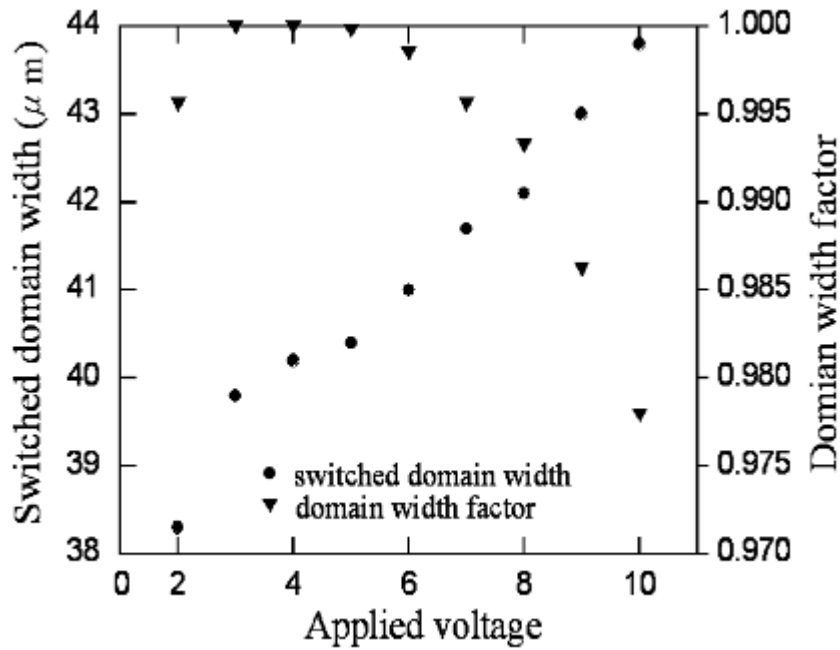
Fig.5-6. Switched domain width and its domain width factor at various driving voltage.
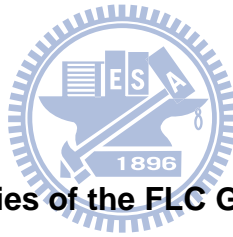
5.5 Electro-Optical Properties of the FLC Grating

The voltage-transmittance curve of an un-patterned R3206-50 cell was characterized by 100 Hz square waves as shown in Fig. 5-7. R3206-50 possesses threshold voltage at 2 V and saturation voltage at about 4.7 V. Fast response times under 1.3 ms (rise: 380 µs, fall: 920 µs) are demonstrated. The diffraction efficiency was characterized by DC voltage. The FLC grating was placed behind a polarizer with the optical axis parallel to the polarizer transmission axis. The voltage dependent, first order diffraction efficiency is shown in Fig. 5-7. The highest diffraction efficiency at 27.29% is shown.
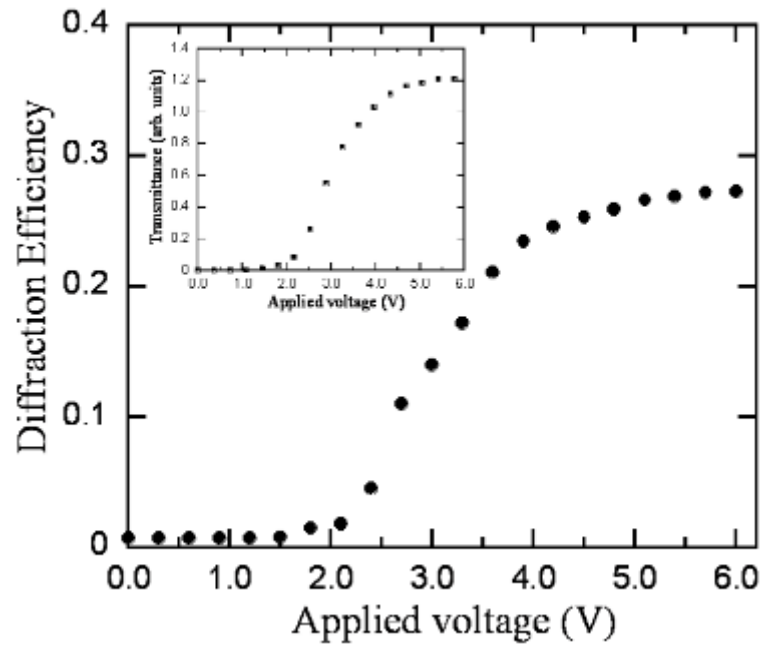
Fig.5-7. Voltage-transmittance curve of the R3206-50 cell and the first order diffraction efficiencies of the R3206-50 grating at various driving voltage. The electro-optic properties were characterized by He-Ne laser (632.8 nm).

Based on Eq. (5.1-5.2), the simulated diffraction efficiencies as a function of cell gaps and cone angles are presented in Fig. 5-8. For the R3206-50 material with 46° cone angle and Δn=0.18, the ideal diffraction efficiency of 40.5% is achieved when the cell gap is 3.1 μm. However, for a FLC device with uniform alignment, the cell gap required, is under 2 μm. The simulated diffraction efficiency of 26.82%, at the cell gap of 1.9 μm, approaches the experimental yield of 27.29%. The matched results indicate that the ideal diffraction efficiency is reached for HV-FLC material with cone angle at 73° and an input wavelength of 632.8 nm. At input wavelengths of 550 nm and 450 nm, the ideal diffraction efficiency is approached at the switched angle of 65° and 54°, respectively. Thus, an FLC grating approaching ideal diffraction efficiency

at the input wavelengths of red, green, and blue is a realistic solution.
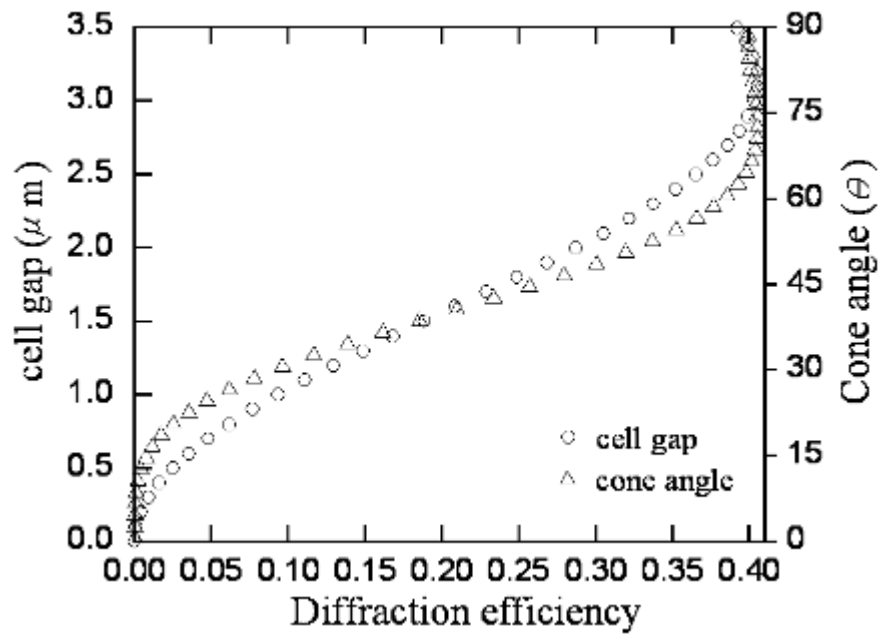
Fig. 5-8. Diffraction efficiencies as a function of cell gaps (at fixed cone angle, $2\theta=46^{o}$) and cone angles (at fixed cell gap =1.9 µm). The parameters are n_e=1.68, n_o=1.5, λ=632.8 nm, and $a=L/2$.

Chapter 6   Cell Gap Issue and FLC's Defect Minimization

6.1   Introduction

Good FLC alignment is able to be achieved by small cell gap, certain pitch design, and surface polarity control which have been illustrated in the previous chapters. The remaining unsolved issue in display applications is the cell process limitation in manufacture. The cell gap of most TFT-LCDs is controlled larger than 3 µm. The minimum cell gap requirement is, at least, 2 times greater than SSFLC cell. As described in Chapter 2, FLC presents three different kinds of molecular arrangements: helical state, splay state, and uniform state depending on FLC's pitch length and cell gap [56]. The larger cell gap is prone to complex alignments. As a result, larger cell gap posts a great challenge for obtaining a good cell performance in HV-FLC and SSFLC cells due to the effective surface boundary condition. In this chapter, we studied a potential approach which can be applied to minimize the alignment defects in the cell gap 3.5± 0.3 µm.

6.2   Alignment of FLC according the pitch length and cell gap

The HV-FLC material R3206, with the pitch length of 0.8 µm and cell gap of 1.6 µm, aligns at helical state (see Fig. 4-1) and shows poly-domains in a rubbed PI cell as shown in Fig. 6-1(a). FLC's alignment is improved by lengthening FLC's pitch length to uniform state as discussed in section 4.2.

Without lengthening the pitch length, in the surface-polarity-controlled asymmetric cell, R3206 presents horizontal-chevron-defect free texture in a cell with very thin cell gap (1.4 μm), as shown in Figs. 6.1(b-c). The asymmetric cell shows ordered LC alignment with striped defects. The alignment of short pitch FLC R3206 is improved by reducing the cell gap and applying asymmetric alignment technique. The result indicates the probability to improve FLC's alignment in addition to uniform state.
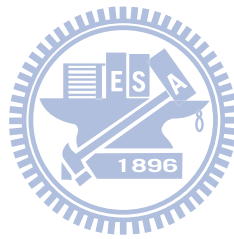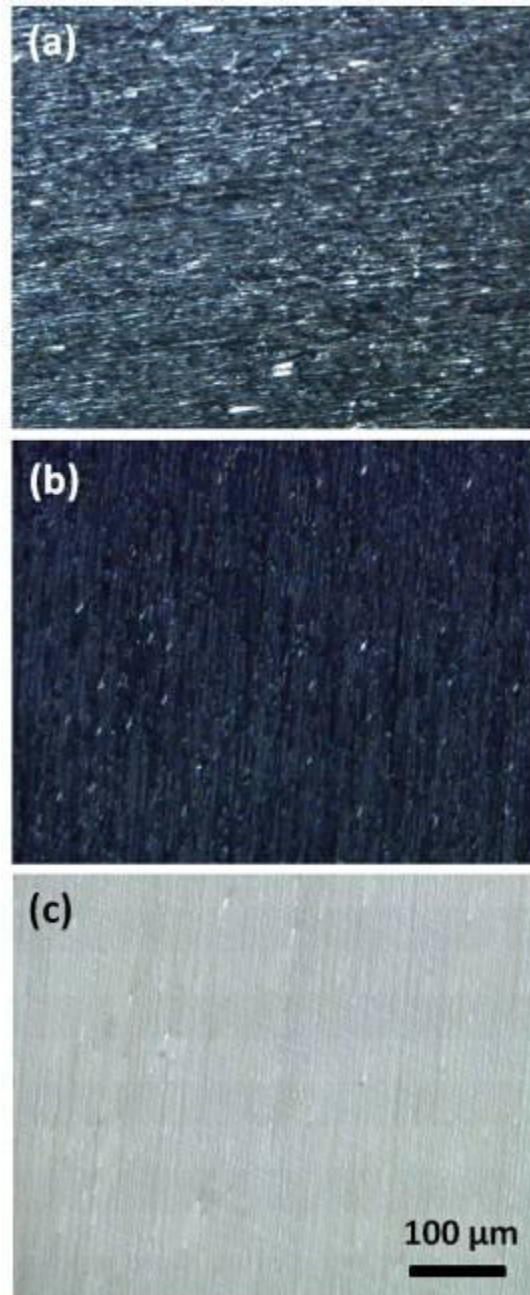
Fig. 6-1. Microscopic textures of R3206 in (a) symmetric cell (both PI treated), (b) surface-polarity-controlled asymmetric cell, and (c) surface-polarity-controlled asymmetric cell with the applied voltage of 100 Hz, 4 V.

According to the results of pitch lengthened and asymmetric surface pre-treated cells discussed in Chapter 4, FLCs tend to have better alignment

as increasing the pitch length. To improve the alignment in a thick cell, FLC's pitch length is further lengthened to more than 12 µm. The *SmC* host R3206H, a racemic mixture of R3206, is prepared to adjust the pitch length of R3206. In the symmetric aligned cell with the cell gap of 3.5 µm, R3206 also shows poly domain alignment. A series of weight differentiated R3206H was mixed into R3206. The pitch diluted mixture, 5% R3206 doped in R3206H (denoted as R3206-05, pitch length: 13.1 µm) shows large domain size with horizontal chevron defect. Within the alignment domain, striped defects present as shown in Fig. 6-2.

In the surface-polarity-controlled asymmetric cell, the horizontal chevron defect still presents in R3026-20 (pitch length: 10.8 µm) as shown Fig. 6-3(a). As increasing FLC's pitch length by doping more *SmC* host, R3206-10 (pitch length 12.3 µm) presents horizontal-chevron-defect free texture with striped defects. To discuss this result based on FLC's free energy, FLC's elastic free energy reduces as increasing FLC's pitch length; therefore, the surface force has better control on FLC's alignment [56]. Fig. 6-4 shows the alignment textures of R3206-10 at various of driving voltages. At the applied voltage of 5 to 10 V, R3206-10 presents poly-domains as shown in Figs. 6-4(b-c). Although the asymmetric alignment method suppresses the horizontal chevron defect of R3206-10, the striped defects remain exist. The pitch length is further diluted with more *SmC* host. The 5% R3206 mixture, R3206-05 shows better alignment with less alignment defects as shown in Fig. 6-5. When en external electric field is applied, R3206-05 shows uniform-domain switching without the presence of striped defects. The study of adjusting FLC's pitch length and surface pre-treatment approaches a promising less-defect FLC device in thick

cell gap to realize the manufacturing of current TFT-LCD.
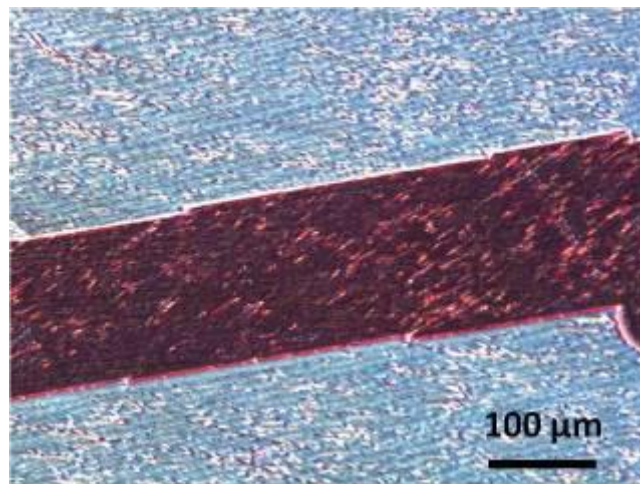
Fig. 6-2. Microscopic texture of R3206-05 in the symmetric cells with the cell gap of 3.3 μm.
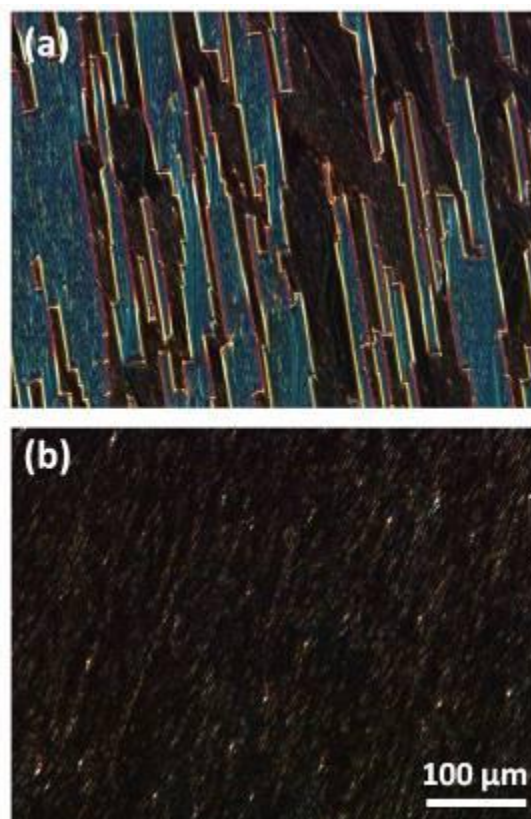
Fig. 6-3. Microscopic texture of (a) R3206-20 and (b) R3206-10 in the asymmetric cells with the cell gap of 3.5 μm.
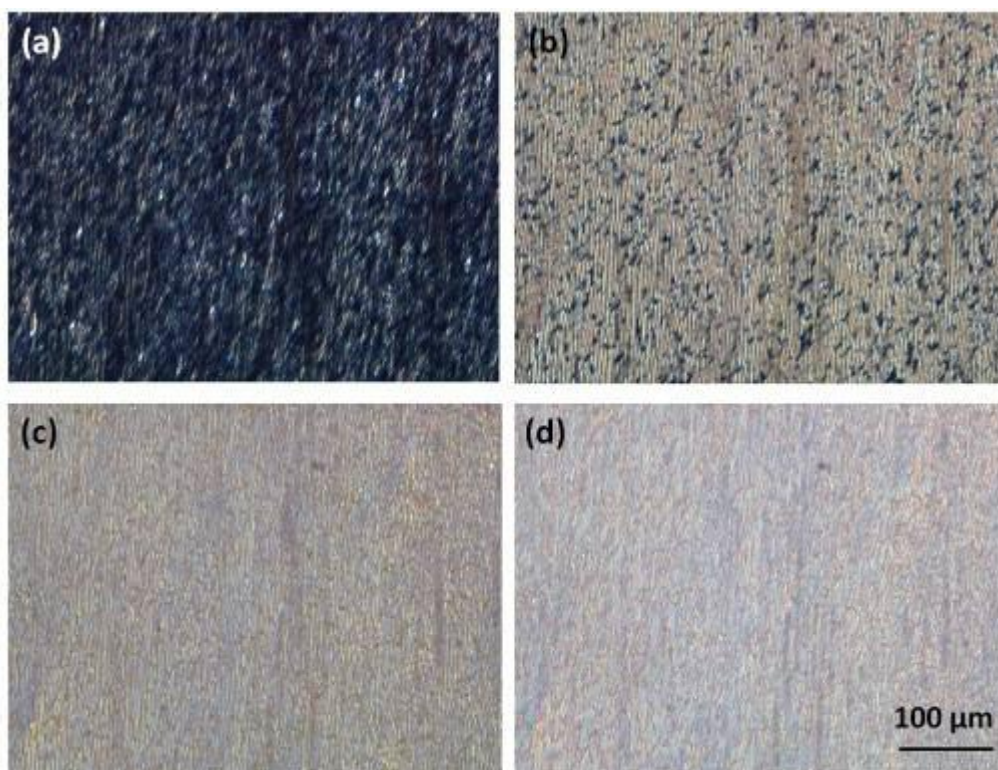
Fig. 6-4. Microscopic texture of R3206-10 at the applied voltage of (a) 5 V, (b) 10 V, (c) 15 V, and (d) 20 V, in the asymmetric cells with the cell gap of 3.5 μm.
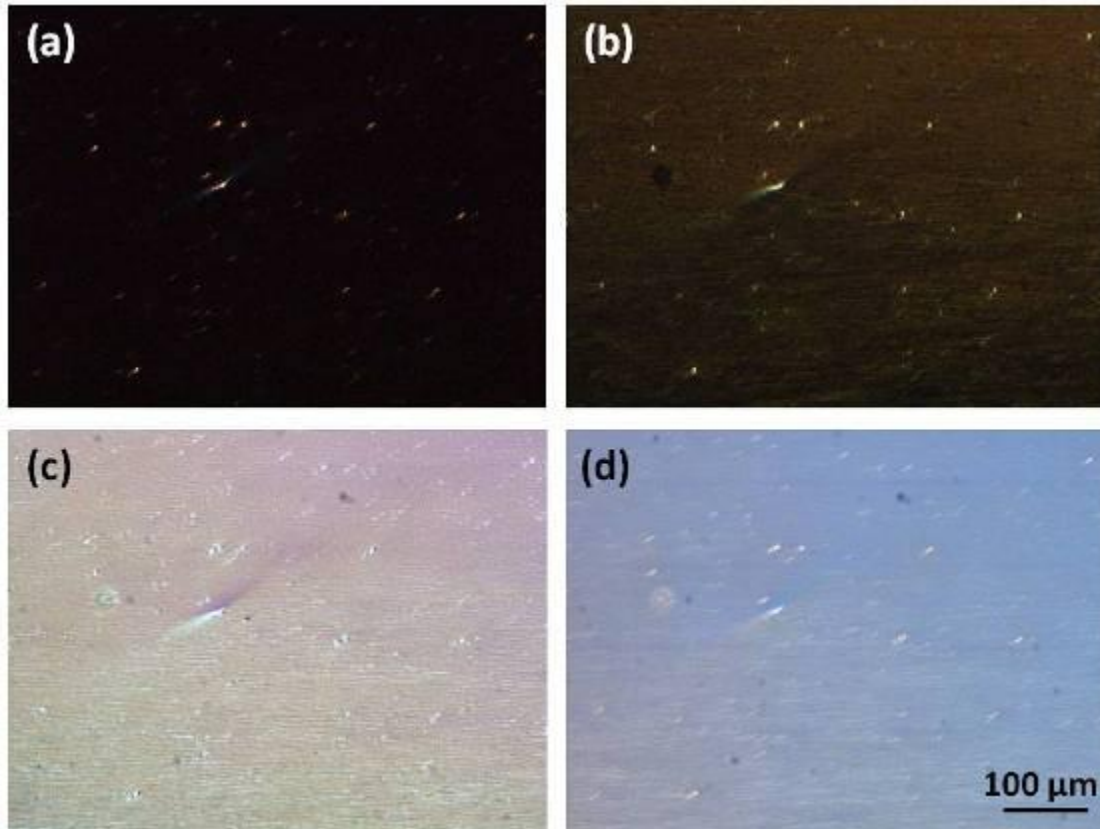
Fig. 6-5. Microscopic texture of R3206-05 at the applied voltage of (a) 0 V, (b) 5 V, (c) 10 V, (d) 20 V, in the asymmetric cells with the cell gap of 3.5 µm.

6.3   Light Scattering FLC devices

The pitch diluted FLC devices appear to have better alignment with large domain size. On the other hand, a short pitch FLC material in a thick cell, the disordered layer structures induce light scattering. The device is accompanied by a randomly aligned domain structure with gray scale capability, derived by tuning the pitch length with an electric field. In contrast to surface-stabilized devices, a short pitch material and a thick cell gap are required to maintain FLC's helical structure. With special surface pre-treatments, short pitch FLC materials display disordered alignment with micro helical domain structures. The micro domains cause light scattering as shown in Fig. 6-6.

The short pitch length (1 µm) HV-FLC material, R3206, is applied in this research. The electro-optical properties with different alignment conditions are studied. Homogeneous alignment (PI) and homeotropic alignment (VA) surfaces are prepared with and without rubbing treatment, respectively. In addition to scattering, the device displays continuous, stable electro-optical properties as shown in Fig. 6-7. The microscopic textures are shown in Fig. 6-8. The device initially shows micro helical domains, inducing scattering. When an external electric field is applied, the pitch is unwound with larger domain size and shows less scattering. The light scattering FLC device with continuous E-O properties has a potential to realize a polarizer-free device [74].

Fig. 6-6 (a) photo and (b) microscopic texture of R3206 in a cell without surface treatment; the cell gap is 5 µm.
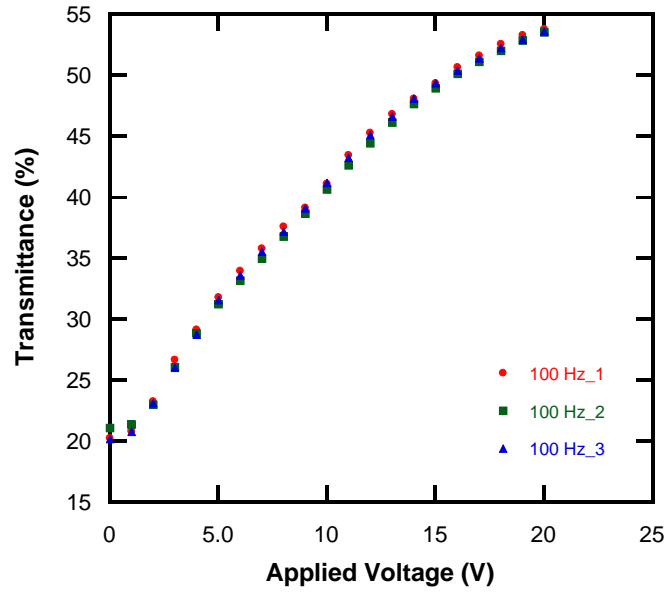
Fig. 6-7. Electro-optical properties of the PI$_{rub}$-VA cell characterized by 100 Hz bipolar square waves. The cell gap is 4.8 μm.
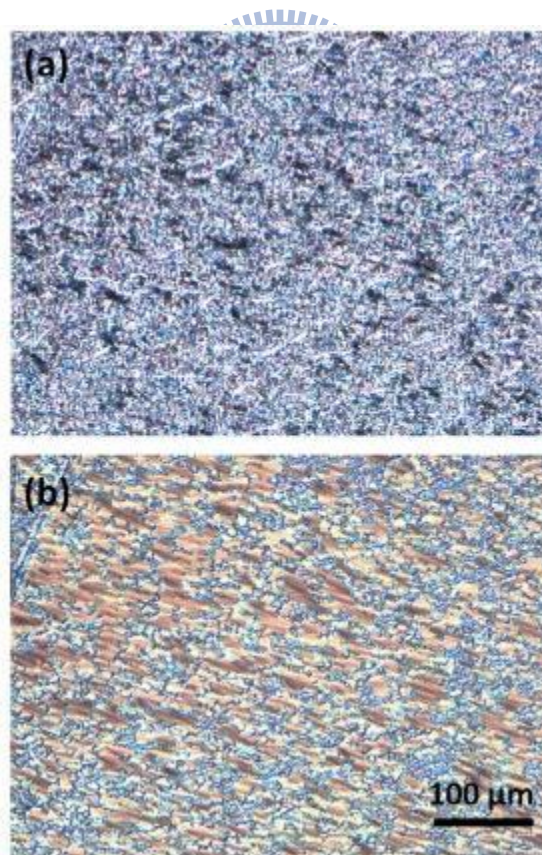
Fig. 6-8. Microscopic texture of R3206 in the PI$_{rub}$-VA cell at the applied voltage of (a) 0 V and (b) 100 Hz, 30V.

Chapter 7   Conclusions and Future Work

7.1   Conclusions

7.1.1   Horizontal Chevron Defect Studied by FLC's Total Free Energy
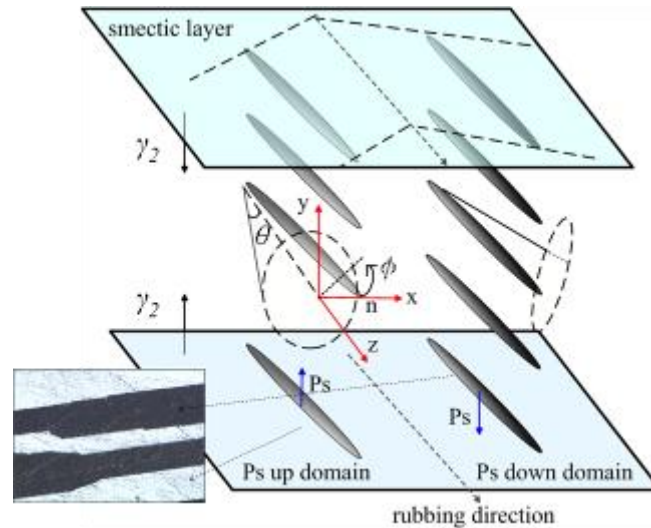
Fig. 7-1. The coordinate system of an H–V FLC device with horizontal chevron defect.

The horizontal chevron alignment defect is caused by the presence of both spontaneous-polarization (P_S) up and down domains when the FLC device is cooled down from its N*-SmC* phase, as shown in Fig. 7-1. The origin of the horizontal chevron alignment defect has been explained in terms of the FLC's free physical energy. The total free energy per unit area of P_S up down domains is expressed in Fig. 7-2. The HV-FLC's total free energy is expressed in terms of elastic free, polar and non-polar surface energies. The ideal uniform state is reached by optimizing the FLC's pitch length (p), cell gap (d), cone angle (θ), elastic constants (K) and the surface interaction coefficients (γ) at the lowest free energy.

The P$_S$ up and down domains co-exist because of the same minimum total free energy in the symmetrical cell. Both top and bottom alignment surfaces have the same polar surface interaction coefficients, i.e. $\gamma_2^{(t)} = \gamma_2^{(b)}$. As a result, a defect-free alignment texture is only achievable when the direction and orientation of the FLC's spontaneous polarization is the same. Based on HV-FLC's total free energy, a large value for $(\gamma_2^{(t)} - \gamma_2^{(b)})$ with asymmetrical alignment surfaces (i.e. $\gamma_2^{(t)} \neq \gamma_2^{(b)}$) holds the key to lowering the FLC's free energy.

Total free energy per unit area

$$F = \int_{-d/2}^{d/2} W_d \, dy + F_s'$$

$$= \int_{-d/2}^{d/2} W_d \, dy$$

$$+ \sin^2\theta (\gamma_1^{(t)} \sin^2\phi + \gamma_1^{(b)} \sin^2\phi) \mp (\gamma_2^{(t)} - \gamma_2^{(b)}) \cos\phi$$

Huge ($\gamma_2^{(t)}$ -$\gamma_2^{(b)}$) value

$$\neq 0$$

1. Different anchoring energy:

$$\gamma_2^{(t)} \neq \gamma_2^{(b)}$$

Strong   Weak

(rubbing   plasma)
10^{-3} 10^{-5} J/m^2
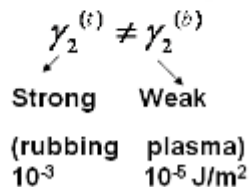
2. Surface Polarity Controlled Asymmetric Cell:

$$\gamma_2^{(b)} \Longrightarrow (-)\gamma_2^{(b)}$$

$$\mp (\gamma_2^{(t)} + \gamma_2^{(b)}) \cos\phi$$

Fig. 7-2. The total free energy of HV-FLC with horizontal chevron defect and the proposed two asymmetric alignment cells in which the polar surface energy term is varied. The minus (–) and plus (+) signs presented in the polar surface energy term indicate the energy of P$_S$ up and down domains in the horizontal chevron defect, respectively.

7.1.2 Defect-Free Asymmetric Alignment Cells

In summary, the horizontal chevron defect-free texture yields from different energy levels between P_S up and down domains. The asymmetrical alignment technique, when $\gamma_2^{(t)} \neq \gamma_2^{(b)}$, is proposed to solve alignment defects. The asymmetrical alignment conditions are achieved by controlling anchoring energies and surface polarities. A defect-free cell can be prepared from PI$_{rub}$–PI$_{plasma}$, PVA$_{rub}$ – PI$_{plasma}$, and PVA$_{rub}$ – PI$_{rub}$ asymmetric cells, with tolerances of progressively increased $(\gamma_2^{(t)} - \gamma_2^{(b)})$ values and cooling rates at 0.1, 1.0, and 3.0°C/min respectively. From a processing point of view, the PVA$_{rub}$–PI$_{rub}$ treated cell, with a large difference in the polar-surface-energy term, appears to align the best even under a fast cooling rate as shown in Fig. 7-3. The contrast ratio was significantly improved to 780:1 in the asymmetrical cell. This alignment technique provided promising FLC material and processing feasibility for fast-switching TFT-LCD applications.
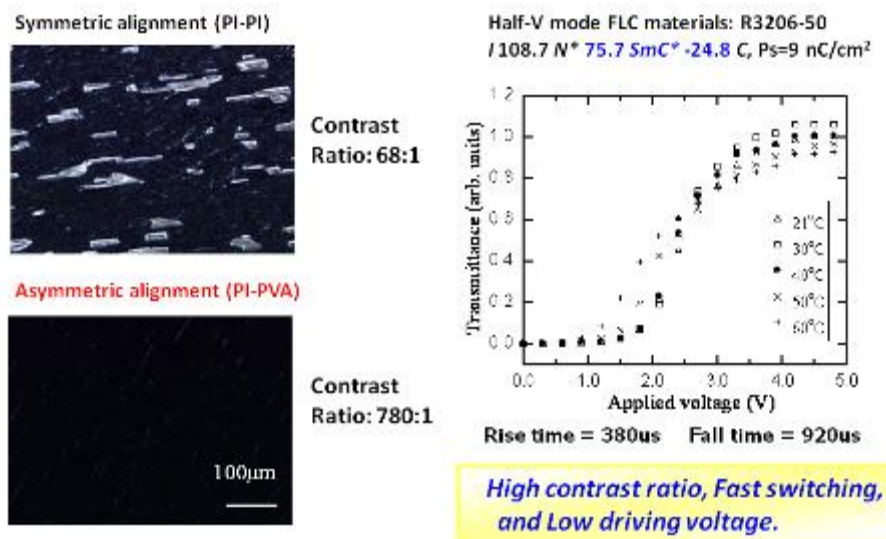
Fig. 7-3. Microscopic textures and electro-optical properties of the surface-polarity-controlled cell.

7.1.3   7Defect-Free H-V FLC Grating Using Striped Electrodes

Electrically tunable FLC grating approaching calculated diffraction efficiency, based on double-side striped electrodes has been demonstrated. Thin striped electrodes with the width designed smaller than half the grating pitch to compensate for the fringe field effect, improve the diffraction efficiency. The domain widths between switched and un-switched domains balance around the saturation voltage of R3206-50. The horizontal chevron defects are suppressed by controlling the alignment surface polarities as shown in Fig. 7-4. The high diffraction efficiency of 27.29% compares well with that of the simulation (26.82%). Under the same experimental condition, the ideal diffraction efficiency is achieved at the input wavelength of red, green, and blue by using HV-FLC material with cone angle of 73°. Fast response time (1.3 ms) are reached with 5V bipolar square waves. This desirable fast switching, low driving voltage and simple process FLC grating has substantial impact on optical system and display applications.
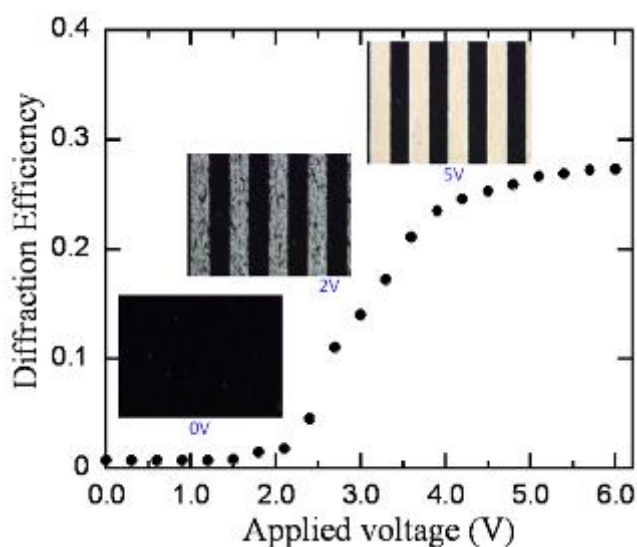
Fig. 7-4. Microscopic textures and diffraction efficiencies of the H-V FLC grating.

7.1.4   Cell gap issue and FLC's defect minimization

HV-FLC's alignment in a 3.5 μm cell is improved by lengthening FLC's pitch length and by applying the surface-polarity-controlled alignment method. The pitch-diluted FLC presents large domain size with horizontal chevron defects and striped defects in symmetric aligned thick cell. To suppress the horizontal chevron defect, the surface-polarity-controlled asymmetric cell is applied. R3206-20 presents horizontal chevron and striped defects as shown in Fig.7-5(a). R3206-10 with the pitch length of 12 μm presents horizontal-chevron-defect free texture; however, striped defects still present as shown in Fig. 7-5(b).   As further diluting the pitch length to 13 μm, R3206-05 shows better alignment with less alignment defects as shown in Fig.7-5(c). The study of adjusting FLC's pitch length and surface pre-treatment approaches a promising less-defect FLC device in thick cell gaps to fulfill the manufacturing of current TFT-LCD.

In contrast to pitch-lengthened FLC device, a short pitch FLC material in a thick cell, the disordered layer structures induce light scattering. The short pitch length (1 μm) HV-FLC material, R3206, under the surface pre-treatment of homogeneous alignment and homeotropic alignment, presents light scattering and displays continuous, stable electro-optical properties. The light scattering FLC device has a potential to realize a polarizer-free device.
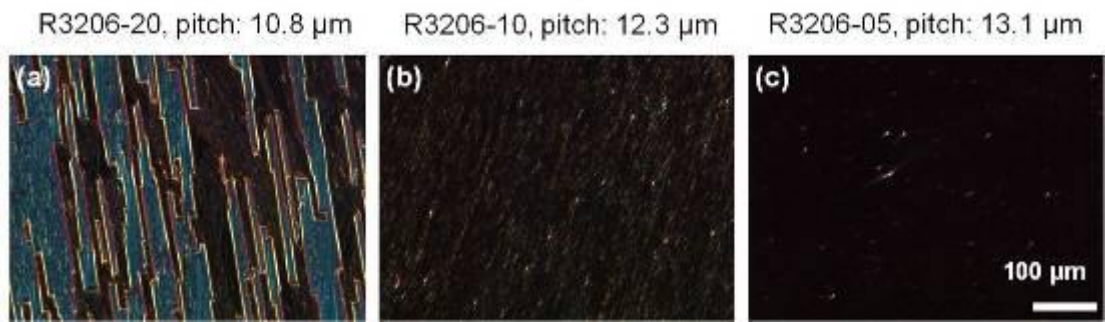
Fig. 7-5. Alignment textures of (a) R3206-20, (b) R3206-10, and (c) R3206-05

in 3.5 µm surface-polarity-controlled cells.

7.2 Future Work

A defect-free HV-FLC device is studied by lengthening FLC's pitch length and by applying the asymmetric alignment technique. For SSFLC or HV-FLC to obtain uniform alignment, the cell gap is limited below 2 µm. However, under such thin cell gap, it is difficult for the manufacturing of TFT-LCD to obtain uniform, large size alignment. Thus, FLC's alignment in a thick cell (3.5 µm) is discussed in Chapter 6. In an asymmetric cell, FLC appears to have better alignment with less alignment defect as lengthening FLC's pitch length to more than 13 µm. However, as diluting FLC material in a *SmC* host, the spontaneous polarization (P_S) reduces as doping more achiral host; therefore, the driving voltage increases. To solve this issue, a long pitch FLC material can be prepared by mixing two positive P_S FLC materials with opposite handedness. Thus, the pitch-diluted FLC keeps the P_S value. Electro-optical properties of the proposed pitch-diluted FLC will be studied.

References

[1] G. W. Gray ed., *Thermotropic Liquid Crystals,* (Jone Wiley & Sons, New York, 1987).

[2] H. G. Kuball, H. Bruning, T. Muller, et al., *J. Mater. Chem.*, **5**, 2167 (1995).

[3] P. Yeh and C. Gu, *Optics of Liquid Chrystal Displays,* (John Wiley & Sons, New York, 1999).

[4] R. B. Meyer, L. Liebert, L. Strzelecki et al., *J. Phys. Lett.*, **36**, 69 (1975).

[5] C. H. Lin, *Appl. Phys. Lett.,* **90**, 151112 (2007).

[6] S. Tahata, A. Tsumura, M. Mizunuma, A. Tamatani, Y. Morii, M. Fujii, and F.Matsukawa, *Proc. SPIE*, ***3015***, 134 (1997).

[7] T. Ishinabe, T. Miyashita, and T. Uchida, *J. Soc. Inf. Display*, **6**, 243 (1998).

[8] S. Meiboom, J. P. Sethna, P. W. Anderson, W. F. Brinkman, *Phys. Rev. Lett.*, **46**, 1216 (1981).

[9] M. J. Costello, S. Meiboom, and M. Sammon, *Phys. Rev. A,* **29**, 2957 (1984).

[10] T. Hatano, K. Yamamoto, H. Takezoe, and A. Fukuda, *Jpn. J. Appl. Phys.*, **25**, 1762 (1986).

[11] J. S. Patel and J. W. Goodby, *J. Appl. Phys.*, **59**, 2355 (1986).

[12] H. Mori and P. Bos, *Jpn. J. Appl. Phys.*, **38**, 2837 (1999).

[13] S. T. Wu and A. M. Lackner, *Appl. Phys. Lett.*, **64**, 2047 (1994).

[14] P. D. Brimicombe and E. P. Raynes, *Appl. Phys. Lett.*, **89**, 031121 (2006).

[15] H. Kikuchi, M. Yokota, Y. Hisakado, H. Yang, and T. Kajiyama, *Nature Materials*, **1**, 64 (2002).

[16] Y. Hisakado, H. Kikuchi, T. Nagamura, and T. Kajiyama, *Adv. Mat.*, **17**, 97 (2005).

[17] N. A. Clark and S. T. Lagerwall, *Appl. Phys. Lett.*, **36**, 899 (1980).

[18] K. Takatoh, M. Hasegawa, M. Koden, N. Itoh, R. Hasegawa, and M.

Sakamoto, *Alignment Technologies and Applications of Liquid Crystal Devices*, (Taylor & Francis, London and New York, 2005).

[19] J. W. Goodby, R. Blinc, N.A. Clark, S.T. Lagerwall, et al., *Ferroelectric Liquid Crystal Principles, Properties and Applications*, (Gordon and Breach Science Publishers, Philadelphia,1991).

[20] Y. Ouchi, J. Lee, H. Takezoe, A. Fukuda, K. Kondo, T. Kitamura, and A. Mukoh, *Jpn. J. Appl. Phys.*, **27**, L1993 (1988).

[21] T. P. Rieker, N. A. Clark, G. S. Smith, D. S. Parmar, E. B. Sirota, and C. R. Safinya, *Phys. Rev. Lett.*, **59**, 2658 (1987).

[22] J. Kanbe, H. Inoue, A. Mizutome, Y. Hanyuu, K. Katagiri, and S. Yoshihara, *Ferroelectrics*, **114**, 3 (1991).

[23] M. A. Hanschy, N. A. Clark, and S. T. Lagerwall, *Phys. Rev. Lett.*, **51**, 471 (1983).

[24] Y. Ouchi, H. Takezoe, and A. Fukuda, *Jpn. J. Appl. Phys.*, **26**, 1 (1987)

[25] Y. Inaba, K. Katagiri, H. Inoue, et al., *Ferroelectrics*, **85**, 643 (1988).

[26] P. J. Bos and K. R. Koehler/Beran, *Ferroelectrics*, **85**, 15 (1988).

[27] Y. Hanyu, K. Nakamura, Y. Hotta, S. Yoshihara, and J. Kanbe, *SID'03 Digest*, **XXIV**, 364 (1993).

[28] N. Itoh, M. Koden, S. Miyoshi, and T. Wada, *Jpn. J. Appl. Phys.*, **31**, 852 (1992).

[29] M. F. Bone, D. Coates, W. A. Crossland, P. Gunn, and P. W. Ross, *Displays*, **8**, 115 (1987).

[30] P. W. H. Surguyc, P. J. Ayliffeb, M. J. Birchb, et al., *Ferroelectrics*, **122**, 63 (1991).

[31] J. C. Jones, C. V. Brown, and P. E. Dunn, *Ferroelectrics*, **246**, 1097 (2000).

[32] M. J. Bradshaw, et al., *Proc. Soc. Inf. Disp.*, **1**, L16 (1987).

[33] J. C. Jones, M. J. Towler, and J. R. Hughes, *Displays*, **14**, 86 (1993).

[34] H. Furue, Y. Iimura, Y. Miyamoto, H. Endoh, H. Fukuro, and S. Kobayashi, *Jpn. J. Appl. Phys.*, **37**, 3417 (1998).

[35] M. F. Bone, D. Coates, W. A. Crossland, et al., *Displays* 115 (1987).

[36] V. Manjuladevi, Yu. P. Panarin, J. K. Song, J. K. Vij, and B. K. Sadashiva, *Appl, Phys. Lett.*, **93**, 093507 (2008).

[37] C. M. Spillmann, B. R. Ratna, and J. Naciri, *Appl, Phys. Lett.*, **90**, 021911 (2007).

[38] E. Pozhidaev, V. Chigrinov, and X. Li, *Jpn. J. Appl. Phys.*, **45**, 875 (2006).

[39] J. S. Patel, *Appl, Phys. Lett.*, **60**, 280 (1992).

[40] Y. Asao, T. Togano, M. Terada, T. Moriyama, S. Nakamura, and J. Iba, *Jpn. J. Appl. Phys.*, **38**, 5977 (1999).

[41] T. Nonaka, J. Li, A. Ogawa, B. Hornung, W. Schmidt, R. Wingen, and H. R. Dubal, *Liq. Cryst.*, **26**, 1599 (1999).

[42] A. Adamski, K. Neyts, and H. Pauwels, *Ferroelectrics,* **330**, 93 (2006).

[43] K. Myojin, H. Moritake, M. Ozaki, K. Yoshino, T. Tani, and K. Fujisawa, *Jpn. J. Appl. Phys.*, **33**, 5491 (1994).

[44] Y. Asao, T. Togano, M. Terada, T. Moriyama, S. Nakamura, J. Iba, *Jpn. J. Appl. Phys.*, **38**, 5977 (1999).

[45] A. Hotta, R. Hasegawa, and K. Takatoh, *Jpn. J. Appl. Phys.*, **43**, 6243 (2004).

[46] S. Kobayashi, J. Xu, H. Furuta, Y. Murakami, S. Kawamoto, M. Oh-kouchi, H. Hasebe, and H. Takatsu, *Opt. Eng.*, **43**, 290 (2004).

[47] M. Okabe, N. Sawatari, M. Ishikawa, and H. Hama, *SID 05 Digest*, 1804 (2005).

[48] T. Tsuchiya, H. Takezoe, and A. Fukuda, *Jpn. J. Appl. Phys.*, **25**, L27 (1986).

[49] A. Hotta, R. Hasegawa, and K. Takatoh, *Jpn. J. Appl. Phys.*, **43**, 6243 (2004).

[50] J. Dijon, C. Ebel, and L. Mulatier, *Ferroelectrics*, **85**, 47 (1988).

[51] D. D. Huang, V. Kozenkov, V. Chigrinov, H. S. Kwok, H. Takada, and H. Takatsu, *Jpn. J. Appl. Phys.*, **44**, 5117 (2005).

[52] C. W. Lin, C. Y. Hsu, and H. M. P. Chen, "Plasma alignment technology for liquid crystal devices", *IDMC 2009* (2009).

[53] H. M. P. Chen and C. W. Lin, *Appl. Phys. Lett.*, **95**, 083501 (2009).

[54] K. Takatoh, H. Nagata, and T. Saishu, *Ferroelectrics*, **179**, 173 (1996).

[55] K. H. Yang, *J. Appl. Phys.,* **64**, 4680 (1988).

[56] T. C. Chieu, *J. Appl. Phys.*, **64**, 6234 (1988).

[57] K. Kondo, F. Kobayashi, H. Takezoe, A. Fukuda, and E. Kuze, *Jpn. J. Appl. Phys.*, **19**, 2293 (1980).

[58] G. Hegde, O. Yaroshchuk, R. Kravchuk, A. Murauski, V. Chigrinov and H. S. Kwok, *J. Soc. Inf. Display*, **16**, 1075 (2008).

[59] K. Takatoh, H. Nagata, and T. Saishu, *Ferroelectrics* **179**, 173 (1996).

[60] T. Hatano, K. Yamamoto, H. Takezoe and A. Fukuda, *Jpn. J. Appl. Phys.*, **25**, 1762 (1986).

[61] C. J. Yu, D. W. Kim, J. Kim, and S. D. Lee, *Opt. Lett.*, **30**, 1995 (2005).

[62] J. A. Davis and G. H. Evans, *Opt. Lett.*, **29**, 1443 (2004).

[63] S. J. Woltman, J. N. Eakin, G. P. Crawford, and S. Zumer, *Opt. Lett.*, **31**, 3273 (2006).

[64] S. Matsumoto, M. Goto, S. W. Choi, Y. Takanishi, K. Ishikawa, and H. Takezoe, *J. Appl. Phys.*, **99**, 113709 (2006).

[65] J. H. Park, L. C. Khoo, C. J. Yu, M. S. Jung, and S. D. Lee, *Appl. Phys. Lett.*, **86**, 021906 (2005).

[66] J. R. Wang, C. R. Lee, and M. R. Lee, and Andy Y. G. Fuh, *Opt. Lett.*, **29**, 110 (2004).

[67] C. Provenzano, P. Pagliusi, and G. Cipparrone, *Appl. Phys. Lett.*, **89**, 121105 (2006).

[68] T. Sasaki, H. Ono, N. Kawatsuki, and M. Kuwabara, *Appl. Phys. Lett.*, **87**, 161112 (2005).

[69] H. Choi, J. H. Woo, J. W. Wu, D. W. Kim, T. K. Lim, and S. H. Song, *Appl. Phys. Lett.*, **91**, 141112 (2007).

[70] C. V. Brown, E. E. Kriezis, and S. J. Elston, *J. Appl. Phys.*, **91**, 3495 (2002).

[71] L. Gu, X. Chen, W. Jiang, B. Howley, and R. T. Chen, *Appl. Phys. Lett.*, **87**, 201106 (2005).

[72] L. M. Blinov and V. G. Chigrinov, *Electrodesoptic Effects in Liquid Crystal Materials* (Springer-Verlag, New York, 1996).

[73] J. W. Goodman, *Introduction to Fourier Optics*, 2nd ed. (McGraw-Hill,

Singapore, 1996).

[74] K. Yoshino and M. Ozaki, *Jap. J. Appl. Phy.*, **23**, L385 (1984).
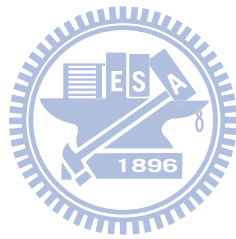
Publication List

Journal Papers

[1] Huang-Ming P. Chen and ***Chi-Wen Lin***, "Free Alignment Defect, Low Driving Voltage of Half-V Ferroelectric Liquid Crystal Device", *Appl. Phys. Lett.*, 95, 083501 (2009)

[2] ***Chi-Wen Lin*** and Huang-Ming Philip Chen, "Defect Free Half-V Mode Ferroelectric Liquid Crystal Device", *Journal of SID*, 18, 976 (2010)

[3] Dick K.G. de Boer, ***Chi-Wen Lin***, Merijn P. Giesbers,et al., "Polarization-independent filters for luminescent solar concentrators", *Appl. Phys. Lett.*, 98, 021111 (2011)

International Conference Papers

[1] ***C. W. Lin*** and H. M. Philip Chen, "Liquid Crystal Gratings Based on Striped Electrodes", *IDMC 2011* (2011/04).

[2] ***C. W. Lin***, Chih-I-Hsu, Chia-Huang Liao, and H. M. Philip Chen, "Horizontal Chevron Defect Free Half-V Mode Ferroelectric Liquid Crystal Devices Based on Asymmetrical Hybrid Alignment Techniques", *SID 2010 Digest*, 391-393 (2010/05)

[3] ***C. W. Lin***, Chih-I-Hsu, and H. M. Philip Chen, "Surface Polarity Controlled Horizontal Chevron Defect Free Surface Stabilized Ferroelectric Liquid Crystal Devices", *SID 2009 Digest*, 1003-1005 (2009/05)

[4] ***C. W. Lin***, Chin-Yi Hsu, and H. M. Philip Chen, "Plasma Alignment Technology for Liquid Crystal Devices", *IDMC 2009* (2009/04).

[5] **_C. W. Lin_**, K. Z. Li, C. W. Yang and <u>H. M. Philip Chen</u>, "Low Driving Voltage with clean Aligned Ferroelectric Liquid Crystal Devices", *SID 2007 Digest*, 622-624 (2007/05)

[6] **_C. W. Lin_**, Y. Y. Tsai, K. G. PaniKumar, C. K. Kim, S. H. Chen and <u>H. M. Philip Chen</u>, "Novel Ferroelectric Glassy Liquid Crystal and Mixtures with Wide SmC* Mesophase", *SID 2006 Digest*, 857-859 (2006/05).

[7] <u>H. M. Philip Chen</u>, Y. Y. Tsai, **_C. W. Lin_**, C. K. Kim, S. H. Chen, "Novel Ferroelectric Liquid Crystals Consisting Glassy Liquid Crystal as Chiral Dopants", *SPIE* 6332-16 (2006).

[8] <u>H. M. Philip Chen</u>, K. G. Pani Kumar, **_C. W. Lin_**, C. K. Kim, S. H. Chen, "Photonic Application of Glassy Liquid Crystals", *SPIE* 587204-1 (2005).

Vita

Name: Chi-Wen Lin 林淇文

E-mail: chiwen.di93g@nctu.edu.tw

Education

- Doctoral Student, Electro-Optical Engineering, National Chiao Tung University, Taiwan. (Sept. 2006 ~ present, Degree Expected: Jul. 2011)
  Advisors: Prof. Huang-Ming Philip Chen

- M.S., Display Institute, National Chiao Tung University, Taiwan.
  (Sept. 2004 ~ Jun. 2006)
  Advisor: Prof. Huang-Ming Philip Chen

- B.S., Department of Electronics Engineering, Yuan Ze University, Taiwan.
  (Sept. 2000 ~ Jun. 2004)

Work

- Guest Researcher, Philips Research, Netherlands (3 Jan. 2010 ~ 28 Dec. 2010)